UNIVERSITY OF CALIFORNIA
RIVERSIDE

Development of Quantitative FRET Technology for SENP Enzyme Kinetics Determinations and High-sensitive High-throughput Screening Assay for Protease Inhibitor Discovery

A Dissertation submitted in partial satisfaction
of the requirements for the degree of

Doctor of Philosophy

in

Bioengineering

by

Yan Liu

December 2012

Dissertation Committee:
- Dr. Jiayu Liao, Chairperson
- Dr. Jerome Schultz
- Dr. David Kisailus
- Dr. Dimitrios Morikis

The Dissertation of Yan Liu is approved:

Committee Chairperson

University of California, Riverside

Acknowledgements

I would like to thank Dr. Jiayu Liao for his great support in my Ph.D training, and Dr. Jerome Schultz, Dr. David Kisailus, Dr. Dimitrios Morikis for their helpful advice. Dr. Morikis and Dr. Chris Kieslich offered the computational method to determine the SUMO4 mutation sites. Dr. Victor Rodgers and Dr. Jerome Schultz provided valuable advice for calculation model optimization. Dr. David Carter helped a lot on compound screening instrumentation. I also have to thank all of the members in Dr. Liao's group for very close collaborative work and helpful discussion, especially Dr. Yang Song and Dr. Yongfeng Zhao's help for teaching and training and Ms. Ling Jiang's technical help, Ms. Hong Xu's help for instrument maintenance. This work is supported by funding from University of California-Riverside and the National Institutes of Health.

The text of this dissertation, in part, is a reprint of the material as is appeared in *Front. Biol.* 2012, Vol 7 (1), p57-64; *Anal. Biochem*. 2012, 422, p14-21. Listed in the publication, Dr. Jiayu Liao supervised the research which forms the basis for this dissertation, Yang Song provided theoretical help for spectrum analysis, Vipul Madahar provided technical help during the research.

Dedication

I would like to dedicate this dissertation to my parents (Haicheng Liu and Qianting Ma) and my boyfriend (Jian Gong) for their constant support and encouragement throughout my Ph.D study.

Abstract of the Dissertation

Development of Quantitative FRET Technology for SENP Enzyme Kinetics Determinations and High-sensitive High-throughput Screening Assay for Protease Inhibitor Discovery

by

Yan Liu

Doctor of Philosophy, Graduate Program in Bioengineering
University of California, Riverside, December 2012
Dr. Jiayu Liao, Chairperson

SUMOylation is an important post-translational protein modification mechanism which plays important roles in a variety of biological processes. Conjugating SUMO to substrates requires an enzymatic cascade. SENP, SUMO specific protease, can either mature pre-SUMO or deconjugate SUMO from its target proteins. To fully understand the roles of SENPs in the SUMOylation cycle, it is critical to understand their kinetics. FRET is an energy transfer phenomenon which occurs between two spectrum-overlapping fluorophores in close proximity. The efficiency of FRET is highly dependent on the distance between the donor and acceptor fluorophores, which makes FRET very powerful in the detection of molecular interactions and biomolecular conformational changes.

A novel highly sensitive FRET-based protease assay was designed and developed to study the activities and specificities of SENP in SUMOylation

signaling pathway and to identify bioactive chemical compounds which can specifically inhibit SENPs' activities. The endopeptidase and isopeptidase activities of SENP1/2/5/6/7c toward SUMO1/2/3 were studied and verified by western-blot assay. A novel quantitative FRET analysis was performed to study the protease kinetics to compare the specificities to substrate. The direct emissions of donor and acceptor were considered in FRET signal analysis. The mathematical algorithm dependent on pre-established standard curves or later optimized internal calibration method related the hydrolyzed substrate concentration to detected fluorescent signals during the dynamic processes, and thus derived the kinetics constants. Then, the developed protease assay and protease kinetics analysis methods were applied to study the pre-SUMO4's maturation and the product inhibition in pre-SUMO's maturation, which indicated the potential application in biomechanism study and chemical compounds' inhibition characterization. Finally, the FRET-based assay was developed to HTS assay to screen small chemical SENP inhibitors. The screening conditions were optimized to achieve satisfactory *Z'* factor value and high signal-to-noise ratio. 55,000 compounds were screened by the developed HTS assay. The general principles of the quantitative FRET analysis in protease kinetics, including the characterization of inhibition, can be applied to other substrate-protease with inhibitors. The FRET-based protease assay as well as the HTS assay provided a powerful tool for large-scale and high-throughput applications.

Table of Contents

List of Figures

List of Tables

List of Abbreviations

SUMO: small ubiquitin-like modifier

Ubl: ubiquitin-like protein

SMT3: suppressor of Mif two 3

SIM: SUMO-interacting motifs

FRET: Förster resonance energy transfer

SENP: Sentrin/SUMO-specific protease

RanGAP: Ran-GTPase-activating protein

PIAS: protein inhibitor of activated STAT

STAT: signal transducers and activators of transcription

DUB: deubiquitinating enzyme

ULP: Ubl-specific protease

NEDD8: neural precursor cell expressed, developmentally down-regulated 8

NLS: N-terminal localization signal

NES: nuclear export signal

NPC: nuclear pore complex

AR: androgen receptor

USP: ubiquitin specific protease

AFC: 7-amino-4-trifluoromethyl-coumarin

SBT: spectral bleedthrough

FLIM: fluorescence lifetime imaging

ACC: 7-amino-4-carbamoylmethyl-coumarin

AMC: 7-amino-4-methyl-coumarin

CFP: cyan fluorescent protein

YFP: yellow fluorescent protein

TR-FRET: time resolved Förster resonance energy transfer

IPTG: isopropyl β-D-thiogalactoside

DTT: Dithiothreitol

SDS-PAGE: sodium dodecyl sulfate-polyacrylamide gel electrophoresis

APC: Allophycocyanin

GST: glutathione S-transferase

T1D: type 1 diabetes

NF*κ*B: nuclear factor *κ*B

AP-1: activator Protein-1

AESOP: analysis of electrostatic similarities of proteins

SPR: surface plasmon resonance

ITC: isothermal titration calorimetry

HTS: high-throughput screening

NEM: N-Ethylmaleimide

DMSO: Dimethyl sulfoxide

INTRODUCTION

SUMO & SUMOylation:

Reversible posttranslational modifications of proteins is an important means to alter their function, activity or localization after their synthesis have been completed [1]. Proteins can be modified by small chemical groups, sugars, lipids, and even by covalent attachment of other polypeptides [2] in two fundamental types: that associated with the incorporation or removal of a functional group and that associated with the introduction of a functional protein (Table 1).

Functional group/entity	Functional protein
Phosphate (-PO_3H)	Ubiquitin
Acetyl (Ac-/CH_3CO-)	SUMO-1,2,3
Methyl (Me-/CH_3-)	NEDD8
Sulphate (-SO_3H)	ISG15
Lipid	FAT10
Carbohydrate	Urm1

Table 1: Types of posttranslational modification.

The most well-known example of polypeptide modifier is ubiquitin, which is a small protein of only 76 amino acids and a molecular weight of ~8.6kDa. Since its first description in 1975 [3], it has been apparent that ubiquitin plays a central role in targeting proteins for proteolytic degradation by the proteasome, although

covalent attachment of ubiquitin to proteins can also regulate localization and/or activity independent of proteolysis.

Ubiquitin is the “parent” of a family of ubiquitin-like proteins (Ulbs) of which at least ten members are currently identified. The Ubls vary widely in their degree of sequence similarity of ubiquitin but share a common chemistry for becoming attached to internal lysine residues in substrate proteins [4]. One Ubl in particular, the small ubiquitin like modifier (SUMO) has been found to covalently attach to the ε-amino groups of lysine residues within substrates and play an important role in a wide variety of biological processes, including gene expression, chromatin structure regulation, signal transduction and maintenance of the genome [1, 2, 4-6]. SUMO is present in all eukaryotic kingdoms [7] and is highly conserved from yeast to humans [4]. NMR studies have shown that SUMO1 and ubiquitin have similar protein fold but only shared 18% sequence identity. Moreover, the surface charge topology of SUMO is very different from that of ubiquitin, with distinct positive and negative regions [8]. SUMOs are ~20 amino acids longer than ubiquitin, and the extra residues are found in an N-terminal extension (Fig. 1). Human SUMO1 (also known as sentrin, Ubl1 and Smt3c) was first discovered in 1996 by homology studies of yeast SMT3 (Suppressor of Mif Two 3) protein and shown to share sequence homology with human ubiquitin protein [9]. SUMO2 (sentrin-3, Smt3a) and SUMO3 (sentrin-2, Smt3b) were identified shortly after the discovery of SUMO1 [10, 11]. SUMO4 was found with high expression level in the kidney, lymph node and spleen until 2004 [12]. All

SUMO genes encode a precursor bearing a short C-terminal peptide (2-11 amino acids), which is cleaved off by its specific protease to produce the mature di-Gly C terminus found in most Ubls.

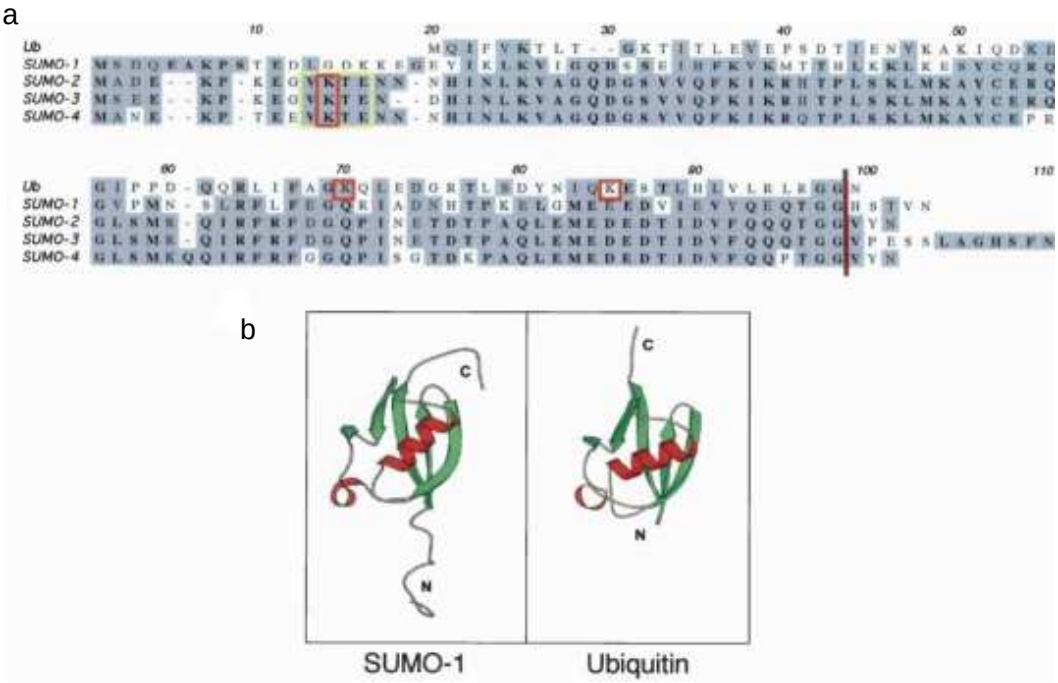

Figure 1 Comparison of SUMO and ubiquitin [2]. (a) Amino acid sequence alignments of ubiquitin and four human SUMO homologs. Identities are indicated in bold and similarities are shaded. A consensus motif for SUMOylation present in SUMO2, 3 and 4 is boxed in yellow; the SUMO acceptor lysine (K) is boxed in red. Ubiquitin Lys48 and Lys63, which serve as common sites for ubiquitin polymerization, are boxed in red. The site of cleavage to produce the mature proteins with C-terminal glycine–glycine residues is also indicated; (b) ribbon diagrams highlight the similarity of the three-dimensional structures of SUMO1 and ubiquitin. Secondary structure elements are indicated: *β* sheets are green and *α* helices are red. Notably, SUMO has an N-terminal extension not found in ubiquitin.

Mammalian SUMO2 and SUMO3 share ~95% sequence identity with each other and are ~45% identical to SUMO1. Cells contain a large pool of free, unconjugated SUMO2/3 but the majority of SUMO1 is conjugated to other proteins at any given time [13, 14]. Conjugation of SUMO2/3 is found to be strongly induced in response to various stresses, but not for SUMO1's conjugation [14]. There is also evidence that different SUMOs are used preferentially for different substrates [14-16]. Polyubiquitin chain is critical for many biological activities. Polyubiquitin is structurally and functionally diverse as multiple Lys in ubiquitin can each serve as a site of ubiquitin attachment (Fig. 1). SUMO2 and SUMO3 contain ΨKXE (Ψ corresponds to a large hydrophobic amino acid, K is a lysine residue, X is any amino acid and E is a glutamic acid residue) sequences in their N-terminal extensions, which can form polySUMO chains but SUMO1 does not have [17]. It is interesting to be found that SUMO1 acts as a polySUMOchain terminator [18]. The role of SUMO4 remains enigmatic but has been found to relate to type I diabetes [12].

Ubls are conjugated to garget proteins by enzymatic cascade involving a Ubl activating enzyme (E1), a Ubl conjugating enzyme (E2) and typically a Ubl protein ligase (E3) (Fig. 2). SUMO conjugation involves the same set of enzymatic steps. The enzymes of the SUMO pathway are specific for SUMO and have no role in conjugating ubiquitin or any other Ubls.

The immature precursors of SUMO need to be leaved prior to protein conjugation (Fig. 2, step 1). This is carried out by SUMO specific protease

(SENP). The mature form has a C-terminal di-Gly motif which is required for efficient adenylation by a heterodimeric SUMO E1 enzyme (SAE1/2, also known as Aos1/Uba2) (Fig. 2, step 2). Once formed, the SUMO adenylate is attached by a conserved Cys on the E1 enzyme to form an E1~SUMO thioester and then transferred to a conserved Cys on a SUMO E2 enzyme (Ubc9) (Fig. 2, step 3). Although the SUMO E2 can directly interact with some SUMO substrates to transfer the SUMO to substrate Lys residues (Fig. 2, step 4) and achieve SUMO post translational modification, E3 ligases often facilitate the final conjugation. SUMO E3 ligases act to either activate Ubc9 or bring Ubc9 and the target protein within close proximity of each other, thus enhancing SUMOylation [19] (Fig. 2, step 5, 6 and 7). Substrates modified by SUMO can contact SUMO-binding proteins through their SUMO-interacting motifs (SIMs) (Fig. 2, step 8). Eventually, SUMO is removed intact from its substrate proteins by SENP and free SUMO may be recycled for another round of conjugation (Fig. 2, step 9).

Like the E1 for ubiquitin, the SUMO E1 catalyzes a three-part reaction. First, the C-terminal carboxyl group of SUMO attacks ATP, forming a SUMO C-terminal adenylate and releasing pyrophosphate. Next, the thiol group of the active site Cys in the E1 attaches the SUMO adenylate, releasing AMP and forming a high-energy thiolester bond between the E1 and the C terminus of SUMO. Finally, the activated SUMO is transferred to a Cys in the E2. Most organisms contain a single SUMO-activating enzyme, which is required for conjugation of all SUMO variants to all substrates [4]. Unlike the ubiquitin

monomer E1, SUMO E1 exists as a heterodimer, with each monomer corresponding to a particular region of the ubiquitin E1. Subunit SAE1(Aos1) shares similarity with the N terminus of the ubiquitin E1, while SAE2 (Uba2) is similar to the C terminus of the ubiquitin E1 [20]. The monomers are never found individually and hence it is assumed that they are unable to function independently [21].

Ubc9 is the only known SUMO E2 enzyme, unlike the ubiquitination pathway where each E2 has a specific set of target proteins [22]. Ubc9 shares considerable sequence similarity with ubiquitin E2s and also assumes essentially the same folded structure, although Ubc9 has a strong overall positive charge [23]. A patch surrounding the active site Cys of Ubc9 binds directly to the ψKXE consensus sequence in the substrate [24, 25]. A second region on Ubc9, separate from the active site, binds directly to SUMO and is involved in transfer SUMO from the E1 [26].

The SUMO E2 is unique among E2 enzymes in its ability to specifically recognize and conjugate SUMO to some substrates in the absence of an E3 ligase, whereas ubiquitin-conjugating enzymes generally require an E3 ligase to impart substrate specificity. However, SUMO conjugation is almost always enhanced in the presence of SUMO E3 ligases.

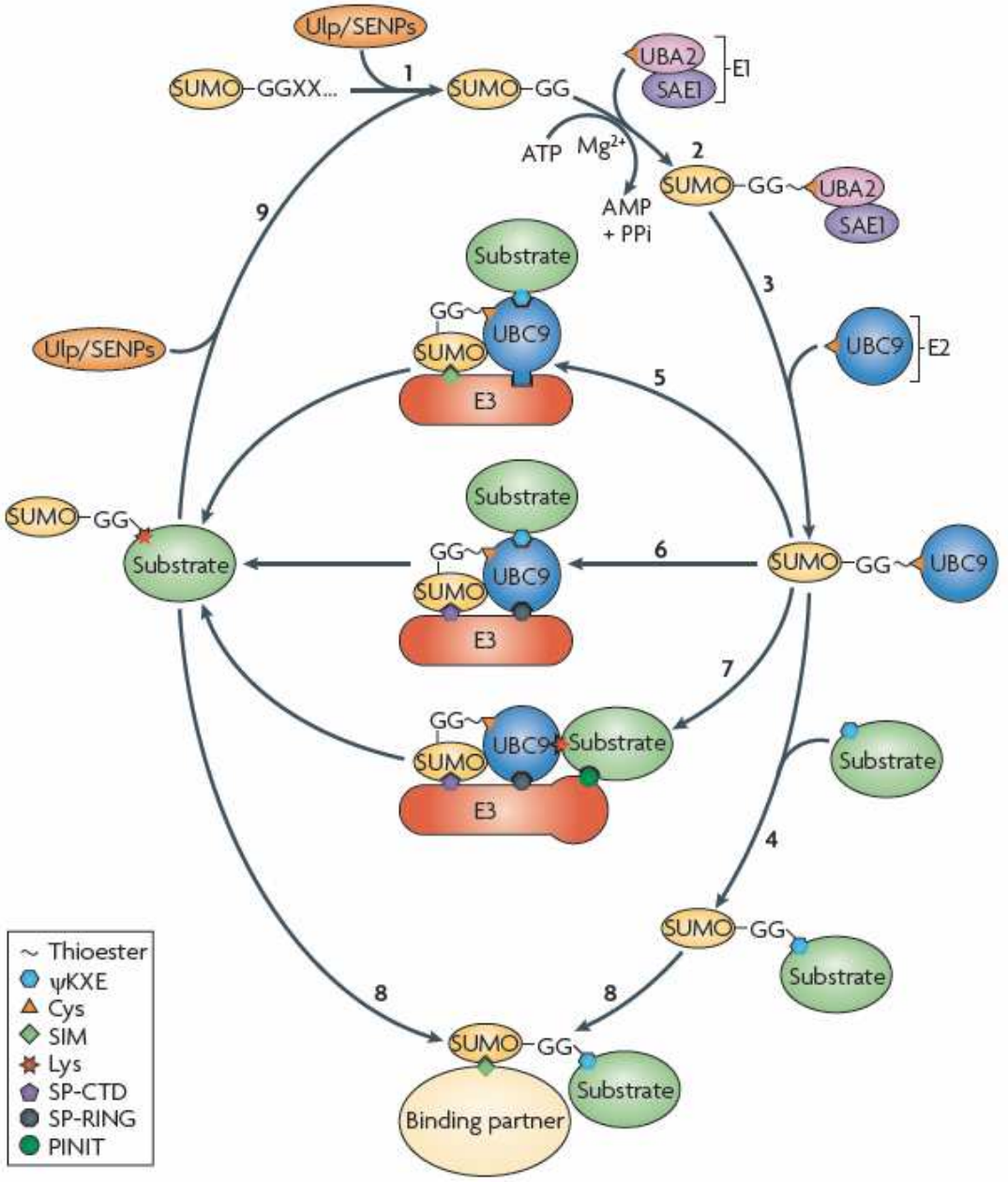

Figure 2. The SUMO conjugation cycle [27].

In contrast to SUMO E2, a larger number of SUMO E3 ligases have been discovered and categorized into three types: a family of SP-RING-containing proteins, including the Siz and the protein inhibitor of activated STAT (PIAS) (STAT: signal transducer and activator of transcription) [6], the nuclear pore proteins Ran binding protein 2 and nucleoporin 358 (RanBP2/Nup358) [28] and the polycomb group protein (PC2) [29], histone deacetylase 4 (HDAC4) [30], topoisomerase I-binding RING finger protein (TOPORS) and Ras homolog enriched in striatum (RHES).

Members of the Siz/PIAS family of E3 ligase include Siz1/2, Mms21 (methyl methanesulphonate-sensitivity protein 21) and Zip3 (molecular zipper protein 3) in yeast and PIS1/3/xα/xβ/y in humans. The Siz and PIAS E3s contact the Ubc9 and SUMO through their SP-RING and Siz/PIAS carboxyl-terminal domain (SP-CTD) domains, respectively (Fig. 2, step 6). The Siz/PIAS E3s also contain a PINIT domain that can contact the substrate, as is the case for the substrate proliferating cell nuclear antigen (PCNA) (Fig. 2, step 7). The second group of SUMO E3 consists of the nuclear pore protein RanBAP2 with only one known substrate, RanGAP (a GAPase activating protein important in nuclear transport of proteins). RanBP2 may coordinate the SUMO-Ubc9 thioester in an optimal conformation for catalysis without directly contacting the RanGAP (Fig. 2, step 5). RanGAP can also be SUMOylated *in vitro* without RanBAP2's assistance (Fig. 2, step 4). The molecular details of how the third SUMO E3 family promotes SUMO modification remain less clear. Substrates modified by SUMO can contact

SUMO-binding proteins through their SUMO-interacting motifs (SIMs) (Fig. 2, step 8), which is always hydrophobic in nature [27, 31].

SENP & De-SUMOylation:

Deubiquitinating enzymes (DUBs) and Ubl-specific proteases (ULPs), the proteins responsible for the removal of Ub and Ubls, act as an additional level of control over the ubiquitin-proteasome system [32]. Likewise, SUMO/Sentrin specific proteases (SENPs) catalyze the removal of SUMO from SUMO-conjugated target proteins as well as the cleavage of SUMO from its precursor proteins. Except that, SENPs also function in polySUMO chain editing (Fig. 3).

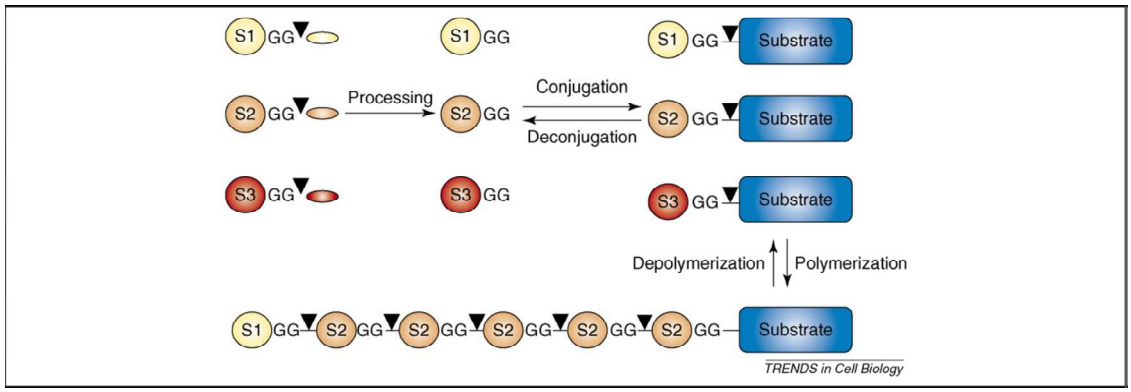

Figure 3. SENPs' function at multiple points in the SUMO pathway [33].

SENPs belong to the CE clan of cysteine protease. They are distinct from their mechanistic relatives, DUBs, which are primarily contained in the peptidase clan CA. They show no sequence similarity to the clan CA proteases although the fold has similarities. Inspection of the clan CE versus clan CA folds reveals

that SENPs have undergone a domain swap during evolution so that they preserve a similar fold to clan CA enzyme, but now have their catalytic features organized differently [34].

Two SUMO specific proteases, Ulp1/2, were first discovered in budding yeast specifically processed Smt3 [35, 36]. Ulp1 has been detected at the nucleoplasmic face of the nuclear pore complex (NPC) [36-38] and functions in both pre-SUMO maturation and SUMO-substrate deconjugation [38]. The non-conversed N-terminal domain of Ulp1 is necessary for the correct localization of Ulp1 at the nuclear envelope [37]. Remarkably, N-terminal deleted Ulp1, suppresses the cellular defects of ulp2Δ mutant cells and substantially reduces Smt3-protein conjugates. The non-catalytic N-terminal domain of Ulp1 functions at a physiologically significant restraint with regard to the subset of SUMOylated proteins which are natural targets of nucleoplasmic Ulp2. Ulp2 is localized predominantly in the nucleus, and its deSUMOylation pattern is distinct from that of Ulp1, but it is dispensable for viability [36].

To date, seven SENPs have been identified in the human genome. Not all SENPs are SUMO-specific, SENP8 (NEDP1/DEN1) has specificity toward another Ubl, NEDD8 [39, 40]. The other six SENPs (SENP1-3, 5-7, Fig. 4) all contain a conserved C-terminal catalytic domain (~250 amino acid residues) that encompasses the catalytic triad residues His478, Asp495 and Cys548 (SENP2 numbering) [34] for selectively deconjugating SUMOylated, but not ubiquitylated proteins [41]. The C-terminal catalytic domain of SENP1 shows a higher homology

to that of SENP2 (59% homology) than to those of SENP3 (42% homology) and SENP5 (44% homology). According to the sequence homology, the SENP family can be divided into 3 subfamilies. SENP1 and SENP2 share a conserved sequence of ~40 residues preceding their catalytic domain and constitute the first SENP subfamily. The catalytic domain of SENP3 is 62% identical to that of SENP5, indicating that SENP5 is more closely related to SENP3. These two SENPs are therefore categorized into the second subfamily. The third subfamily of SENPs consists of SENP6 and SENP7, both of which contain an insertion of ~180 or ~50 residues in their conserved catalytic domain. Phylogenetic analysis indicates that Ulp1 is related to SENP1, 2, 3 and 5, while Ulp2 is related to SENP6 and 7 [42].

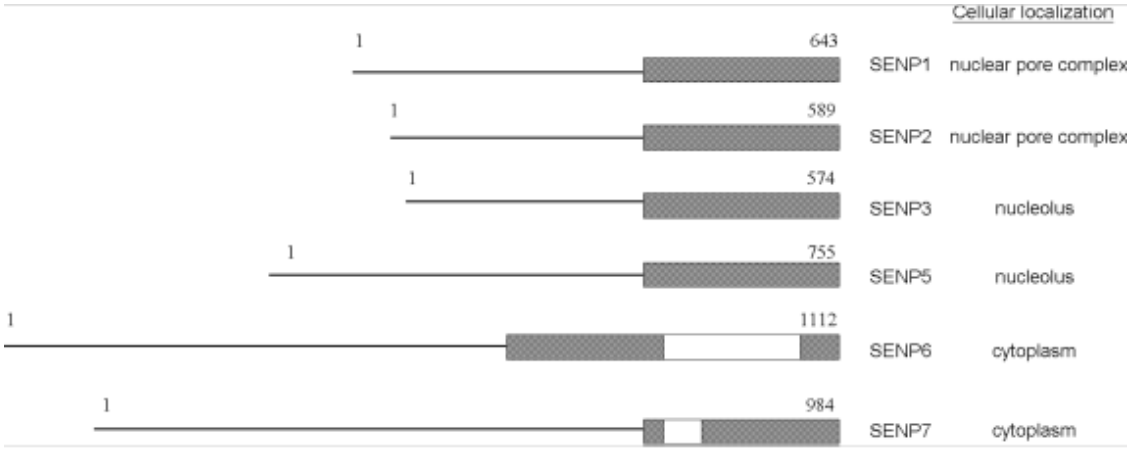

Figure 4. Structure and localization of human SUMO specific protease (SENP). The N-terminal nonconserved domain is associated with subcellular localization and substrate specificity. The C-terminal conserved catalytic domain is shown as a hatched box. Insertion of ~180 and ~50 amino acid residues in the catalytic domain of SENP6 and SENP7 is shown as an open box [42].

The less conserved N-terminal domain of SENP is responsible for cellular localization and substrate specificity during deconjugation [37]. SENP1 contains both N-terminal localization signals (NLS) and nuclear export signals (NES), but the primary location of SENP1 is in the nucleus [43-45]. Probably, SENP1 localization might be controlled by the extracellular signaling pathways with concurrent post-translational modifications such as phosphorylation or SUMOylation, although any data that can prove the hypothesis has not yet been reported [46]. SENP2 is closely related to SENP1; it is primarily found in the nuclear envelope in association with the nuclear pore complex (NPC) [47, 48]; it also accumulates in distinct subnuclear bodies [49]. It has been reported that SENP2 has both NLS and NES within its non-conserved N-terminus. Using a series of SENP2 mutants and interspecies heterokaryon assay, it was found that SENP2 shuttles between the nucleus and the cytoplasm. Interestingly, the SENP2 in the cytoplasm is efficiently polyubiquitinated and triggered to be degraded by the 26S proteasome pathway [50]. In addition, alternative mRNA splicing generates at least three different SENP2 isoform with strikingly distinct cellular localization (Axam, Axam2 and SuPr-1). Axam localizes to the nucleoplasmic face of the NPC [48], Axam2 and SuPr-1 have been detected in the cytosol and PML bodies [51, 52]. This pattern of isoform localization underscores the notion that a distinct subcellular distribution might contribute to the substrate specificity of the Ulp/SENPs. SENP3 and 5 are detected predominantly in the

nucleolus [53, 54]. SENP6 was originally reported to be located in the cytoplasm [55], but recent reports suggest that it is located in the nucleus [56].

There have been many structural and biochemical investigations of SENPs to identify their specific for SUMO isoforms, in addition to the differentiation among maturation, deconjugation and chain editing reactions (Table 2) [34, 57]. Crystal structures of SENPs have revealed that these proteases have narrow and tight active site tunnels for Gly-Gly motif recognition and utilize conserved tryptophans to clamp down on the C-terminal Gly-Gly motif of SUMO within a hydrophobic channel [58-60].

SENP Paralog	Maturation	Deconjugation	Chain editing
SENP1	SUMO1>SUMO2>SUMO3	SUMO1~SUMO2/3	No
SENP2	SUMO2>SUMO1>SUMO3	SUMO2/3>SUMO1	No
SENP3	Unknown	SUMO2/3	No
SENP5	SUMO3	SUMO2/3	No
SENP6	No	SUMO2/3	SUMO2/3
SENP7	No	SUMO2/3	SUMO2/3

Table 2: SENPs' substrate specificities of catalytic activity.

All SUMO paralogs are expressed in their precursor forms. Human SENP2 and yeast Ulp1 were the first SUMO proteases reported to be functional in SUMO maturation [55, 58]. Several lines of evidence later demonstrated that the

catalytic domain of SUMO proteases exhibit different maturation efficiencies to different SUMO precursors. SENP1 matured pre-SUMO1 with greater efficiency than pre-SUMO2, but shows limited activity towards pre-SUMO3 [61, 62]. SENP2 has been shown to contain the highest maturation efficiency to pre-SUMO2 than pre-SUMO1, but again processes pre-SUMO3 poorly [60, 63]. Because SENPs directly recognize the newly translated pre-SUMOs in these reactions, determinants of this specificity must lie within the pre-SUMO sequences themselves. By mapping the residues of SUMO precursors, the difference of the sequence after the Gly-Gly motif of pre-SUMOs has been show to influence maturation efficiency [60, 62]. Pro94 of pre-SUMO3 is particularly important for its inefficient maturation [62]. In addition, SENP1 processing of pre-SUMO1 is enhanced by a histidine residue in the pre-SUMO1 C-terminal tail (His98, P1 position in pre-SUMO1 tail) [61]. Pre-SUMO C-terminal tails likewise determine the efficiency of SENP2 processing [60] and Pro94 of pre-SUMO3 again contributes towards its inefficient maturation by SENP2. In contrast to SENP1 and SENP2, SENP5 is essentially inactive for pre-SUMO1 processing, but efficiently catalyzes pre-SUMO3 maturation [54, 64]. SENP6 and SENP7 do not function as a processing enzyme for pre-SUMO maturation [65].

SUMOylation is a dynamic process that is reversible by removing the SUMO moiety from the substrates by SENPs. This is necessary to control the half-lives of SUMO conjugates and regulate their effects on downstream cellular events [66], while the SUMO moiety released can be recycled for another conjugation

process. The deconjugation process involves cleavage of the amide bond between the carbonyl group of the C-terminal glycine in SUMO and the ε-amino group of the target lysine in the conjugate proteins. The importance of deconjugation has been demonstrated by investigating the biological effects of substrates upon conjugation and deconjugation. The residues 418-587 of Ran-GTPase activating protein1 (RanGAP1), a major SUMO conjugation substrate, were used to study the SENP deconjugating SUMO activities. As the binding interfaces between SENPs and mature SUMO2 or SUMO3 are identical, it seems unlikely that there is substantial discrimination between these paralogs during deconjugation [61, 63]. Nevertheless, SENPs can clearly differentiate SUMO1 from SUMO2/3 [61, 63, 64]. SENP1 deconjugates RanGAP1-SUMO1 and RanGAP1-SUMO3 with indistinguishable efficiencies [59, 61]. Conversely, SENP2 is less efficient at deconjugation of RanGAP1-SUMO1 than RanGAP1-SUMO2 [63]. SENP3 and SENP5 are more active in deconjugating SUMO2/3 conjugated targets than SUMO1-containing species [54, 64]. The SENP6 and SENP7 have been characterized to exhibit slight specificity for SUMO2/3 [65].

The depolymerization process is chemically equivalent to that of deconjugation, but instead of cleavage of the isopeptide bond between the C-terminal glycine of SUMO and the ε-amino group of target lysine of the substrate proteins, target lysine in SUMO2/3 or Smt3 is involved. An evolutionary conservation analysis suggests that SENP6 and SENP7 are responsible for dismantling the SUMO polymers. Val713 in SENP6/7 is substituted by Glu in

SENP1/2. Removal of the Glu for Val diminishes SENP7 activity with regard to poly SUMO2/3 chains [65].

Biological Significance of deSUMOylation

The interruption of SENPs has been implicated in embryonic and carcinoma cells, indicating that a proper balance of SUMO conjugation and deconjugation is crucial. Clearly SENPs are vital for the process because SUMO precursors must have their C-terminal tails removed before ligation. But it is far from clear what role the isopeptidase activity (deSUMOylation) has to play in most of these events, although all authors point to the dynamic process of SUMOylation/deSUMOylation as likely regulation points [34].

DeSUMOylation in yeast. The isopeptidase activity of Ulp1 is essential for growth of yeast cells, particularly at the G_2/M transition. The catalytic domain of Ulp1 is sufficient to rescue the growth defect of Ulp1 deletion in yeast [37]. This nuclear detect is dependent on the isopeptidase activity because it is not rescued by the mature form of Smt3. Interestingly, Ulp1 exhibits a cell cycle-specific pattern of localization. During the S and G_2 phases, Ulp1 is localized at the nuclear periphery. However, during mitosis, Ulp1 is localized in the nucleus. Ulp2-null cells exhibit temperature sensitive growth, chromosome instability and hypersensitivity to DNA-damaging agents [36]. More recently, it was shown that

Ulp2 is required for resumption of cell division following DNA damage-induced arrest but is not required for DNA double-strand break repair [67].

Transcription regulation. More than 120 mammalian SUMO substrate proteins have been identified. Two thirds of them are transcription factors and co-regulators [68, 69]. However, an increasing number of investigations have shown that SUMOylation can also activate transcription. SENPs use their isopeptidase activity on SUMOylated transcriptional factors and nuclear receptors that bind promoter elements and directly mediate gene transcription. In addition, the isopeptidases also modulate the activity of SUMO-conjugated coregulatory proteins. These proteins can either facilitate (co-activator proteins) or inhibit (corepressor proteins) the transcriptional activity of specific transcription factors or nuclear receptors to which they are bound. Overexpression of SENP1 enhances androgen receptor (APR)-dependent transcription [70, 71]. Enhancement of AR-dependent transcription is not medicated by deSUMOylation of AR, but rather is processed by the deconjugation of histone deacetylase 1 (DHAC1), thereby reducing its deacetylase activity [70]. SENP1 and SENP2 have been observed to independently regulate the transcriptional activity of c-Jun [52, 72] although c-Jun is not a direct target of SENP2. SENP1 deconjugates SUMOylated c-Jun co-activator p300. SUMOylation of p300 is responsible for the cis-repression function of the CRD1 domain of p300 and prevents the transactivation capabilities of p300. SENP1 relieves this internal repression and enhances p300-mediated transactivation. SENP2 regulates the SUMOylation

and function of Sp3, a member of the GC box-binding transcription factors [49]. Conjugation of SUMO to Sp3 represses Spe-mediated transcription while the deSUMOylating ability of SENP2 prompts Sp3 transcriptional activation. SENP2 has also been shown to modulate the Wnt signaling pathway via regulation of the co-activator β-catenin and the transcription factor Tcf-4 [73-75]. The highly conserved Wnt pathway mediates the transcription of gene that is critical for development and carcinogenesis. The expression of Axam2, the mouse homolog of SENP2, directly facilitated degradation of β-catenin but required an intact isopeptidase domain to prompt this change in β-catenin levels. SENP3 reverses the modification to augment the transcriptional and myogenic activities of SUMO target MEF2, a transcriptional activator of muscle differentiation [76]. A yeast two-hybrid demonstrated that SENP6 deSUMOylated RXRα (retinoid X receptor α) but not two other SUMO conjugated nuclear receptors AR or PPARγ (peroxisome proliferator-activated receptor γ), and increases the RXR transcriptional activity [77].

Development. The characterization of a random retroviral insertional mutation in the mouse orthology of SENP1 highlights the critical importance of regulating the levels of SUMOylation during mouse embryogenesis, which suggests a non-redundant and essential role of SENPs during development [78]. A significant reduction in the SENP1 expression has been attributed to the physical disruption of an intron enhancer elements; this mutation reduces both deconjugation and processing of SUMO1. Loss of SENP2 in mice also causes

embryonic lethality due to a placental defect [79]. SENP2 ablation increases p53 levels and thereby impairs cell cycle progression and maturation of trophoblasts.

Cell growth and differentiation. Small interference RNA (siRNA) knockdown of SENP5 leads to decreased cell proliferation in HeLa Cells [64]. SENP5 downregulation increases the number of binucleate cells that are due to defects in mitosis and cytokinesis; hence SENP5 mediate normal cell division. SENP1 and SENP7 also appear to positively regulate cell proliferation. Stable overexpression of SENP1 enhances the cell cycle regulator cyclin D1 whereas the expression of the catalytically inactive SENP1 mutant has no effect [80]. Retroviral SENP1 inhibits cell proliferation without inducing apoptosis or necrosis in human foreskin fibroblast cells [81]. SENP1 deficient fibroblast cells undergo cellular senescence and hence are arrested in the G_1 phase of the cell cycle. Absence of p53 activity with either shRNA treatment or stable overexpression of a p53 dominant negative mutant prevented cellular senescence induced with SENP1 knockdown suggesting that the senescence response is mediated via a p53-dependent pathway. Downregulation of SENP2 and SENP7 also inhibited cell proliferation and caused cellular senescence. Interesting, SENP2 ablation in a mouse model produces a defect in the G_1-S transition with increased number of trophoblast stem cells in the G_1 phase [79]. Elevated p53 levels are observed in the SENP2 knockout trophoblasts which prompt G_1 arrest and prevent trophoblast differentiation. The critical role of SENP1 in tumor necrosis factor (TNF) α-induced ASK (apoptosis signal-regulating kinase) 1-JNK activation and

endothelial cell apoptosis is conferred by the translocation of SENP1 from cytoplasm to the nucleus in response to TNF [82]. In endothelial cells, TNF prompts the translocation of SENP1 to the cytoplasm, SENP1 mediated deSUMOylation of homeodomain-interacting protein kinase (HIPK) 1 and subsequent ASK1 dependent apoptosis [82].

Cancer and other disease. As more oncogenes and tumor suppressor genes are identified as SUMO conjugates [83], the role of SUMO in cancer development seems more obvious and direct. It is now believed that alteration of gene expression of components in the SUMOylation system is associated to carcinogenesis and cancer progression [84]. The isopeptidase activity of SENP is heavily dependent upon the level expressed in the cell. Under normal physiological conditions, a balance must exist between the level of SUMO conjugated and deconjugated target proteins. Changes in the expression level of one SENP would greatly affect this equilibrium; where induction of a specific SENP would facilitate greater deSUMOylation of cellular substrates and inversely reduction of a SENP would enhances SUMO conjugation of target proteins. Thus, it is feasible that shifts in this SUMOylation/deSUMOylation equilibrium could contribute to the onset of various pathophysiological conditions. Elevated SENP1 mRNA levels are observed in thyroid oncocytic adenocarcinoma and prostate cancer [80, 85]. The upregulation of SENP1 is a relatively early event in the carcinogenesis of the prostate. Persistent elevation of SENP1 was found to directly facilitate the transformation of the normal prostate gland to dysplastic

state as observed in transgenic mice model [80]. SENP1 enhances the transcriptional activity of the AR via deSUMOylation of the corregulatory protein HDAC1[70], which potentiates SENP1 expression as feedback loop. The intriguing relationship between SENP1 and AR initiates a prominent signal cascade for the development of prostate cancer [86]. SENP3 is also elevated in prostate cancer and additional carcinomas, including ovarian, lung, rectum and colon [87]. The tumor suppressor protein $p19^{ARF}$ is known to dictate SENP3 turnover; it initiates SENP3 phosphorylation, ubiquitylation and subsequent proteosomal-mediated degradation [88]. Loss of ARF is observed with the onset of several human cancers [64, 89], and hence, deregulation of the ARF-medicated SENP3 turnover could attribute to the elevated SENP3 levels observed in various carcinomas. Overexpression of SENP3 can facilitate the expression of HIF1α-regulated vascular endothelial growth factor (VEGF), which is critical for vascular development. When SENP3 was stably overexpressed in HeLa cells and subsequently xenografted into nude mice, the SENP3 overexpression produced more aggressive tumors, as exemplified via the greater tumor volume and angiogenesis in the xenograft animals [86]. Whereas the induction of SENP1 and SENP3 in prostate cancer would favor enhanced deSUMOylation of cellular substrates, it is likely that SUMOylation would be prevalent in breast carcinomas. Augmentation of SUMO conjugation -- specifically, SUMO1, Ubc9 and PIAS3 -- in breast cancer cells increases tumor formation [86, 90, 91]. Decreasing SUMOylation with the expression of the dominant negative Ubc9 inhibits tumor

volume in the xenograft models [92]. A recent report demonstrated downregulation of SENP6 mRNA in breast tumor tissue as compared to normal tissue based on bioinformatics analysis of published microarray data [93]. It is possible that restoring reduced SENP6 levels in breast cancer cells could produce results similar to the dominant negative Ubc9 and inhibit tumor formation. Hence, in some cancers, enhancing net SUMO conjugation (possibly via downregulation of one or more SENPs) may contribute to the progression of the carcinoma. Altered subcellular localization of SENP5 in patients with oral squamous cell carcinoma (OSCC) has been discovered. SENP5 predominantly localized to the cytoplasm of OSCC and SENP5 expression was associated with differentiation of OSCC cells [94]. SENP6 was found to fuse to the novel gene T-cell lymphoma breakpoint associated target 1 (TCBA1) in the HT-1 cell line which is derived from a T-cell lymphoblastic lymphoma [95]. The fusion gene may contribute to tumorigenesis but the mechanism remains undefined. The roles of SUMoylation in cancer metastasis have also been demonstrated by isolating the SENP1 and SENP6 associated *β*-catenin-reptin chromatin remolding complex which regulates a metastasis suppressor gene KAI1 [96, 97] and inhibits the progression of tumor metastasis [98].

RNA biogenesis. It has been reported that the two SUMOylated proteins, CPSF73 and symplekin, involved in the pre-mRNA 3' processing. SENP2 was found to interact with these proteins and inhibits 3' processing in HeLa nuclear extracts *in vitro* [99]. SENP3 has been shown to be crucial for 32S rRNA

processing in the nucleolus via cleaving SUMO2 from NPM1 (nucleophosmin 1), in which is critical for 28S rRNA maturation in the nucleolus [100]. Knockdown of SENP5 reduces the amount of the primary 47S rRNA transcript, indicating that SENP3 and SENP5 play a role in ribosome biogenesis by acting on distinct substrates [100].

Small Chemical Compounds as SENP Inhibitor

The balance of SUMOylation and deSUMOylation plays an important role in many biological processes including regulation of immune signal transduction, stabilization of target proteins and maintenance of chromosomal integrity. It has remained difficult to globally assess the temporal aspects of the SUMOylation in the regulation of basic biological processes due to the highly dynamic process of protein SUMOylation and deSUMOylation. Given the important roles SENPs play, knockout of SENP genes can have serious effects and may even kill the transgenic animals, which make genetic studies quite difficult. To overcome these difficulties, new tools besides the traditional biochemical and genetic approaches are needed to study the SENPs functions. Furthermore, increasing reports, as stated above, suggest an oncogenic function of SENPs required for cancer cell survival or proliferation and have generated interests in SENPs as targets for therapeutic intervention.

An attractive strategy to further the understanding of proteolytic enzymes is the design of selective inhibitors. Indeed, this approach has been successfully applied to the caspase [101] and cathepsin [102] families as well as the individual enzymatic activities of the proteasome [103]. Compared with other biological approaches, bioactive small chemical compounds not only offer better spatial and temporal control of biological processes but can also be used to investigate the biological function of proteins when gene knockout is not feasible. In that way, small molecule inhibitors of SENPs are wanted to facilitate the interrogation of the intracellular SUMO network and to investigate the potential of SENPs as cancer drug targets. Surprisingly, very few small molecule tools have been developed for exploring SENPs.

The first generation of ubiquitin specific protease (USP) and Ubl-specific protease inhibitors is based on the entire Ub/Ubl protein itself modified at the C terminus with electrophilic entities capable of reacting with the active-site cysteine thiol, present in most Ub and Ubl-specific proteases. These electrophilic traps include aldehydes [103, 104], nitrile derivatives [105], Michael acceptors (including vinyl sulfone (VS), vinyl methyl ester (VME)) [106, 107], and alkyl halides [108, 109]. Co-crystallization of yeast SUMO (Smt3) aldehyde with the yeast deSUMOylating enzyme Ulp1 has been used to probe the enzyme-substrate interactions [58]. SUMO1 and SUMO2 aldehydes are highly specific inhibitors of SENPs and have utilities in the stabilization of SUMO-protein conjugates *in vitro*, enhancing their accumulation in cell lysates and tissue extracts [56, 103]. The

commercially available full-length SUMO vinyl sulfone inhibitor has also been developed into an active site probe by addition of an HA tag at the N terminus to allow detection by western blotting [110]. In addition, a biotinylated vinyl sulfone-based inhibitor containing the final five amino acids of the C terminus of SUMO was shown to label at least one protein in cell lysates in a dose-dependent manner [106]. Labeling of this protein could also be competed away be addition of full-length SUMO. However, the identity of the target has never been confirmed.

The first report on design and synthesis of SENP1 inhibitor based on structure-activity was in 2011. A series of benzodiazepine-based SENP1 inhibitors were designed and synthesized to inhibit the cleavage of SUMO-ΔRanGAP as benzodiazepine improved stability and bioavailability in peptidomimetic chemistry [111]. One leader synthesized compound 38 can covalently bind Cys603 of SENP1 and was discovered to have other favorable interactions, including hydrogen bond with Gly531, π-π interaction with His529, nonpolar interaction with Val532 and the insertion of Cbz moiety into the hydrophobic pocket consisting of Phe496, Thr495, Thr499, Phe498, Ile528 and Pro527 (Fig. 5-a). The inhibition of synthesized compounds were tested in SUMO-ΔRanGAP PLA_2 reporter assay and prostate cancer cell (PC3) line. None specificity and toxicity was tested.

In the same year, a library of small chemical cysteine protease inhibitors in lysates of the human parasite pathogen *Plasmodium falciparum* was screened to identify compounds that blocked endopeptidase processing of recombinant pre-

SUMO [112]. One lead compound JCP666, which contained a reactive aza-epoxide eletrophile linked to an extended, nonnatural peptide backbone structure that effectively blocked *Pf*SENP activity. JCP666 (Fig. 5-b) and its derivatives can effectively inhibit endopeptidase activity of hSENP1/2/5/7, but showed high nonspecific labeling properties when used in complex proteomes [113].

Peptide acyloxymethyl ketone (AOMK)s have been successfully used as covalent, irreversible probes of multiple classes of cysteine protease [114-116]. Furthermore, these compounds can be readily synthesized using solid-phase synthesis methods [117]. Peptide AOMKs with retained overall structure of identified JCP666 and large aromatic O-acyl group were synthesize as covalent inhibitors which function as highly selective probes of SENP activity [113]. The IC_{50} value of one of the peptide AOMK derivative, VEA-499 (Fig. 5c), was 3.6 ± 0.3 μM of human SENP1 and 0.25 ± 0.03 μM of SENP2 to the fluorogentic substrate QTGG-ACC (7-amino-4-trifluoromethyl-coumarin), a non-native SUMO substrate. However, the side effects such as toxicity to cell, antibacterial activities and inhibition of other protease or proteins have not been characterized yet.

In order to find small chemical compounds targeting the deSUMOylation step with higher potency and specificity, there is an urgent need in the development of high-throughput screening assays to test compounds from small molecule libraries.

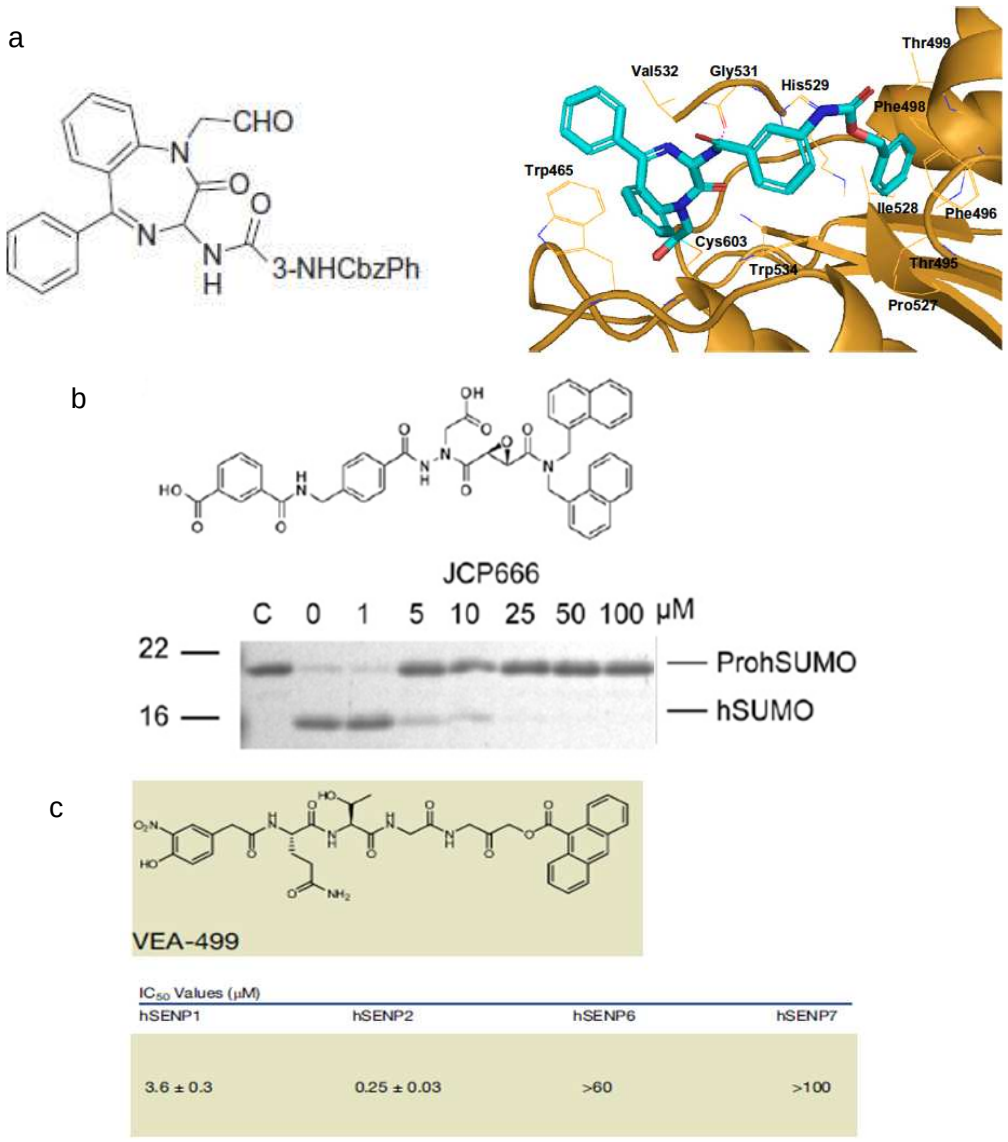

Figure 5. Synthesized or discovered small chemical SENP inhibitors [111-113]. (a) Structure of compound 38 (left) and binding model of 38 in SENP1 catalytic site (right), cyan sticks-compound 38, yellow ribbons-SENP1 protein, yellow lines-SENP1 residues, magenta dashed line-hydrogen bond; (b) structure of JCP666 (upper) with treatment of hSENP1C (100 nM) and pre-SUMO1 substrate (lower); (c) structure of VEA499 (upper) and IC_{50} for hSENP1/2/6/7C to QTGG/LRGG-AFC non-natural SUMO substrate (lower).

Förster Resonance Energy Transfer (FRET) and quantitative analysis

The historical precursors for the theory of FRET data back to the 19th and early 20th centuries with emerging understanding of electromagnetic and quantum mechanics. The energy transfer was noted to be distance-dependent and occur over a specific range (15-25nm) in 1920s by Perrin. The required distance was corrected as 1-10nm by German scientist Förester in the mid-1940s [118] (Fig. 6-a).

The most basic characterization of the theory of FRET is nonradiative energy transfer from an excited chromophore (donor) to a proximal ground state chromophore (acceptor) through a long-range dipole-dipole coupling mechanism. The interaction occurs between oscillating dipoles with similar resonance frequencies and depends on the spectroscopic and geometric properties of the donor-acceptor pair. The rate of transfer for a donor and acceptor separated by a distance r can be expressed in terms of the Förester distance R_0 (Fig. 6-d), which is the distance between donor and acceptor at 50% energy transfer efficiency. R_0 can be calculated from the spectral properties of the donor and acceptor species:

$$R_0^6 = \frac{9000(\ln 10)Q_D\kappa^2}{125\pi^5 N n^4} J(\lambda)$$

where $Q_D$is the quantum yield of the donor in the absence of acceptor; n is the refractive index of the medium, typically 1.4 for biomolecules in aqueous solution; N is Avogadro's number; $J(\lambda)$ is the overlap integral expresses the degree of

spectral overlap between the donor emission and the acceptor absorption (Fig. 6-b):

$$J(\lambda) = \frac{\int_0^\infty F_D(\lambda)\varepsilon_A(\lambda)\lambda^4 d\lambda}{\int_0^\infty F_D(\lambda)d\lambda}$$

where $F_D(\lambda)$ is the corrected fluorescence intensity of the donor in the wavelength range λ to $\lambda + \Delta\lambda$ with the total intensity normalized to unity; $\varepsilon_A(\lambda)$ is the extinction coefficient of the acceptor at λ, which is typically in units of $M^{-1}{\cdot}cm^{-1}$.

The efficiency of energy transfer (E) is the fraction of photons absorbed by the donor which are transferred to the acceptor. This fraction is given by:

$$E = \frac{k_T(r)}{\tau_D^{-1} + k_T(r)}$$

which is the ratio of the transfer rate to the total decay rate of the donor in the presence of acceptor, as $k_T(r) = \tau_D^{-1}(R_0/r)^6$, the above equation can be easily rearranged to yield:

$$E = \frac{R_0^6}{R_0^6 + r^6}$$

The orientation factor (κ^2) (Fig. 6-c) depends on the relative orientation of the donor and acceptor dipoles and is given by:

$$\kappa^2 = (cos\theta_T - 3cos\theta_D cos\theta_A)^2$$

where θ_T is the angle between the donor and acceptor transition moments, θ_D is the angle between the donor moment and the line joining the centers of the

donor and acceptor, and θ_A is the angle between the acceptor moment and the line joining the centers of the donor and acceptor.

Unlike the molecular distance (r) and the spectrum overlap integral (J), the value of κ^2 is often hard to obtain experimentally due to the uncertainty of molecular motions. Stryer analyzed the probability distribution of donor-acceptor relative angles and showed that, while the theoretical value of κ^2 can vary from 0 to 4, its range is narrow in practice and will introduce no more than 20% variation to the determination of donor-acceptor distance. In most FRET studies, the value of κ^2 is assumed to be 2/3, which corresponds to the ideal case in which both the donor and acceptor undergo unrestrictive motion [119, 120].

The theory of FRET has been validated by many subsequent studies, and the effects of different parameters on FRET efficiency have been carefully examined. A poly-L-proline with up to 12 residues was synthesized as the linker to separate a pair of fluorophores, and correlated the observed efficiencies of energy transfer with the reverse sixth power of the donor-acceptor distances [121]. An r^{-6} dependence was also confirmed by Bücher et al. with fatty acid layers of known dimensions to separate donor and acceptor [122]. The dependence of FRET efficiency on the spectrum overlap integral (J) was later verified by Haugland et al. as J was varied over 40-fold by changing the solvent and found to have a linear relationship to the energy transfer rate constant [123].

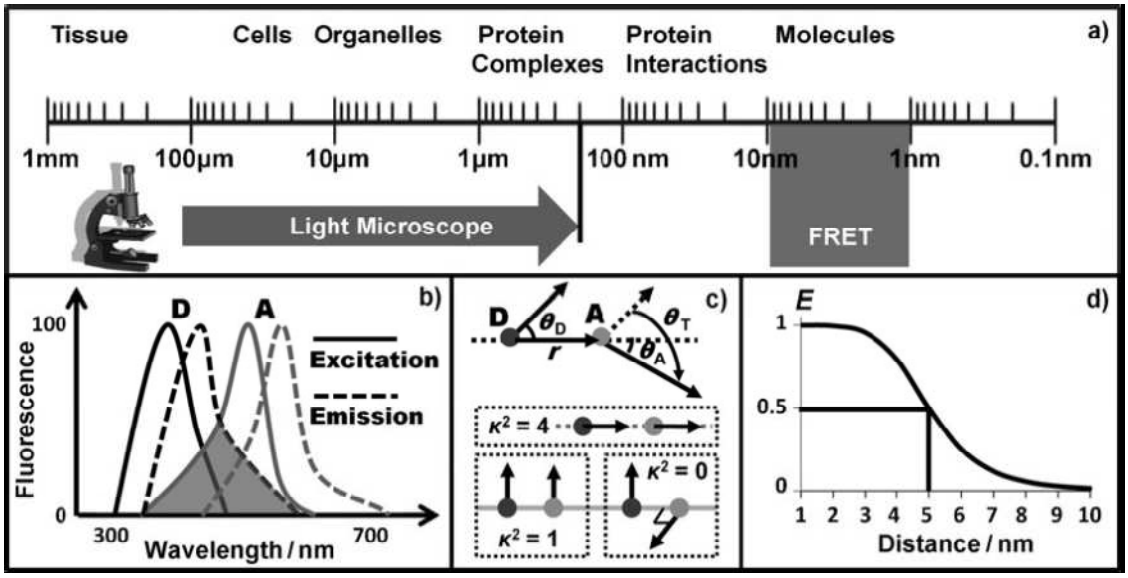

Figure 6. Basic concepts of FRET [118]. FRET is nonradiative energy transfer from an excited-state donor (D) to an acceptor (A) in the ground state, in close proximity (1–10 nm) through a long-range dipole–dipole coupling mechanism. (a) Thus, FRET can be used to detect the interaction between fluorescently labeled cellular components within 1–10 nm, far beyond the resolution limit of a light microscope. Other than the D–A distance, FRET also requires two other conditions: (b) significant overlap between the donor emission and the acceptor excitation spectra (covered by the gray area); (c) a favorable dipole moment κ^2, κ^2 cannot be 0 for FRET to occur, and a larger κ^2 increases the likelihood of FRET. (d) Since the energy transfer efficiency E from the donor to the acceptor is dependent on the inverse of the sixth power of the distance between them measuring E provides a sensitive indication of the change in D–A distance around the Förster distance, as seen by plotting the relationship between the distance and the E of a single D–A pair, given its Förster distance of 5 nm.

The inverse sixth power relationship between energy transfer rate and donor-acceptor distance makes FRET very sensitive to changes in molecular distance. When the distance of the donor and acceptor narrows from R_0 to $0.5R_0$, the efficiency of FRET increases from 50% to near maximum. On the other hand,

when the donor-acceptor distance increases by 100% of R_0, FRET efficiency decreases to an almost undetectable level of 1.5% (Fig. 6-d). This high sensitivity serves as the basis of two types of FRET-based applications: FRET can be used as a spectroscopic ruler to precisely measure molecular distance when the donor and acceptor distance is not far from their R_0; the "on" and "off" status of FRET can be monitored to determine the status of molecular interaction.

Suitable fluorophore FRET pairs are the key to the success of a FRET application. A larger R_0will increase the likelihood of a FRET event and can be achieved by using a donor with a higher quantum yield, an acceptor with a larger extinction coefficient, and a FRET pair with a larger spectral overlap. Many visible fluorescent proteins have been employed in combination with FRET microscopy/spectroscopy to visualize dynamic protein interactions under physiological conditions [124-127] . The development of novel organic dyes that exhibit improved photo- and pH-stability, as well as excellent spectral characteristics, provides additional choices for FRET imaging [128]. There are also applications in which only labeled antibodies will enable the researcher to establish interactions between cellular components with FRET microscopy, albeit almost exclusively in fixed specimens [129, 130]. Although the new semiconductor nanocrystal quantum dots are still in the early application phase of biomedical FRET imaging, they have been successfully used as donors for *in vitro* FRET biological assays [131-134]. By utilizing long-lifetime chelates of lanthanides such as europium as the donor probe, time-resolved FRET approaches have been used

for *in vitro* drug screening studies [135-137]. Since the europium probe has a much longer lifetime than organic compounds, imaging in a time-resolved manner can easily eliminate background fluorescence from most compounds and dramatically increase the sensitivity of FRET signals [138, 139].

The most commonly used FRET method is detection of the sensitized emission—the FRET signal—by exciting a specimen containing both D and A at the D excitation wavelength. However, in most situations this FRET signal cannot be directly used for analysis due to spectral bleedthrough (SBT) contained in the signal, a byproduct of the necessary spectral overlap between the FRET pair. There are usually two major contaminants: donor SBT resulting from the D emission detected in the FRET channel and acceptor SBT caused by direct excitation of A at the D excitation wavelength (see Fig. 6-b). Over the years, many sensitized emission FRET microscopy/spectroscopy methodologies have been developed to remove SBT, as well as to analyze and quantify the FRET signal.

Ratiometric FRET analysis was the initial method used in FRET analysis and is commonly employed for screening purposes. It is a simple way to demonstrate differences between a control specimen and some intervention or a “before-and-after” event. When the D is excited, the emission signals of D and A are obtained: that obtained in the D emission (D channel) is the quenched donor signal and the other, obtained in the A emission (FRET channel), is the uncorrected FRET signal, which contains both FRET and SBT signals. For biological systems such

as FRET-based biosensors, in which D and A are linked at a fixed stochiometry (usually 1:1 for FRET-based biosensors), the ratio of the two channel signals measured in ratiometric FRET analysis can quantitatively indicate the FRET significance [140-143]. However, it should be noted that the ratiometric FRET analysis cannot correct the fluorescent contamination signal as it does not distinguish the contributions of donor, acceptor and FRET signals. A series of approaches then have been developed to correct SBTs.

One FRET measurement employs “three-cube FRET” fluorescence microscopy/spectroscopy. To account for the fluorescence contamination, except the detection through an optical FRET filter set selecting acceptor emission during donor excitation (I_{DA} image), two additional images are acquired: acceptor fluorescence during acceptor excitation (I_{AA}) and donor fluorescence during donor excitation (I_{DD}). The crosstalk coefficients of acceptor and donor in the FRET filter set are given as a and d, respectively, which are constant and assume no other crosstalk components [144, 145]. In this way, the sensitized emission, F_c, can be calculated by linear unmixing of the I_{DA} intensity as:

$$F_c = I_{DA} - aI_{AA} - dI_{DD}$$

Based on the “three-cube FRET” theory, a variety of methods have been developed to characterize the FRET signal and applied in biological research. One of the methods requires prior knowledge of the dye concentration and absorption coefficients. It also assumes that the acceptor is not excited at the

donor excitation wavelength, and thus, there is no fluorescence contamination in the donor channel. This method was applied to directly observe a specific mRNA in a single living cell [146]. The same assumptions were applied to another developed method, except for the donor. The same approach was utilized to observe the dynamics of myosin motor by characterizing the FRET between GFP and BFP [147]. These methods are most appropriate for monitoring dynamic FRET as only one sample was required during detection, although both donor and acceptor fluorophores were present.

Other methods were developed to provide FRET signal with more complete SBT. The underlying assumption is that the amount of cross-talk is independent of the absolute intensity of the fluorophore and thus can be calibrated by ratiometric analysis of donor and acceptor signals. This permits the off-line calibration of SBT ratios in samples containing only one of the two fluorophores at arbitrary concentrations. These methods have been applied to study cell-surface staining (FRET pair: FITC-Tritc) [144], cytoskeletal components of cell adhesion (FRET pair: FITC-rhodamine) [148], Bcl-2-Berclin interaction on chromosome (FRET pair: FITC-rhodamine) [145], Ber-2-Bax interaction in mitochondria (FRET pair: BFP-GFP) [149], and functional expression analysis of protein subunits in rat neurons (FRET pair: CFP-FP) [150].

In contrast, a step-by step algorithm was developed to remove SBT contamination in FRET images collected by wide-field, confocal, and two-photon FRET microscopy, in which the SBT ratios were not considered constant but

were determined at different fluorescent intensities [151]. Different methods of characterizing FRET efficiency and FRET index were compared by a self-developed Monte Carlo simulation algorithm and a surface FRET system with controlled amounts of donor and acceptor fluorophores and controlled distances between them. It was concluded that optimized donor-to-acceptor ratios provides higher energy transfer efficiencies. Moreover, the FRET signals have been characterized by a complex matrix of fluorescent intensities of donor, acceptor and FRET, according to the concentration of free donor and acceptor and energy transfer "linking" the donor-acceptor pair with α, β, γ and ξ, where α characterizes contaminated FRET signal (direct excitation of acceptor by the donor excitation wavelength), β characterizes spectral bleed-through (spillover of donor emission into the acceptor emission channel), γ characterizes the ratio of extinction coefficient of acceptor/donor at donor's excitation wavelength, and ξ characterizes fluorescent intensity of the acceptor's sensitized emission signal to the fluorescence intensity that would have arisen from the quenched donor. This complex matrix has been used to study the cellular protein binding affinities (K_d) by three dimensional FRET microscopy images [152] and dynamic protein interaction to insulin secretory granule behavior with total internal reflection fluorescence (TIRF) microscopy [153].

An alternative approach for quantitative characterization of FRET signal is photobleaching, which is comparatively simple to perform on a conventional fluorescence microscope. Photobleaching can be used in multiple ways. The

donor bleach rate is directly related to the excited state lifetime and, thus, provides a way to detect change lifetime, which can be monitored by fluorescence lifetime imaging (FLIM). FLIM is independent of changes in probe concentration, excitation intensity and other factors that limit intensity based steady-state measurements [128]. Instrumental methods for measuring fluorescence lifetimes can be divided into frequency domain and time domain, either of which can be used in one- or two-photon FRET-FLIM microscopy. FLIM can independently determine FRET efficiency without being affected by concentrations and allows the measurement of dynamic events at very high temporal resolution (ns). Whereas one- or two-photon FRET produces “apparent” energy transfer efficiency, the donor lifetimes obtained by FRET-FLIM usually exhibit as a combination of quenched and unquenched, which allows a more precise estimate of distance than that based on FRET donors only.

A tandem construct with EGFP-mCherry FRET pair linked with a thrombin cleavage site was developed to be quantitatively analyzed by FRET-FLIM spectroscopy. A spectral bleed-through index (CT), which is the ratio between the required correction (cross-excitation plus cross-emission contributions) and the measured fluorescence signal, was applied to characterize the FRET properties. A lower CT index is preferable when choosing FP pairs in FRET [154]. A new concept of a minimal fraction of donor molecules involved in FRET (mf_D) was applied to monitor dynamic changes in protein-protein interactions between the bromodomains of TAF_{II250} and acetylated histones H4 at high spatial and

temporal resolution in living cells by fast acquisition time domain FLIM. This method quantitatively determines multi-lifetime donors in FRET-FLIM without fitting procedures [155]. The requirements of FRET-FLIM technique are that the acceptor is photostable and the donor is photolabile. A variant is measurement of the photobleaching of the acceptor in response to excitation via FRET [156-158], which requires the acceptor to be photolabile and the donor is photostable.

A more straightforward approach is to use direct acceptor photobleaching, which frustrates the occurrence of FRET and monitors the reappearance of the donor fluorescence. The basic principle is the measure donor intensity before and after complete acceptor bleaching, thus providing an internal control by eliminating the occurrence of FRET. The increase in donor intensity can be directly related to the FRET efficiency and should be corrected for bleed-through of the acceptor into the donor detection channel. As its working principle, this method requires that acceptor bleaching be complete, which is difficult due to the low excitation intensities. This limitation was solved by a gradual acceptor photobleaching method, which monitored the donor and acceptor continuously during acceptor photobleaching. It requires curve fitting to determine the FRET efficiency and was relatively simple to use on a normal wide-field microscope [158]. This method was adapted to study the complex formation of sterile 2 α-factor receptor protein (Ste2p) in vivo with a scanning laser confocal microscope. The developed method included correction for donor bleaching, both for the“complete” and gradual acceptor bleaching. The spectra determined by fitting the measured

spectrum were expressed by the normalized spectra of donor and acceptor with scaling factors, which represented the individual amounts of fluorescence emitted [159].

In addition to the above methods, various strategies correct FRET contamination in special cases (e.g., quantum dots used as FRET donor [160, 161], single-molecule FRET spectroscopy [162], and FRET between a flat surface and a spherical shell [163].

CHAPTER I: Development of FRET-based Protease Assay for SENP Endopeptidase Activity Study and Quantitative FRET Analysis in Enzyme Kinetics Parameters Determination

Abstract

Förster resonance energy transfer (FRET) technology has been widely used in biological research. SUMOylation is an important posttranslational protein modification with critical roles in multiple biological processes. Conjugating SUMO to substrates requires an enzymatic cascade. SUMO-specific proteases (SENPs) act as an endopeptidase to process the pre-SUMO or as an isopeptidase to deconjugate SUMO from its substrate.

A novel highly sensitive FRET-based protease assay was developed for SENP endopeptidase activity and specificity study. The developed theoretical and experimental procedures to determine the kinetic parameters is based on the quantitative analysis of the FRET signal in the total fluorescent signal, which consists of three components: donor (CyPet–SUMO1) direct emission, acceptor (YPet) direct emission, and FRET-induced acceptor's emission during the pre-SUMO processing. Standard curves were pre-established to relate protein concentration with fluorescent reading. The kinetics of pre-SUMO1's maturation by SENP1 was studied by the developed protease assay. Importantly, the general principles of this quantitative FRET-based protease kinetic determination can be applied to other proteases.

Introduction

Reversible posttranslational modifications of proteins with ubiquitin or ubiquitin-like proteins (Ubls) are one of general mechanisms to regulate protein activity and have diverse roles in many important biological events. SUMO (Small Ubiquitin-like Modifier) belongs to a family of ubiquitin-like proteins (Ubl) that, similar to ubiquitin, are conjugated to their substrates by a dedicated ligation system. Conjugation of SUMO in most cases results in altered subcellular localization of the modified protein, with consequent effects on its activity. The list of proteins subjected to SUMOylation is rapidly growing, and includes protein localized in most subcellular compartments that are involved in the regulation of cell cycle, transcription, cell survival and apoptosis, DNA damage response, heat shock, and stress response, as well as endoplasmic reticulum and plasma membrane-associated proteins, receptors, and viral proteins [2, 4, 83].

Modification of proteins by SUMO is a dynamic and reversible process. The SUMO cycle begins when pre-SUMOs are processed to remove short C-terminal extensions, thereby uncapping the C-terminal Gly-Gly motif that is essential for conjugation. SUMO ligases conjugate the protein, via its C-terminal carboxylate, to the side-chain lysine of target proteins to generate an isopeptide linkage. Eventually, SUMO is removed intact from its substrate SUMOylated proteins, and thus the SUMOylation/deSUMOylation cycle regulates SUMO function. The SUMO pathway differs from the ubiquitin pathway insomuch as mammals contain

at least four SUMO family members, SUMO1-4. Mammalian SUMO2 and SUMO3 share ~95% sequence identity with each other and are ~45% identical to SUMO1.

A group of proteases knows as SENPs are involved in both the maturation of SUMO precursors (endopeptidase cleavage) and deconjugation of the targets (isopeptidase cleavage) [18, 33, 34]. These two activities share a common catalytic mechanism, although the substrates differ insomuch as processing involves hydrolysis of an *α*-linked peptide bond and deconjugation catalyzes hydrolysis of the *ε*-linked lysine isopeptide bond [63]. Biochemical and bioinformatic approaches have identified several members of the SENP protease family in human, SENP1-3 and SENP5-7. The subcellular localization of the SENP protease family is diverse in nucleus, nuclear pore or cytoplasm. In most instances, nonconserved N-terminal domains (from 355 residues for SENP3 up to 663 for SENP7) direct subcellular localization. Subcellular localization of SENP family members contributes, in part, to SENP function by restricting protease activity to distinct areas of the cell.

Although subcellular localization has been recognized as a determinant in regulating the activities of SUMO proteases, the diversity of human SENP family members suggests the possibility that SUMO proteases might also participate in specific interactions with particular SUMO-conjugated substrates or SUMO precursors. It has been reported that different SENPs demonstrate various specificities toward pre-SUMO substrates. SENP1 and SENP2 can process all

the three pre-SUMOs. SENP3 and SENP5 prefer SUMO2/3 than SUMO1. SENP6 and SENP7 function in de-polySUMO editing [34, 164, 165].

The catalytic efficiency or specificity of an enzyme is best characterized by the ratio of the kinetic constants, k_{cat}/K_M. The accuracy of proteases kinetic parameters is not only important for understanding protease activity in normal physiological processes but also critical in drug discovery and development in estimating inhibitor potency and efficacy. Several methods are commonly used to determine k_{cat}/K_M, such as the enzymatic digestion in solution, followed by the polyacrylamide gel based western blot method, radioactive-labeled substrate, dialysis of digested substrate, fluorescent compound-labeled peptide substrate, and fluorescent protein-labeled substrate.

The kinetic parameters of SUMO–SENP pairs have been determined in several studies, albeit with substantive differences in observed k_{cat} and K_M values (Fig. 7; Table 3) [61, 63, 164, 166, 167]. While these differences may be attributable to indirect methodologies used to extract kinetics parameters from the experimental data, it is also possible that utilization of chemical or genetic modifications C-terminal to the SUMO scissile peptide bond might interfere with accurate assessment of protease activity. AMC (7-amino-4-methyl-coumarin) or ACC (7-amino-4-carbamoylmethyl-coumarin) tagged tetrapeptide QTGG or mature SUMO are commonly used substrates in proteolytic assays because the moiety was quenched in the intact substrate but became highly fluorescent upon cleavage by SENPs [168, 169]. However, the determined k_{cat}/K_M of SENP1 to

QTGG peptide was ~300 $M^{-1} \cdot s^{-1}$, which was up to two orders of magnitude lower than the natural substrates as the SUMO substrates differ outside of the catalytic cleft (di-Gly motif) have significant impact to the binding step (K_M). The SUMO-AMC/ACC system cannot clearly differentiate the isopeptidase and endopeptidase activities of SENPs as there is no specific sequence of either SUMO tail or SUMO-specific substrate after the AMC/ACC moiety.

Recently, FRET-based protease assays were used to study the deubiquitinating enzymes (DUBs) or SENPs. FRET pair Eu-cryptate and APC (allophycocyanin) were tagged to anti-Myc and anti-FLAG, which interacted with Myc and FLAG on the N- and C-terminus of pre-Nedd8 [170]. Terbium (Tb) and YFP (yellow fluorescent protein), another FRET pair, were tagged on SUMO and anti-RanGAP individually to study the SUMOylation and SENP's deconjugation [171]. The same FRET pair was used to tagged on N- and C- terminus of ubiquitin to study the DUBs' processing by time-resolved FRET (TR-FRET) technology [166]. However, these assays require additional steps for immune antibodies conjugation or chemical conjugation of thiol-reactive Tb chelate to ubiquitin-AC or other fluorofores. The conjugation efficiency and side effect may lead to inaccurate result for quantitative analysis. Fluorescent proteins can be genetically tagged to interested proteins. ECFP (enhanced cyan fluorescent protein) and YFP were used as FRET pair to study the SENP1's activities [61]. However, all of the above FRET-based protease assay used the ratio of acceptor's emission to donor's emission (under the excitation of donor) to characterize the FRET signals

without consideration about self-fluorescence from donor and acceptor, which lead to an inaccurate FRET signal analysis [145, 172]. In addition, the low FRET efficiencies of these fluorescent proteins and the complexity of fluorescence emissions of the donor and acceptor limit assay reliability and sensitivity.

In this chapter, I will describe the development of the highly sensitive FRET-based protease assay to study the endopeptidase activity and specificity of SENPs. An engineered FRET pair, CyPet and YPet, with significantly improved FRET efficiency and fluorescence quantum yield [173], were used to generate the CyPet-(pre-SUMO)-YPet substrate. Substrate specificities of SENP1/2/5/6/7 processing pre-SUMO1/2/3 were demonstrated by the developed protease assay. Quantitative FRET analysis considering about the self fluorescence of donor and acceptor was applied to develop the novel methodology of determination of kinetic parameters of pre-SUMO1 maturation by SENP1. The absolute fluorescent signals were converted into protein concentrations by pre-established standard curves. The methodology can be expended to study other protease as well.

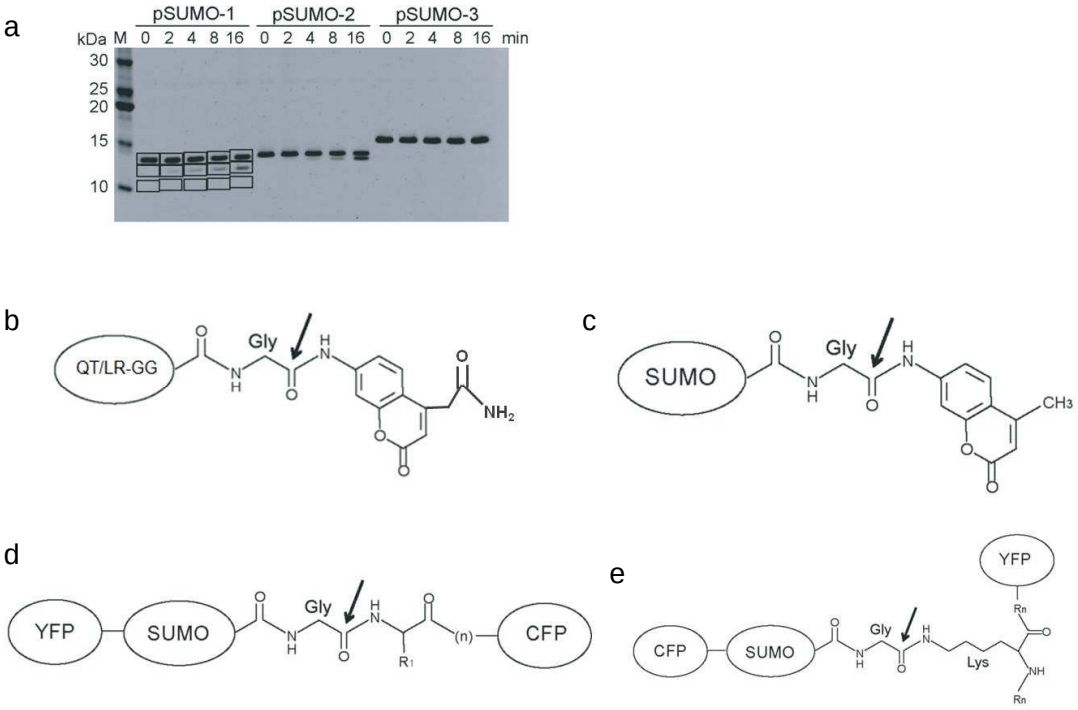

Figure 7. Examples of previous studies about SUMO-SENP pair. (a) Western-blot analysis of SENP2 processing pre-SUMO1/2/3 [63]; (b) tetrapeptide SUMO substrate in SENP activity profiling, QTGG is used to study SENP1/2/3/5, LRGG is used to study SENP6/7/8 or ubiquitin, the fluorophore ACC tagged after Gly-Gly will emit highly fluorescent signal after released by SENP [168]; (c) mature SUMO substrate in SENP specificity studying, similar as (b), organic fluorophore AMC tagged after Gly-Gly becomes high fluorescent after released by SENP [169]; (d) Fusions in a single polypeptide of the SUMO precursor with the YFP at the N-terminus and the CFP at the C-terminus, the detected disrupted FRET signal was used to characterize SENP1/2 endopeptidase activities [61, 167]; (e) Fusion of SUMO with the CFP at the N-terminus forming an isopeptide bond with a Lys of a SUMO substrate fused to YFP, similar as (d), the detected change of FRET signal was used to characterize SENP1 isopeptidase activities [61].

SENP1 Substrate	K_M (μM)	k_{cat} (s^{-1})	k_{cat}/K_M ($M^{-1} \cdot s^{-1}$)
CFP-pre-SUMO1-YFP [61]	0.098 ± 0.005	3.73 ± 0.05	(3.81 ± 0.98) x 10^7
CFP-SUMO1-RanGAP1-YFP [61]	0.15 ± 0.015	8.27 ± 0.26	(5.53 ± 1.96) x 10^7
QTGG-ACC [168]			325.7 ± 21.4
SUMO1-AMC [169]	0.0159	0.039	2.4 x 10^6
SUMO2-AMC [169]	0.0425	0.024	5.6 x 10^5
CFP-pre-SUMO3-YFP [61]	0.126 ± 0.012	0.075 ± 0.002	(5.95 ± 1.46) x 10^5
CFP-SUMO3-RanGAP1-YFP [61]	0.242 ± 0.024	18.2 ± 0.62	(7.52 ± 1.97) x 10^7

SENP2 Substrate	K_M (μM)	k_{cat} (s^{-1})	k_{cat}/K_M ($M^{-1} \cdot s^{-1}$)
pre-SUMO1 [63]	27.9 ± 3.7	0.72 ± 1.5	2.6 x 10^4
SUMO1-RanGAP1 [63]	33.1 ± 3.2	50.4 ± 2.2	1.5 x 10^6
QTGG-ACC [168]			196.1 ± 34.4
SUMO1-AMC [169]	0.0328	0.0059	1.8 x 10^5
SUMO2-AMC [169]	0.0197	0.0019	9.9 x 10^4
pre-SUMO2 [63]	2.0 ± 0.6	0.77 ± 0.07	3.8 x 10^5
pre-SUMO3 [63]	2.2 ± 0.3	0.11 ± 0.01	5.0 x 10^4
SUMO2/3-RanGAP1 [63]	5.47 ± 0.7	31.0 ± 1.5	5.7 x 10^6

SENP5 Substrate	K_M (μM)	k_{cat} (s^{-1})	k_{cat}/K_M ($M^{-1} \cdot s^{-1}$)
SUMO1-AMC [169]	0.176	0.011	6.1×10^4
SUMO2-AMC [169]	0.0523	0.084	1.6×10^6

SENP6 Substrate	K_M (μM)	k_{cat} (s^{-1})	k_{cat}/K_M ($M^{-1} \cdot s^{-1}$)
QTGG-ACC [168]			0.24 ± 0.01
LRGG-ACC [168]			35.67 ± 7.57
SUMO2-AMC [169]	0.0802	0.00021	2.1×10^3
SUMO2-AMC [169]	0.0974	0.0095	9.8×10^4

SENP7 Substrate	K_M (μM)	k_{cat} (s^{-1})	k_{cat}/K_M ($M^{-1} \cdot s^{-1}$)
QTGG-ACC [168]	0.098 ± 0.005	3.73 ± 0.05	0.12 ± 0.01
LRGG-ACC [168]	0.15 ± 0.015	8.27 ± 0.26	13.57 ± 0.51
SUMO2-AMC [169]			2.6×10^3

Table 3 Previous kinetics analysis of SUMO-SENP pair.

Material and Methods

Molecular clone of DNA constructs

The open reading frames of CyPet, YPet and pre-SUMO1/2/3 were amplified by PCR and the PCR products were cloned into PCRII-TOPO vector (Invitrogen). The fragments encoding pre-SUMO1/2/3 were extracted by SalI/XhoI digestion and inserted into PCRII-CyPet plasmid which was linearized by SalI/XhoI. Then, the CyPet-(pre-SUMO1/2/3) were extracted by NheI/XhoI digestion and inserted into PCRII-YPet plasmids which were linearized by NheI/SalI. After the sequences were confirmed, the cDNA encoding CyPet-(pre-SUMO1/2/3)-YPet were cloned into the NheI/NotI sites of pET28(b) vector with an engineered 6x His on N-terminus (Novagen). The construct encoding ECFP-(pre-SUMO1)-YFP (as control) was obtained by same strategy (Fig. 8-a).

The open reading frame of mature SUMO1 was amplified by PCR and the PCR products were cloned into PCRII-TOPO vector (Invitrogen). The fragments encoding mature SUMO1was extracted by Sal/NotI digestion and inserted into PCRII-CyPet plasmids which was linearized by SalI/NotI. After sequences were confirmed, the cDNA encoding CyPet-SUMO1 was cloned into the NheI/NotI sites of pET28(b) vector with an engineered 6x His on N-terminus (Novagen) (Fig. 8-b)

The open reading frames of YPet and catalytic domain of SENP1/2/3/5/6/7[164] (SENP1/2/3/5/6/7C, Fig. 8-d) were amplified by PCR and the PCR products were

cloned into PCRII-TOPO vector (Invitrogen). After the sequences were confirmed, the cDNA encoding YPet and SENP1/2/3/5/6/7C were cloned into the SalI/NotI sites of pET28(b) vector with an engineered 6x His on N-terminus (Novagen) (Fig. 8-c).

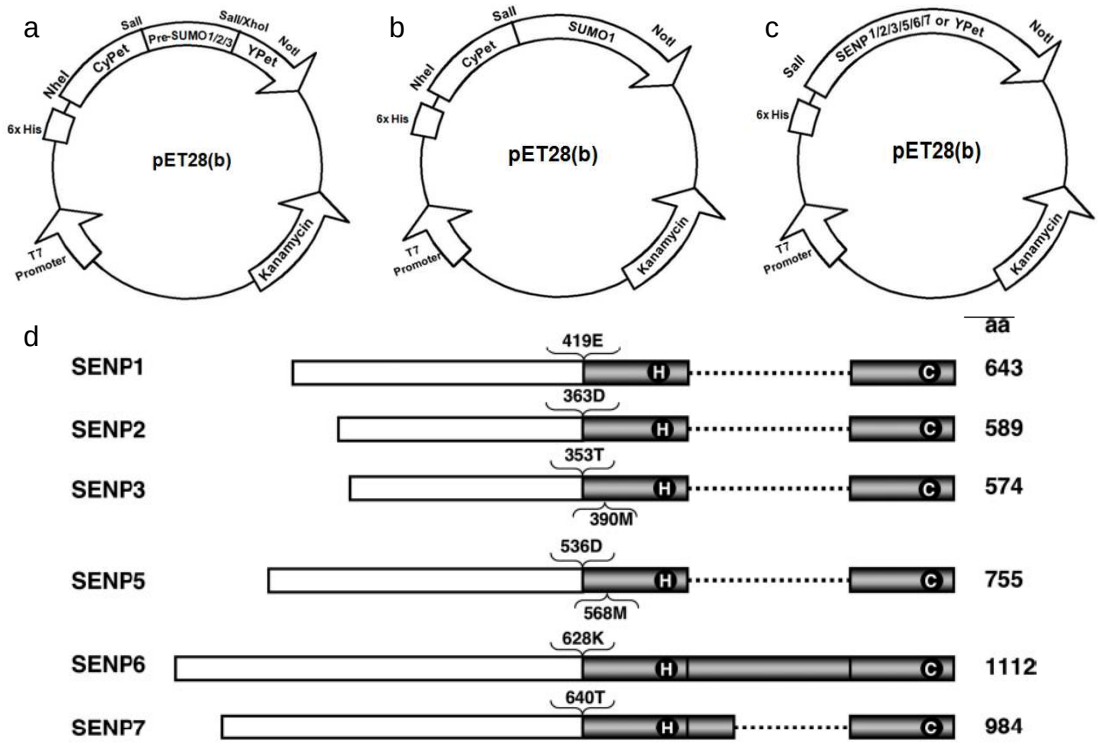

Figure 8 Map of the bacterial expressional plasmids encoding CyPet-(pre-SUMO1/2/3)-YPet (a), CyPet-SUMO1 (b) and Ypet or SENP1/2/3/5/6/7 C (c) and the schematic representation of SENPs (d). The open reading frames were fused with a poly-histidine tag so that the recombinant proteins can be purified with Ni-NTA affinity chromatography. The expression of proteins is driven by T7 promoter and induced by addition of IPTG to the culture medium. The conserved catalytic domain is represented in gray with catalytic residues in circles. The catalytic domain limits used in the study are defined in braces. The dotted line illustrates insertions within the catalytic domain in SENP6/7.

Recombinant protein expression and purification

BL21 (*DE3*) *Escherchia coli* (*E. coli*) cells were transformed with pET28 (b) vectors encoding CyPet-(pre-SUMO1/2/3)-YPet, ECFP-(pre-SUMO1)-YFP, CyPet-SUMO1, YPet, and SENP1/2/3/5/6/7C. The transformed bacteria were plated on LB agar (10 g Bacto-tryptone, 5 g Bacto-yeast extract, 10 g NaCl, 15 g agar in 1L distilled H_2O, pH adjusted to 7.5, sterilize by autoclaving) plates containing 50 µg/ml kanamycine, and single colony was picked up and inoculated in 2xYT medium (16 g Bacto-tryptone, 10 g Bacto-yeast extract, 5 g NaCl in 1L distilled H_2O, pH adjusted to 7.0, sterilize by autoclaving) to an optical density at 600nm of 0.4-0.5 by induction with 100 µM IPTG (isopropyl β-D-thiogalactoside) for 16hr at 25℃. Bacterial cells were spinned down at 6000 rpm 10 min, and resuspended in binding buffer (20 mM Tris-HCl, 0.5 M NaCl, 5 mM imidazole, pH 7.4) and sonicated with an ultrasonic liquid processor (Misonix). Cell lysate containing recombinant proteins was cleared by centrifugation at 35000 g 30 min. The recombinant proteins were then bound to Ni^{2+}-NTA agarose beads (Qiagen) followed by washing buffer I (20 mM Tris-HCl, 0.3 M NaCl, pH 7.4), washing buffer II (20 mM Tris-HCl, 1.5 M NaCl, 0.5% Triton-100, pH 7.4), washing buffer III (20 mM Tris-HCl, 0.5M NaCl, 10 mM imidazole, pH 7.4), eluted by elution buffer (20 mM Tris-HCl, 0.2 M NaCl, 150 mM imidazole, pH 7.4) and dialyzed overnight in dialysis buffer (20 mM Tris-HCl, 50 mM NaCl, 1 mM DTT (Dithiothreitol), pH 7.4). The purity of the proteins was confirmed by SDS-PAGE and Coomassie blue staining. Concentrations of protein were determined by

Coomassie Plus Protein Assay (Thermo) with known quantities of bovine serum albumin (BSA) as standards. Aliquots of final products were stored in -80℃.

Protease assay and Western blot confirmation

FRET-based pre-SUMO processing assays were conducted by measuring the emission intensity of CyPet at 475 nm and YPet at 530 nm with an excitation wavelength of 414nm in a fluorescence multiwall plate reader FlexStation II^{384} (Molecular Devices, Sunnyvale, CA).

To compare the sensitivity of FRET pair CyPet-YPet and ECFP-YFP, recombinant protein CyPet-(pre-SUMO1)-YPet or ECFP-(pre-SUMO1)-YPet was incubated with SENP1C (1:1 molar ratio) at 37℃ in low-salt reaction buffer (20 mM Tris-HCl, 50 mM NaCl, 1 mM DTT, 0.1% Tween-20, pH 7.4) and transferred into a 384-well plate (glass bottom, Greiner). The final concentration of proteins in reaction was 300 nM. Reactions were stopped at 1 hr and were analyzed by fluorimeter.

To test the substrate specificities, recombinant protein CyPet-(pre-SUMO1/2/3)-YPet was incubated with SENP1/2/5/6/7C (1:1 molar ratio) at 37℃ in low salt reaction buffer and transferred into a 384-well plate. The final concentration of reacted proteins was 100 nM. Reactions were stopped at 1 hr and were analyzed by fluorimeter and western blot. Three samples were repeated in each concentration. The results were reported as mean ± SD.

The western blot was performed by standard procedure: protein were separated by SDS-PAGE for 2 hr (running buffer: 25 mM Tris-base, 192 mM glycine, 0.1% SDS) and then transferred to nitrocellulose membrane at 100 V in Tris-Glycine buffer (25 mM Tris-base, 192 mM glycine, 20% methanol) for 2 hr. The membrane was blocked by 5% milk in TBST (Tris-buffered saline (25 mM Tris-base, 150 mM NaCl, 2 mM KCl, pH 7.4) with 0.05% Tween-20) for 2 hr at room temperature, followed by incubating in 1st antibody at ratio of 1:1500 5% milk in TBST (anti-SUMO1, Sigma; anti-SUMO2/3, Cell Signaling) at 4℃ over night. After washed with TBST for three times, the membrane was incubated in 2nd antibody at ratio of 1:3000 2% milk in TBST (anti rabbit, Sigma) for 1 hr at room temperature. The membrane was developed by SuperSignal West Dura Chemiluminescent Substrate (Thermo) and imaged by BioSpectrum 500 Imaging System (UVP, LLC, upland, CA).

Protease kinetics assay

For the validation of the protease kinetics assay, 8 μM CyPet-(pre-SUMO2)-YPet and 0.6 nM SENP2C were mixed in the low salt reaction buffer in a total volume of 80 μl and transferred into a 384-well plate. Reactions were tested every 2-5 minutes until all the pre-SUMO2 have been processed.

For the kinetics study of pre-SUMO1's maturation by SENP1C, CyPet-(pre-SUMO1)-YPet was incubated with SENP1C at 37℃ in low salt reaction buffer to a total volume of 80μl and transferred into a 384-well plate. The final

concentration of SENP1C was fixed at 0.8 nM, and the final concentration of CyPet-(pre-SUMO1)-YPet was varied as 115.3, 241.2, 406.9, 594.2, 725.3 nM and as 1.471, 1.899, 2.300 μM. Reactions were tested within original 5 min with 10 sec intervals. One phase association model was used to fit the exponential increased reaction velocity. Data were analyzed by the developed method and plotted in GraphPad Prism V software fitting the Michaelis–Menten equation. Five samples were repeated in each concentration. The results were reported as mean ± SD.

Self-fluorescence cross-talk ratio determination

To determine the cross-talk ratio of CyPet and YPet's self-fluorescence, purified CyPet-SUMO1and YPet were incubated individually in 37℃ in low salt Tris buffer to a total volume of 80 μl in the concentration of 10 nM, 20 nM, 50 nM, 100 nM, 200 nM and 500 nM for 10 minutes and added to each well of a 384-well plate.

Fluorescent missions of CyPet at 475 nm and 530 nm individually were detected in a fluorescence multi-well plate reader (Molecular Devices, Flexstation II^{384}) under the excitation at 414 nm to determine the cross-talk ratio α; fluorescent emissions of YPet at 530 nm were detected under the excitation at 414nm and 475nm individually to determine the cross-talk ratio β. Three samples were repeated for each concentration.

Standard curve establishment

CyPet-(pre-SUMO1)-YPet was incubated at 37°C in low salt reaction buffer to a total volume of 80 µl and added to each well of a 384-well plate. The emission signals at 475 nm were collected after excitation at 414 nm. The concentration was varied from 0.02 to 0.6 µM.

CyPet-SUMO1 and YPet were incubated at 37°C in low salt reaction buffer to a total volume of 80 µl with 1:1 molar ratio and added to each well of a 384-well plate. The emission signals at 475 nm were collected after excitation at 414 nm. The concentration of CyPet-SUMO1 was varied from 0.02 to 0.2 µM.

Results

Designing a highly sensitive FRET-based assay for SENP's endopeptidase activity study

The general strategy for the FRET-based protease assay was based on fluorescent protein-tagged substrate (Fig. 9-a&b). The SENP substrate, pre-SUMOs, was flanked by a FRET pair, CyPet and YPet. This pair has more than 20-fold of improved energy transfer efficiency achieved by engineering CFP and YFP, respectively, to yield a high dynamic range and sensitivity for the FRET assay [173]. The fused recombinant protein is cleaved by the protease SENPs to release two products: the CyPet-SUMO and the SUMO tail with YPet, which led to the disruption of FRET resulting in an increase of CyPet's emission and a dramatic decrease of YPet's emission under the excitation of CyPet. The decreased fluorescent emission of YPet after the cleavage can be used to characterize the kinetic properties of SENPs in real time.

The fusion substrates, CyPet-(pre-SUMO1/2/3)-YPet, and SENP1/2/3/5/6/7C were cloned into the bacterial protein expression vector pet28(b). The recombinant proteins were expressed and purified by Ni-NTA agrose (Fig. 9-c). The SENP3C was insoluble, and stayed in the inclusion body during the protein purification even treated with 6M Guanine-HCl. In that way, only SENP1/2/5/6/7C were obtained and characterized in the developed protease assay.

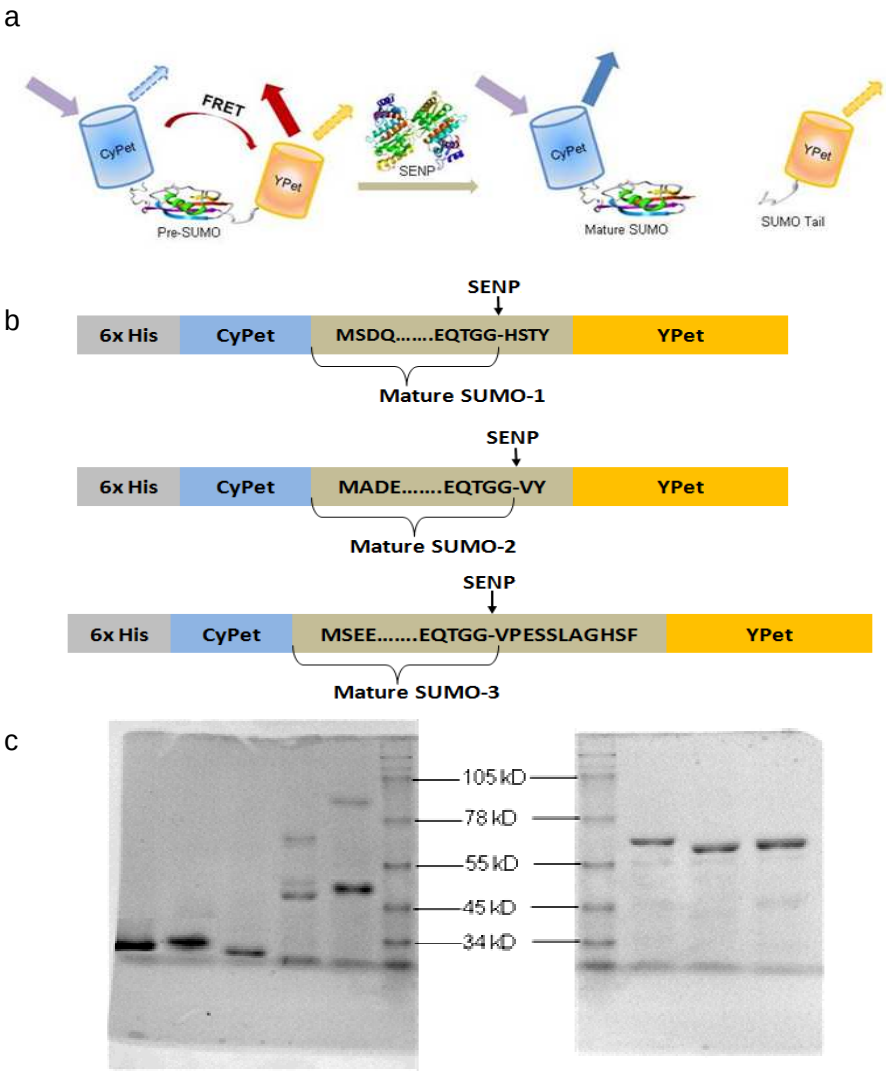

Figure 9 Design of FRET-based protease assay. (a) Schematic depicting the CyPet-(pre-SUMOs)-YPet substrate indicating the principle of FRET from CyPet (donor, excitation peak: 414nm, emission peak: 475nm) to YPet (acceptor, excitation peak: 475nm, emission peak: 530nm). Once cleaved by SENPs, the distance between the fluorescent proteins is increased beyond a FRET-sensitive distance and thus CyPet emission measured at 475 nm is increased while the YPet FRET induced emission is reduced; (b) Schematic of the 6xHis-CyPet-(pre-SUMO1/2/3)-YPet constructs, the arrow indicates the cleavage site by SENP; (c) Coomassie staining of purified SENP1/2/5/6/7C (31kD, 31kD, 29kD, 47kD, 49kD, left to right, left sub-figure) and CyPet-(pre-SUMO1/2/3)-YPet (~68 kD, left to right, right sub-figure)

To test the sensitivity and dynamics of this FRET assay, CyPet–(pre-SUMO1)–YPet or ECFP-(pre-SUMO1)-YFP was incubated with SENP1C (1:1 molar ratio, 0.3 μM each, 37°C, 1 hr). A significant signal change was observed from the CyPet–(pre-SUMO1)–YPet substrate after processing, while the signal change of ECFP-(pre-SUMO1)-YFP substrate after maturation is much less (Fig.10-a).

The excitation and emission peak wavelengths of CyPet and YPet are 414 nm/475 nm and 475 nm/530 nm, respectively. After incubation with SENP1C, the emission ratio (FL_{530}/FL_{475} under excitation of 414 nm) of the CyPet–YPet pair exhibited more than six folds of signal changes (4.23–0.63). In contrast, the control fusion protein, ECFP–(pre-SUMO1)–YFP, showed only more than two folds of signal changes (1.10–0.49) (Fig. 10-b). Since the two constructs used in this study, ECFP–(pre-SUMO1)–YFP and CyPet– (pre-SUMO1)–YPet, have the same length and similar structures, the result suggests that the CyPet–YPet pair has higher energy transfer efficiency and provides substantially more sensitivity than the ECFP–YFP pair.

a

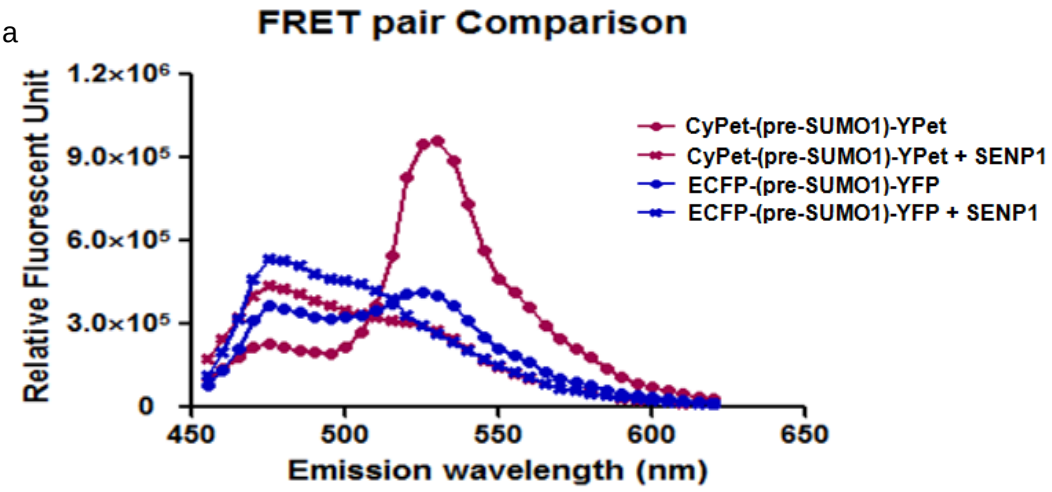

b

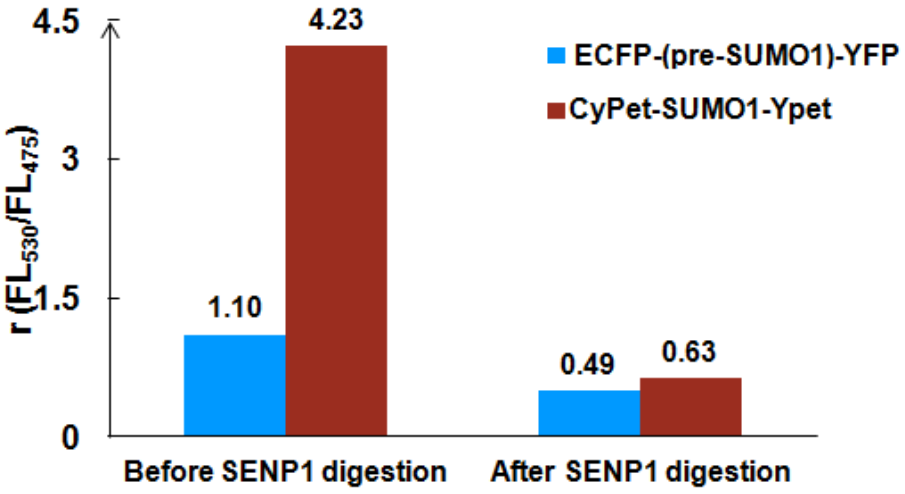

Figure 10. Comparison of FRET pair in the developed protease assay. (a) Emission spectrum of CyPet–(pre-SUMO1)–YPet or ECFP-(pre-SUMO1)-YFP (300 nM) with incubation of SENP1C (300 nM) for 1 hr under excitation at 414 nm; (b) ratiometric measurement ($r = FL_{530}/FL_{475}$) of CyPet–YPet pair and ECFP-YFP pair under excitation at 414 nm before and after SENP1C processing.

SENPs belong to the family of cysteine proteases. The SENP protease family contains six members in the human genome with different specificities for SUMO substrates [34, 57]. Previous studies suggested that SENP1 catalytic residue mutant (C603A) increases the level of SUMO1's conjugation [44]. SENP6 and SENP7 have no endopeptidase activity on pre-SUMOs [65, 164]. To test the substrate specificities of SENPs toward pre-SUMOs by the developed FRET-based protease assay, CyPet-(pre-SUMO1/2/3)-YPet was incubated with SENP1/2/5/6/7C (1:1 molar ratio, 300 nM each) at 37°C for 1hr. The fluorescent emission ratio (FL_{530}/FL_{475}) under the excitation of 414 nm was used to characterize the FRET signal. The obtained results were highly consistent with the ones in previously published papers: SENP1/2 can process pre-SUMO1/2/3 and SENP6/7 showed almost no processing activity toward pre-SUMOs (Fig. 10-a, b, c). The reactions were performed and confirmed in biochemistry assay (western-blot) in parallel (Fig. 10-d, e, f), indicating that the developed protease assay can not only be applied to study the substrate specificities of different SENP-SUMO family members, but also be explored to study other substrate-protease pairs.

a

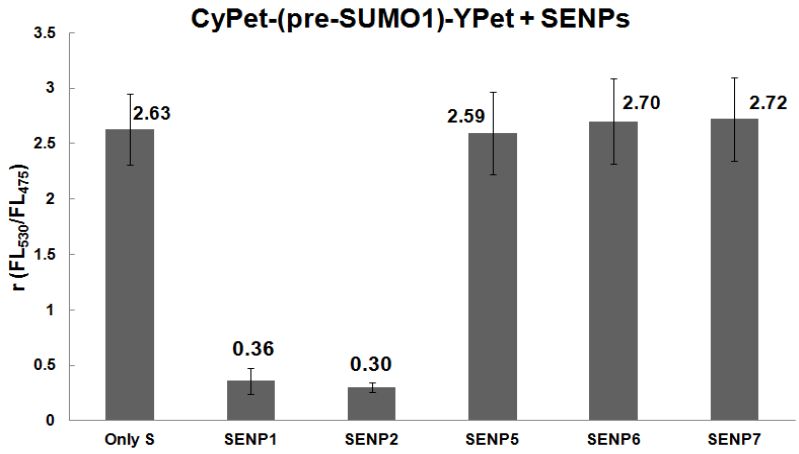
CyPet-(pre-SUMO1)-YPet + SENPs
r (FL530/FL475)
3.5
3
2.5
2
1.5
1
0.5
0
2.63
0.36
0.30
2.59
2.70
2.72
Only S
SENP1
SENP2
SENP5
SENP6
SENP7

b

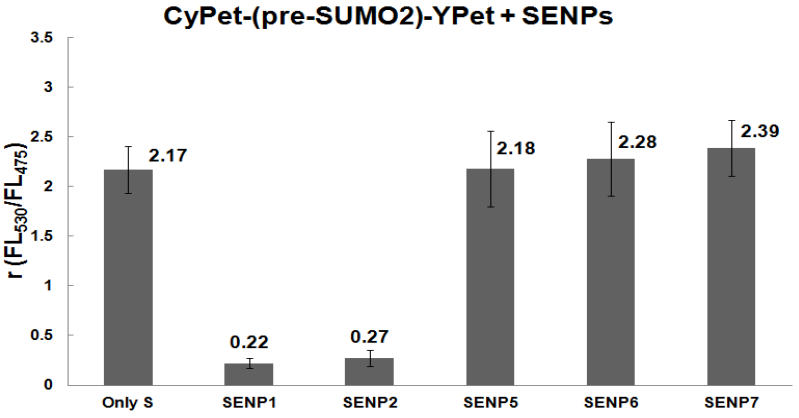
CyPet-(pre-SUMO2)-YPet + SENPs
r (FL530/FL475)
3.5
3
2.5
2
1.5
1
0.5
0
2.17
0.22
0.27
2.18
2.28
2.39
Only S
SENP1
SENP2
SENP5
SENP6
SENP7

c

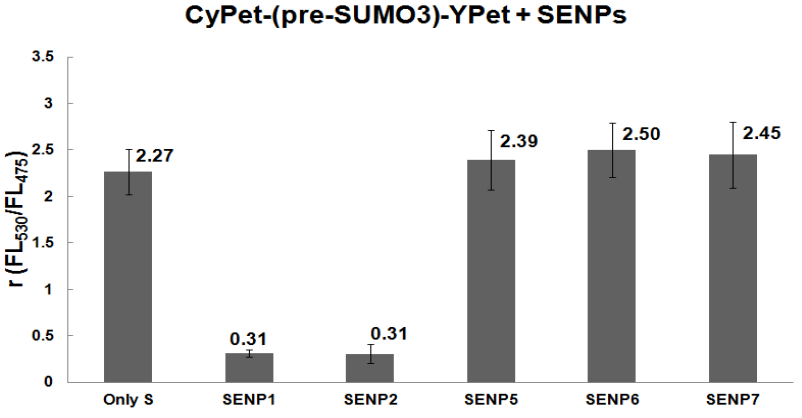
CyPet-(pre-SUMO3)-YPet + SENPs
r (FL530/FL475)
3.5
3
2.5
2
1.5
1
0.5
0
2.27
0.31
0.31
2.39
2.50
2.45
Only S
SENP1
SENP2
SENP5
SENP6
SENP7

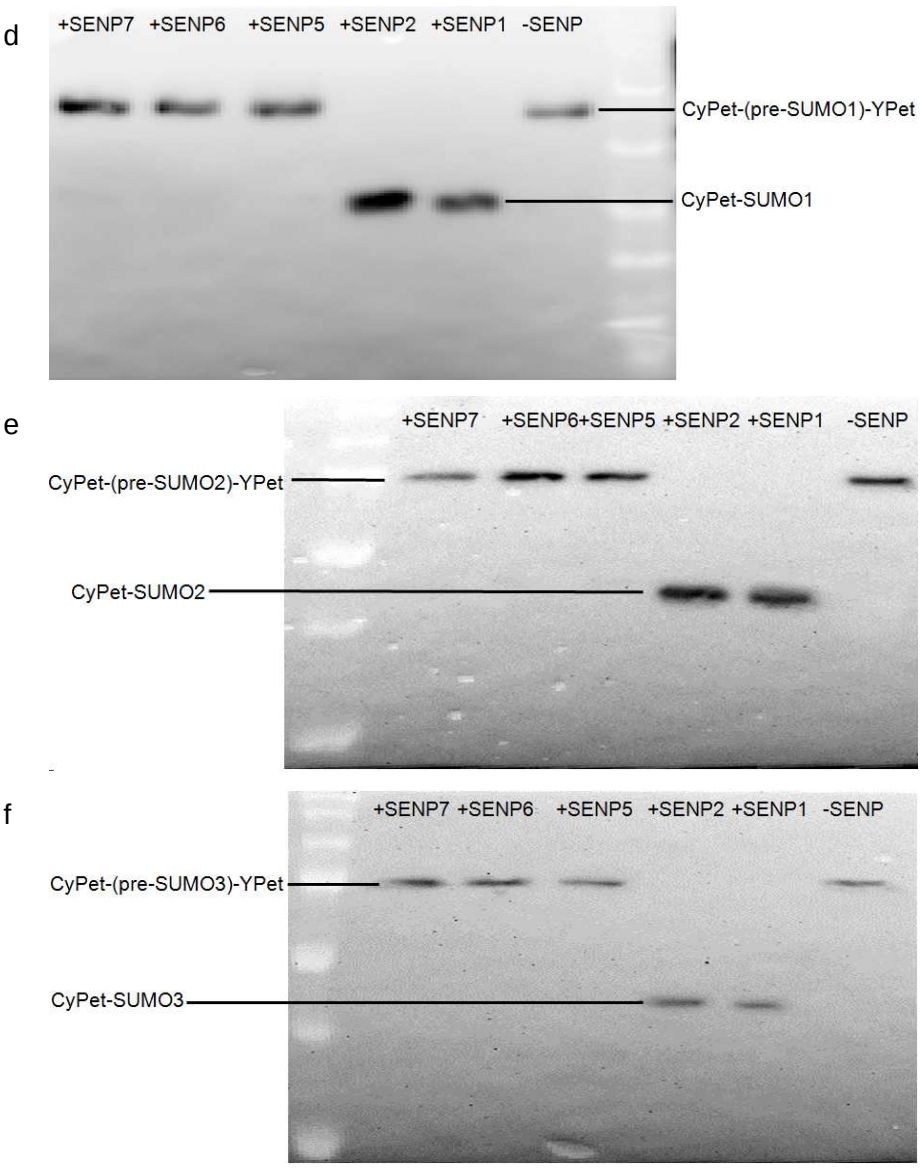

Figure 11 Characterization of CyPet-(pre-SUMO1/2/3)-YPet processing by SENP1/2/5/6/7C by developed FRET-based protease assay (a, b, c) and confirmed in biochemistry western-blot analysis (d, e, f). Reactions were incubated in low salt reaction buffer at 37°C for 1hr. Final concentration of CyPet-(pre-SUMO1/2/3)-YPet or SENP1/2/5/6/7C was 300 nM.

To explore the possibility that whether the developed FRET-based protease assay is able to monitor the maturation process in real-time and determine reliable kinetic parameters of SENPs, CyPet-(pre-SUMO2)-YPet and SENP2C (8 µM and 0.6 nM respectively) were incubated at 37°C in low salt reaction buffer. The emission spectrum under excitation of 414 nm was monitored every 2-5 minutes until the substrate has been totally processed (Fig. 12). The result showed that CyPet's emission increased and YPet's emission decreased when the pre-SUMO2 was gradually matured by SENP2C. The SENP2C exhibited excellent activities even at this 13,333:1 ratio of substrate to enzyme.

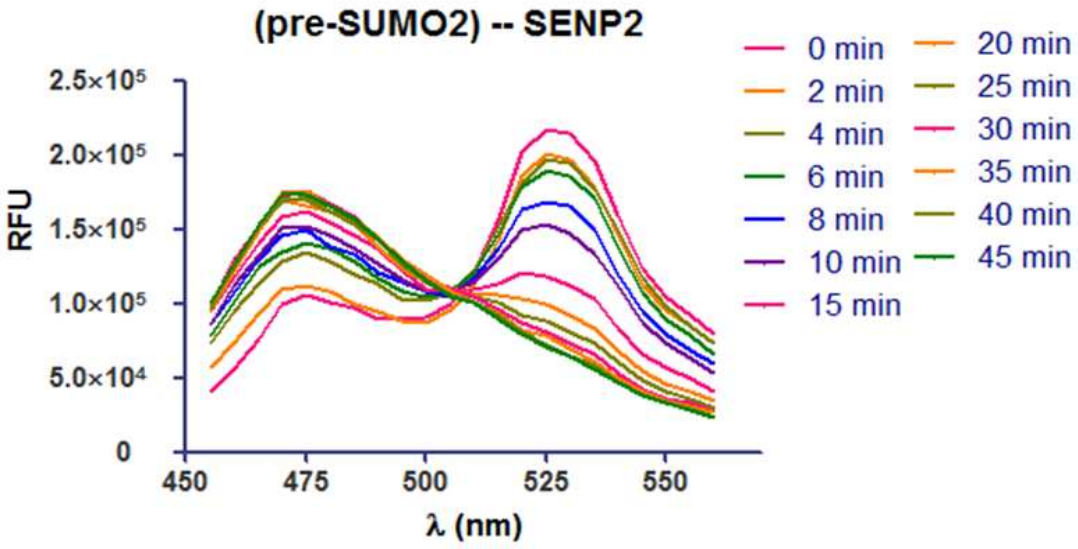

Figure 12 Emission spectrum of CyPet-(pre-SUMO2)-YPet (8 µM) digested by SENP2C (0.6 nM) under excitation of 414nm. The process was monitored every 2-5 minutes until the substrate had been totally matured.

Fluorescence emission spectrum analysis and standard curves for donor and acceptor direct emissions and FRET signals

Pre-SUMO1 and SENP1C are used as an example in this chapter to describe the developed methodology in enzyme kinetics analysis. To determine the kinetics parameters of SENP1 by developed FRET assay, two issues must be addressed: how to determine the absolute FRET signal that is corresponding to digested substrate concentration and how to convert the absolute FRET signal into related protein concentration. For the first issue, the fluorescence signal of FRET has to be distinguished from the direct fluorescence signals of donor and acceptor at the emission wavelength of acceptor (Fig. 13-a). The absolute FRET signal will determine the amount of undigested substrate, excluding interference of donor and acceptor direct emissions from both digested and undigested substrates. For the second issue, standard curves are needed to convert FRET signal to concentrations of corresponding proteins.

Before digested by SENP1C, the total fluorescent emission of CyPet-(pre-SUMO1)-YPet at 530nm under the excitation at 414nm can be divided into three parts: FRET-induced acceptor's emission (I_{da}), donor's direct emission ($I_{d530/414}$) and acceptor's direct emission ($I_{a530/414}$) as shown in Fig. 13-a:

$$FL_{530/414} = I_{da} + I_{d530/414} + I_{a530/414} \quad \text{[Eq. 1]}$$

The cross-talk ratio of CyPet's self-fluorescence (α) is the ratio of CyPet-SUMO1/2/3's emission at 530 nm ($I_{d530/414}$) to 475 nm ($I_{d475/414}$) under excitation at 414 nm (Fig. 13-b).

$$\alpha = \frac{I_{d530/414}}{I_{d475/414}} \quad \text{[Eq. 2]}$$

The determined value of α is 0.332 for CyPet-SUMO1.

The cross-talk ratio of YPet's self-fluorescence (β) is the ratio of Ypet's emission at 530 nm under excitation at 414nm ($I_{a530/414}$) to emission at 530 nm under excitation at 475 nm ($I_{a530/475}$) (Fig. 13-c).

$$\beta = \frac{I_{a530/414}}{I_{a530/475}} \quad \text{[Eq. 3]}$$

The determined value of β is 0.026.

According to the determined α and β:

$$FL_{530/414} = I_{da} + \alpha I_{d475/414} + \beta I_{a530/475} \quad \text{[Eq. 4]}$$

where $I_{d475/414}$ is CyPet's emission at 475 nm under excitation at 414 nm, $I_{a530/475}$is YPet's emission at 530 nm under excitation at 475 nm.

After the distion by SENP1C, the fluorescent signal at 530 nm was decreased and fluorescent signal at 475 nm was increased due to the disruption of FRET. The remaining fluorescent emission at 530nm ($FL'_{530/414}$) can still be divided into the same three parts:

$$FL'_{530/414} = I'_{da} + \alpha I'_{d475/414} + \beta I'_{a530/475} \quad \text{[Eq. 5]}$$

where I'_{da} is the remaining FRET-induced acceptor's emission, $I'_{d475/414}$ is the fluorescent emission of CyPet at 475 nm, which can be divided into two parts: from the undigested CyPet-(pre-SUMO1)-YPet and the digested CyPet-SUMO1, $I'_{a530/475}$ is the fluorescent emission of YPet, which is constant whether substrate has been digested or not, therefore, the fraction $\beta I_{a530/475}$ remained the same.

After treatment with SENP1C, the remaining FRET-induced acceptor's emission (I'_{da}) is:

$$\frac{C-x}{C} \times I_{da} = \frac{C-x}{C} \times (FL_{530/414} - \alpha I_{d475/414} - \beta I_{a530/475}) \quad \text{[Eq. 6]}$$

where C is the total concentration of CyPet-(pre-SUMO1)-YPet (μM) (before SENP1C added into the reaction system) in 80 μl; x is the concentration of digested CyPet-(pre-SUMO1)-YPet (μM) in 80μl at different detected time point.

Standard curves were created by plotting the fluorescent emissions against related protein concentrations. For undigested CyPet-(pre-SUMO1)-YPet, the fluorescence emissions of various concentrations at 475 nm under excitation at 414 nm were determined and plotted with protein concentrations (Fig. 14-a). For the digested CyPet–SUMO1, different concentrations of CyPet–SUMO1 were mixed with YPet with a molar ratio of 1:1 and the emissions at 475 nm with excitation at 414 nm were determined, then were plotted against the protein concentration (Fig. 14-b). Slopes value as k = 230800 and j = 326700, respectively, described the linear relationship between the detected fluorescent signals and the protein concentrations.

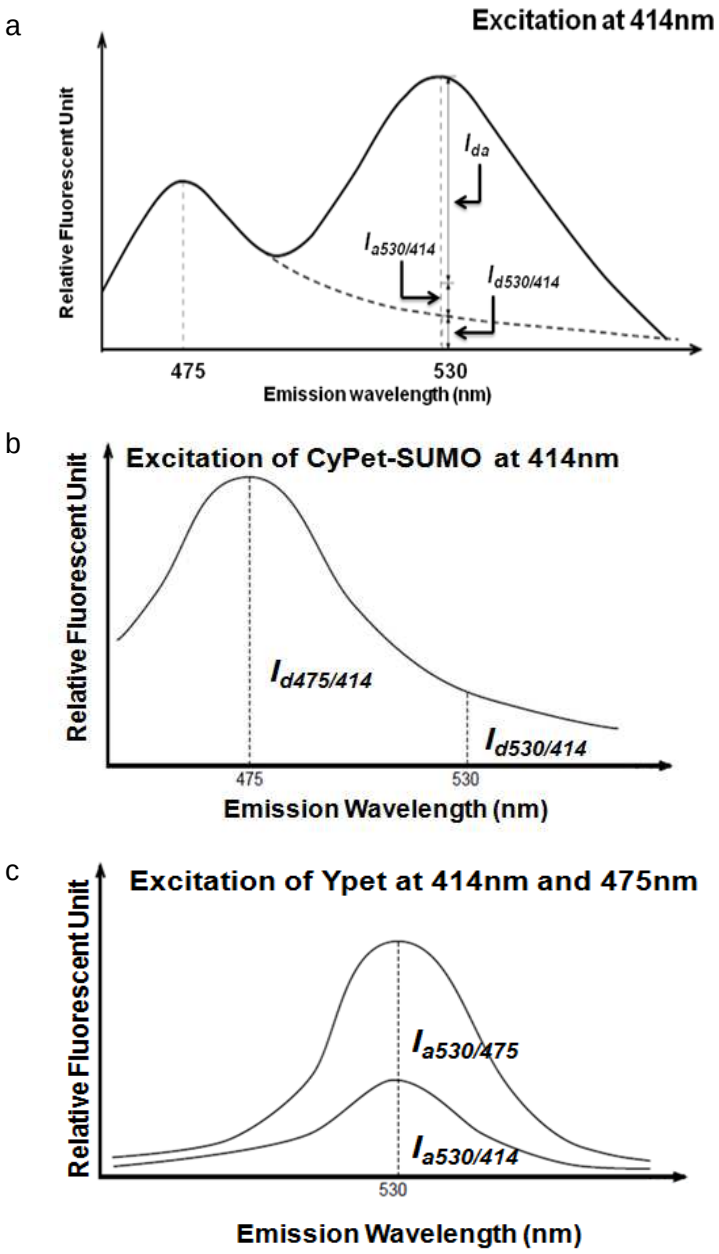

Figure 13 Quantitative analysis of fluorescent signals. (a) Fluorescent emission at 530 nm at the excitation wavelength of 414 nm ($FL_{530/414}$) can be divided into three components: FRET-induced YPet's emission (I_{da}), direct emission of unquenched CyPet ($I_{d530/414}$), and direct emission of YPet ($I_{a530/414}$); (b) determination of α factor using CyPet-SUMO1; (c) determination of β factor using YPet.

a

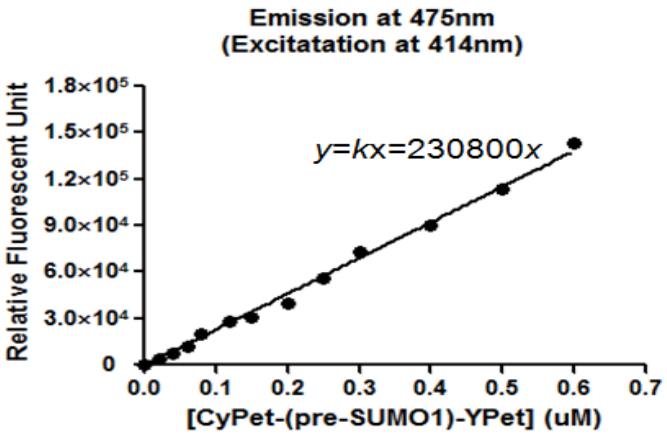

b

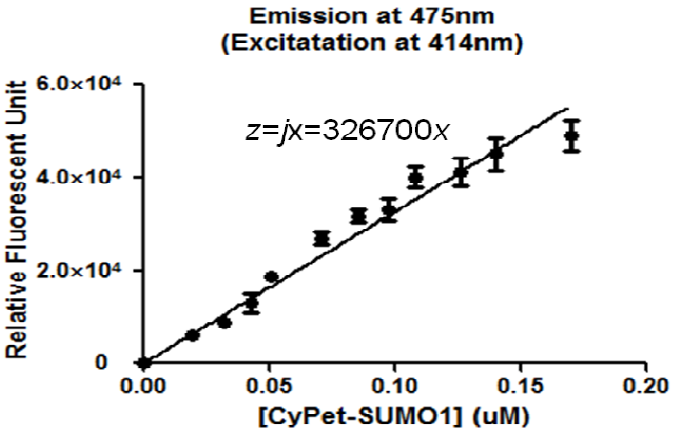

Figure 14 Standard curves of fluorescent signal versus related protein concentration. (a) Emission of CyPet–(pre-SUMO1)–YPet at 475 nm under excitation at 414 nm; (b) emission of CyPet–SUMO1 + YPet (1:1 molar ratio) under excitation at 414 nm (the x axis is the protein concentration of CyPet–SUMO1).

According to the standard curves:

$$I_{d475/414-csy} = y = k(C - x) \quad \text{[Eq. 7]}$$

$$I_{d475/414-cs} = z = jx \quad \text{[Eq. 8]}$$

where $I_{d475/414-csy}$ (y in standard curve) is emission of CyPet-(pre-SUMO1)-YPet at 475nm under excitation of 414nm, k is slope of the standard curve for I_{d-csy} to concentration of CyPet-(pre-SUMO1)-YPet (μM), $I_{d475/414-cs}$ (z in standard curve) is emission of CyPet-SUMO1 at 475 nm under excitation of 414nm, and j is slope of the standard curve for I_{d-cs} to concentration of CyPet-SUMO1 (μM).

Combine the above analyzed items, the detected fluorescent signal at 530nm under excitation of 414nm when substrate CyPet–(pre- SUMO1)–YPet treated with protease SENP1C was:

$$FL'_{530/414} = \frac{C-x}{C} \times \left(FL_{530/414} - \alpha I_{d475/414} - \beta I_{a530/475}\right) + \alpha[k(C-x) + jx] + \beta I_{a530/475} \quad \text{[Eq. 9]}$$

During the experiments, the direct emissions CyPet and YPet as well as the total fluorescent emissions at 530 nm were firstly determined: the emission of CyPet–(pre-SUMO1)–YPet was measured at 475 nm when excited at 414 nm to determine the CyPet direct emission ($\alpha I_{d475/414}$); the emission was measured at 530 nm when excited at 475 nm to determine the YPet direct emission

($\beta I_{a530/475}$); and the emission was measured at 530 nm when excited at 414 nm to determine the total emission ($FL_{530/414}$).

After the treatment of SENP1C, the total emission ($FL'_{530/414}$) was obtained at 530 nm when excited at 414 nm and related to digested concentrations of CyPet– (pre-SUMO1)–YPet (x) from the parameters determined above (Eq.9)

Ratiometric FRET analysis

To compare with the most used traditional ratiometric analysis of FRET signal, the ratios $FL_{530/475}$ during the maturation process were also calculated.

The ratio of fluorescent emission at 530 nm to 475 nm under the excitation at 414 nm was obtained from CyPet-(pre-SUMO1)-YPet ($r_{(CyPet-preSUMO1-YPet)}$) and CyPet-SUMO1 with YPet (1:1 molar ratio) ($r_{(CyPet-SUMO1+YPet)}$). In that way, the ratio is directly proportional to SUMO substrate concentration as:

$$\frac{C-x}{C} = \frac{FL'_{530/414}/FL'_{475/414}}{r_{(CyPet-preSUMO1-YPet)} - r_{(CyPet-SUMO1+YPet)}} \qquad \text{[Eq. 10]}$$

where $FL'_{530/414}$ and $FL'_{475/414}$ are detected fluorescent emission at 530 nm and 475 nm under excitation of 414 nm at different time points. C is the total concentration of CyPet-(pre-SUMO1)-YPet (µM) in 80 ul; x is the amount of digested CyPet-(pre-SUMO1)-YPet (µM) in 80 µl.

Determination of the initial velocity

The pre-SUMOs' maturation by SENP1C can be determined by monitoring the changes of fluorescent signal at 530 nm during the process. Changes of absolute FRET signal and other fluorescence components can be analyzed with the calculations from standard curves (Fig. 14). Different concentrations of the substrate, ranging from 0.115 to 2.300 μM, were incubated with 0.8 nM of SENP1C. The remaining fluorescence intensity ($FL'_{530/414}$) were monitored and the digested substrate (x) was calculated according to Eq. 9. The digested substrate concentration showed very good dose-dependent digestion with the amount of substrate (Fig. 15). This dose-dependent cleavage of substrate suggests that SENP1C presented excellent activities even at 1:5000 ratio of enzyme/substrate.

According to the theory of chemical reactions' rates, at the start of the reaction, the finite amount of S is $[S]_0$. At any time later, the amount of substrate remaining ($[S]_t$) will be less than $[S]_0$. The amount of substrate will decline with time until there is no substrate left, at which point the reaction will stop. The reaction rate (v) is expected to be proportional to the amount of substrate present:

$$v = -\frac{d[S]}{dt} = k[S] \qquad \text{[Eq. 11]}$$

where k is a constant of proportionality referred to at the rate constant.

To integrate this differential equation, it is obtained:

$$-\int d[S] = \int k[S]dt \qquad \text{[Eq. 12]}$$

As the digested substrate (or product) concentration increases exponentially from 0 when t=0, to $[S]_0$ at infinite time:

$$[S]_t = [S]_0(1 - e^{-kt}) \qquad \text{[Eq. 13]}$$

The initial reaction velocity is the initial linear portion of the enzyme reaction when less than 10% of the substrate has been depleted or less than 10% of the product has formed. Under these conditions, it is assumed that the substrate concentration does not significantly change and the reverse reaction does not contribute to the rate. Accordingly, the original velocity (v_0) is:

$$v_0 = \frac{d[S]_t}{dt}\Big|_{t=0} = k[S]_0 \qquad \text{[Eq. 14]}$$

The original velocities were calculated by Eq. 14 under different substrate concentrations (Table 4). For comparison, the original velocities were also calculated by Eq. 14 under the same substrate concentrations but the FRET signal was analyzed by traditional ratiometric analysis (Eq. 10).

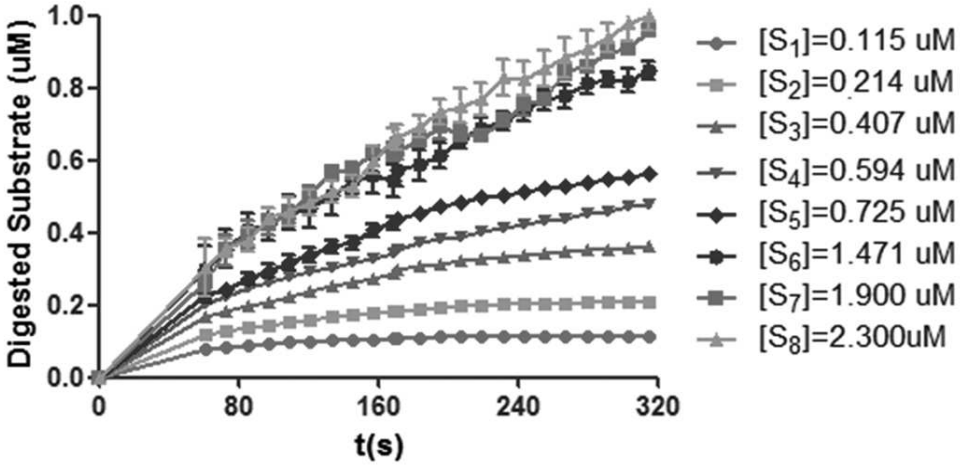

Figure 15 Quantitative analysis of CyPet–(pre-SUMO1)–YPet digested by different ratio of SENP1C. Reactions were monitored within original 5 min.

[CyPet-(pre-SUMO1)-YPet] (μM)	v_0 (x10^{-3} μM/s)	
	Quantitative FRET Analysis	Ratiometric FRET Analysis
0.115	1.96 ± 0.03	2.66 ± 0.04
0.214	2.54 ± 0.03	3.36 ± 0.04
0.407	3.20 ± 0.06	3.84 ± 0.07
0.594	3.58 ± 0.09	3.93 ± 0.07
0.725	4.12 ± 0.11	4.82 ± 0.10
1.471	5.15 ± 0.38	4.58 ± 0.17
1.900	5.18 ± 0.31	4.09 ± 0.24
2.300	5.00 ± 0.41	3.70 ± 0.56

Table 4. Initial velocities determined by quantitative and ratiometric FRET analysis.

.

Michaelis–Menten analysis and kinetic parameters determination

Michaelis–Menten kinetics is one of the simplest and best-known models of enzyme kinetics. The model takes the form of an equation describing the rate of enzymatic reactions, by relating reaction rate v to $[S]$, the concentration of a substrate as:

$$v = \frac{V_{max}[S]}{K_M + [S]} \qquad \text{[Eq. 15]}$$

K_M is the substrate concentration that results in half-maximal velocity for the enzymatic reaction, or it represents the substrate concentration at which half of the enzyme active sites in the sample are filled by substrate molecules in the steady state.

The K_M and V_{max} values can be obtained from the Michaelis–Menten equation by plotting the various velocities of SENP1C digestion versus the corresponding different concentrations of substrate. The value of k_{cat} can be directly calculated by dividing the experimentally determined value of V_{max} by $[E]$ as:

$$k_{cat} = \frac{V_{max}}{[E]} \qquad \text{[Eq. 16]}$$

The value of k_{cat} is sometimes referred to as the *turnover number* for the enzyme, since it defines the number of catalytic turnover events that occur per unit. As k_{cat} relates to the chemical steps subsequent to formation of the ES complex, changes in k_{cat}, brought about by changes in the enzyme, in solution conditions, or in substrate identify, define perturbations that affect the chemical

steps in enzymatic catalysis. In other words, changes in k_{cat} reflect perturbations of the chemical steps subsequent to initial substrate binding.

The catalytic specificity and efficiency of an enzyme for a specific substrate is best defined by the ratio of the kinetic parameters, k_{cat}/K_M. This ratio is generally used to compare the efficiencies of different enzymes with one substrate or the use of different substrates by a particular enzyme.

The Michaelis–Menten graph was plotted for the data in Table 4 (Fig. 16). k_{cat}, K_M, and the k_{cat}/K_M ratio were obtained by both the quantitative and ratiometric FRET analysis. To compare these two FRET analysis methods completely, the kinetics of ECFP-(pre-SUMO1)-YFP treatment with SENP1C was also studied in quantitative and ratiometric FRET analysis (Table 5).

The k_{cat}/K_M from the quantitative FRET analysis (CyPet-YPet pair) was (2.49 ± 0.37) x 10^7 $M^{-1}\cdot s^{-1}$, which was close to that in one of the previous SENP1 endopeptidase function studies [61], however, the individual k_{cat} and K_M were quite different. Similarly, ECFP-YFP can also provide consistent results. It has to be noted that the errors of ratiomatric FRET analysis were relatively larger than the ones of quantitative FRET analysis.

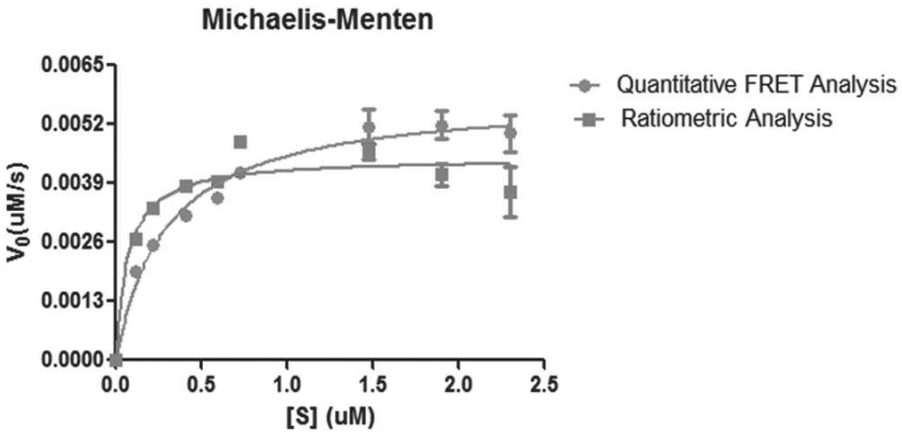

Figure 16 Michaelis–Menten graphical analysis of CyPet–(pre-SUMO1)–YPet's processing by SENP1C. Data were plotted and analyzed by GraphPad Prism 5 of nonlinear regression.

FRET pair	FRET analysis method	K_M(μM)	k_{cat} (s^{-1})	k_{cat}/K_M ($\mu M^{-1} \bullet s^{-1}$)
CyPet-YPet	Quantitative	0.29 ± 0.042	7.27 ± 0.29	24.9 ± 3.7
	Ratiometric	0.067 ± 0.026	5.57 ± 0.30	83.1 ± 32.7
ECFP-YFP	Quantitative	0.15 ± 0.018	6.3 ± 0.25	41.0 ± 2.8
	Ratiometric	0.089 ± 0.020	5.43 ± 0.29	50.9 ± 7.0
	Ratiometric [61]	0.098 ± 0.005	3.73 ± 0.05	38.06 ± 9.8

Table 5. Kinetic parameters of CyPet-(pre-SUMO1)-YPet's and ECFP-(pre-SUMO1)-YFP's maturation by SENP1C determined by quantitative and ratiometric FRET analysis.

Discussion

A highly sensitive quantitative FRET-based protease assay for characterizing SENP's endopeptidase activities was developed and described in this chapter. FRET pair, CyPet and YPet, was genetically tagged to pre-SUMOs' N- and C-terminus. The emission of quenched CyPet will be increased and FRET-induced YPet's emission will be decreased when pre-SUMOs cleaved by their specific protease SENPs at di-Gly active sites, which results in the disruption of FRET. The FRET pair, CyPet and YPet, demonstrated higher FRET efficiency compared to ECFP-YFP pair in the study.

Except for SENP3, all SENP paralogs (SENP1/2/5/6/7) were studied in the developed FRET-based protease assay for pre-SUMO1/2/3's maturation. Different SENP paralogs showed different specificities towards various pre-SUMO substrates. SENP1 and SENP2 can mature all the three pre-SUMOs, while SENP5, SENP6 and SENP7 almost have no endopeptidase activities, which were confirmed by biochemistry western-blot assay. The results indicate a potential application in studying the digestion of other substrate–protease.

The ratio of kinetic parameter, k_{cat}/K_M is the best characterization of the catalytic efficiency or the enzyme specificities of different substrates for a particular enzyme. A novel methodology for k_{cat}/K_M measurements in solution with the developed FRET-based protease assay in the steady state was demonstrated by using the example of (pre-SUMO1)-SENP1 pair. In contrast to

the previous ratiometric FRET analysis, I fundamentally improved the approach in both a new theory of FRET signal characterization for enzymatic kinetics analysis and an experimental procedure to derive kinetic parameters by quantifying the contributions of absolute fluorescence signals from direct emission of donor and acceptor, and real FRET-induced acceptor's emission. This quantitative FRET analysis can differentiate the quantitative contributions of each component, whereas traditional ratiometric measurement of FRET cannot.

The k_{cat}/K_M value from the developed quantitative FRET analysis study, (2.49 ± 0.37) x 10^7 $M^{-1}{\cdot}s^{-1}$, was more convergent and close to that from the previous ratiometric analysis (3.806 ± 0.98) x 10^7 $M^{-1}{\cdot}s^{-1}$ using the ECFP/YFP pair, but the individual measurements of K_M and k_{cat} were three to seven times larger than their apparent K_M and k_{cat} [61]. However, analyzing the same fluorescent readings by ratiometric FRET analysis produced a slightly higher k_{cat}/K_M, (8.31 ± 3.27) x 10^7 $M^{-1}{\cdot}s^{-1}$, with much higher variations. The small numeric differences between these two approaches reflected a fundamental difference of the FRET signal analysis. The discrepancy between these two approaches might due to the inclusion of direct emission of donor and acceptor in the ratiometric analysis method. Based on quantitative FRET analysis method, the donor's direct emission at the acceptor's emission peak wavelength (530 nm) is proportional to the donor's emission at its own emission peak wavelength (475 nm). Because the fluorescent emission of the donor is quantitatively related to the protein concentrations, and this relationship is different from the undigested

CyPet–(pre-SUMO1)–YPet and digested CyPet–SUMO1, the donor's direct emission at 530 nm needs to be divided into two parts: the digested substrate and the remaining substrate, both of which are changed during the pre-SUMO's digestion process. The decreased fluorescent signal at 530 nm is correlated to the disrupted energy transfer from the donor to the acceptor and is also affected by the changes of the donor's direct emission as the two donor populations change during the digestion process. Traditional ratiometric measurements of FRET do not consider the direct emissions and simply convert all of the signal change to disrupted energy transfer, which may result in an overestimation of kinetic parameters from the Michaelis–Menten equation due to an overestimation of FRET emission signal (containing donor and acceptor direct emission) and an overestimation of FRET donor emission (increasing with digested substrate). The overestimations of FRET signal might not greatly affect the final k_{cat}/K_M ratio, but the effect is more obvious when studying the individual parameters, K_M and k_{cat}, which are important in determining the rate-limiting step and inhibitor potency of enzymes.

Compare to ECFP and YFP, CyPet-YPet pair can provide more energy to transfer, and thus increases the sensitivity of the protease assay. The results in Table 5 showed that the differences of kinetics constant k_{cat}/K_M values determined by quantitative FRET analysis and ratiometric FRET analysis were larger in the CyPet-YPet protease assay than those in the ECFP-YFP protease

assay. I believe the differences can prove the sensitivity of the improved FRET pair.

Fluorophores and fluorescent proteins have been widely used in various biological studies recently. The method developed in this study is environmentally friendly and requires only molecular cloning and protein expression without radioactive labeling or expensive instruments. The fluorescent-tagged proteins are in the aqueous phase, which is mostly close to their natural environment in cells. Fluorescence intensity can be determined by general fluorescence spectroscopy or fluorescence plate readers, which are widely available. Compared with the traditional ‘‘gel-based’’ method, the developed FRET-based protease assay offers several advantages, including increased sensitivity, real-time measurement, and less time and labor needed. In addition, the highly sensitive FRET-based assay can be used in high-throughput biological assays such as protease inhibitor screenings. The kinetic study can also be used to characterize the properties of the inhibitors (e.g., K_i, IC_{50}).

Therefore, the highly sensitive quantitative FRET-based protease assays could be a powerful approach in developing genome-wide protease–substrate profiling and inhibitor screenings.

CHAPTER II: Development of Quantitative FRET Analysis in Internal Calibration to study SENP kinetics

Abstract

Defining the kinetics of key regulatory reactions is necessary for understanding their actions. SUMOylation is an important post-translational modification of critical proteins in multiple processes. SENPs act as can either process pre-SUMO or deconjugate SUMO from its substrate.

Förster resonance energy transfer (FRET) technology has been widely used in biomedical research and is a powerful tool for elucidating protein interactions. A novel quantitative FRET-based protease assay was developed to study SENP activity with consideration of the direct emissions of donor (CyPet) and acceptor (YPet). The fluorescent emission of both donor and acceptor were detected in real-time of the pre-SUMO maturation or SUMO deconjugation process. The improved quantitative FRET analysis in internal calibration was applied to characterize the protease kinetics of the pre-SUMO1/2/3's maturation by SENP1/2C and deconjugation of SUMO1 from RanGAP1 by SENP1C with comparison to previous results and analysis in structure complex. Compare to the previously developed standard curve-dependent quantitative FRET analysis, internal calibration method can provide more accurate and consistent results for kinetic constants determination.

Introduction

Proteases are one of the most important enzyme classes in various signaling pathways, including proliferation and apoptosis, cellular signal transductions, protein maturation and trafficking, and are involved in many human diseases, ranging from cardiovascular disorders, autoimmune diseases, metabolic diseases to cancers [174, 175]. The accuracy of proteases kinetic parameters is not only important for understanding protease activity in normal physiological processes but also critical in drug discovery and development in estimating inhibitor potency and efficacy.

SUMO (small ubiquitin-like modifier) covalently modifies and regulates the activities of proteins with important roles in diverse cellular processes, including regulation of cell cycle, cell survival and apoptosis, DNA damage response, and stress responses [2, 4, 5, 19, 27]. Mammalian cells usually express four SUMO paralogues (SUMO1–4). Mammalian SUMO2 and SUMO3 share ~95% sequence identity with each other and are ~45% identical to SUMO1. Different SUMOs are used preferentially for different substrates [14-16]. SUMO2 and SUMO3 can form polySUMO chains but SUMO1 does not have [17]. The role of SUMO4 remains enigmatic but has been found to relate to type I diabetes [12].

Like ubiquitylation, SUMO conjugation occurs through a cascade of reactions by an activating enzyme (E1), a conjugating enzyme (E2) and, usually, a SUMO ligase (E3). SENPs (Sentrin-specific proteases) perform two critical functions via

an encoded cysteinyl protease activity. The first involves proteolysis of SUMO C-terminal amino acid residues to release a mature form of the SUMO terminated with a di-Gly motif, the only known form of SUMO that can be activated and conjugated to other proteins. The second protease activity catalyzes SUMO deconjugation from the target protein, releasing the target lysine and SUMO [34]. SENPs participate in diverse biological pathways, including transcriptional regulation, development, cell growth and differentiation, cancer, and ribosome biogenesis [57]. Different SENPs demonstrate various specificities toward SUMO substrates. The isopeptidase and endopeptidase activities of one SENP to the same SUMO substrate are not the same.

Analysis of SUMOylation and deSUMOylation generally involves detection of the modified species by SDS-PAGE, immunoblotting or autoradiography. These techniques are not only time- and material-consuming, but are also not easily applicable for kinetic, quantitative or high-throughput assays.

Förster resonance energy transfer (FRET) is widely used in biological and biomedical research, including cell biology, medical diagnostics, optical imaging and drug discovery [176-179]. FRET occurs when the donor fluorophore and acceptor fluorophore are close to each other (1–10 nm) with favorable orientations. Excitation of the donor elicits energy transfer that induces emission from the acceptor and results in quenching of donor and excitation of acceptor. Fluorescent proteins are being increasingly used in FRET systems due to the ease of genetic labeling. Energy transfer based protease assays have been used

to study the de-ubiquitinating enzymes (DUBs) or SENPs [61, 166, 167, 170, 171, 180] (Fig. 17) in the recent years.

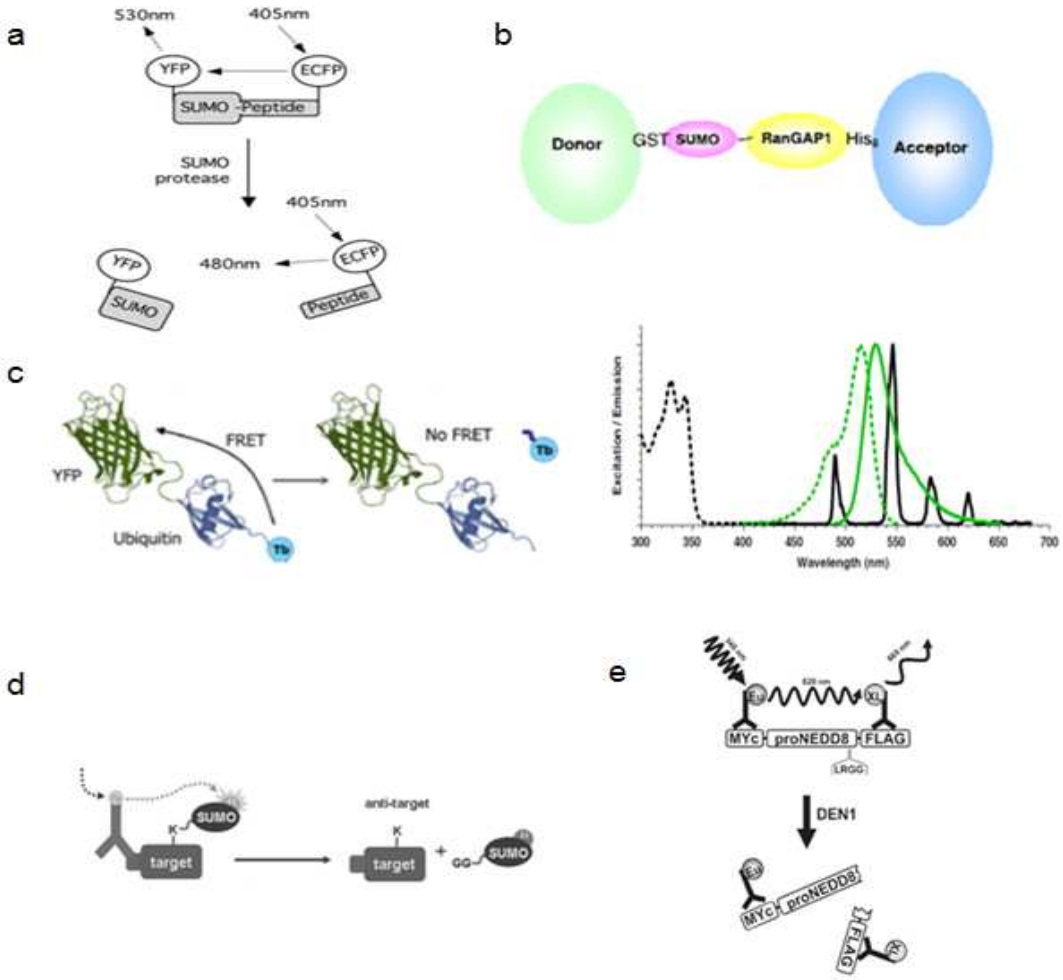

Figure 17 Examples of energy transfer-based assay to study SENP or DUBs. (a) YFP-SUMO (full length)-ECFP substrate for SENP study; (b) ALPHA to study SENP cleavage of SUMOylated RanGAP1; (c) substrate for DUB activity based on TR-FRET between terbium and YFP (left) and excitation (- - -) and emission spectra (—) of donor (terbium, black) and acceptor (YFP, green) (right); (d) LanthaScreen assay for SENP study, fluorescein -SUMO with terbium labeled antibody which is specific to SUMO target proteins; (e) TR–FRET-based DEN1 peptidase assay monitoring the maturation of pre-NEDD8.

ALPHA (Amplified Luminescent Proximity Homogeneous Assay), first described in 1994, is a bead-based technology based on the principle of luminescent oxygen channeling with inherent high sensitivity [181, 182]. The donor beads contain a photosensitizer that converts ambient oxygen to an excited form of singlet oxygen upon illumination at 680 nm. Singlet oxygen diffuses up to 200 nm in solution before it decays. Thus, if a biomolecular interaction brings the donor beads into close proximity with the acceptor beads, singlet oxygen will activate thioxene derivatives in the acceptor beads, leading to the emission of light between 520 and 620 nm [182-184]. In the absence of acceptor beads, the singlet oxygen falls to the ground state with no light emission. Donor beads can release up to 60,000 singlet oxygen molecules per second, resulting in signal amplification. Because signal detection is performed in a time-resolved manner and at a lower wavelength than is excitation, background interference is very low [180]. The larger diffusion distance of the singlet oxygen enables the detection of binding distance up to 200nm.

The premise of a TR-FRET (Time-resolved fluorescence resonance energy transfer) assay, first described in 1988 [185], is the same as that of a standard FRET assay. In contrast to standard FRET assays, TR-FRET assays use a long-lifetime lanthanide chelate as the donor species. Lanthanide chelates are unique in that their excited state lifetime (the average time that the molecule spends in the excited state after accepting a photon) can be on the order of a millisecond or longer. This is in sharp contrast to the lifetime of common fluorophores used in

standard FRET assays, which are typically in the nanosecond range. TR-FRET assays are performed by measuring FRET after a suitable delay, typically 50 to 100 microseconds after excitation, by a flashlamp excitation source in a microtiter plate reader. This delay not only overcomes interference from background fluorescence or light scatter, but also avoids interference from direct excitation due to the non-instantaneous nature of the flashlamp excitation source.

The most common lanthanides used in TR-FRET assays are terbium and europium. Terbium offers unique advantages over europium when used as the donor species in a TR-FRET assay. In contrast to europium-based systems that employ Allophycocyanin (APC) as the acceptor, terbium-based TR-FRET assays can use common fluorophores such as fluorescein as the acceptor. In terbium-based TR-FRET assays, fluorescein-labeled reagents may be used rather than biotinylated molecules that must then be indirectly labeled via streptavidin-mediated recruitment of APC as is commonly performed in europium-based assays. However, these assays require additional steps for immune antibodies conjugation or chemical conjugation of thiol-reactive Tb chelate to ubiquitin-AC or other fluorofores. The conjugation efficiency and side effect may lead to inaccurate result for quantitative analysis. Fluorescent proteins can be genetically tagged to interested proteins.

In this chapter, I will describe the improvement of the internal calibration quantitative FRET analysis to enzyme kinetics study for the endopeptidase and isopeptidase activity of SENPs by the developed highly sensitive FRET-based

protease assay in Chapter I. The pre-established standard curves, which related the fluorescent reading to protein concentration, were not required in the improved internal calibration method. Instead of only obtaining the fluorescent reading at 530 nm (acceptor's emission wavelength) during the SENP hydrolysis process, the fluorescent reading at 475 nm and 530 nm (donor and acceptor's emission wavelength) were required in the internal calibration quantitative FRET analysis. The improved quantitative FRET analysis was applied to study the kinetics of pre-SUMO1/2/3's maturation by SENP1/2C and the SUMO1-RanGAP1C deconjugation by SENP1C. The specificities were also compared of different pre-SUMO substrates to SENP1/2C, SUMO1/2-RanGAP1 deconjugation by SENP1/2C as well as the differences of endopeptidase and isopeptidase of SUMO1-SENP1C.

The improved internal calibration method can also diminish the errors of the pre-established standard curve (also simplify the operation) and minimize the variations from the fluorometer, thus makes the determined kinetics parameters more accurate and consistent.

Material and Methods

Molecular clone of DNA constructs

The open reading frame of mature SUMO2, SUMO3 and C-terminal domain (420-587) of RanGAP1 (RanGAP1C) were amplified by PCR and the PCR products were cloned into PCRII-TOPO vector (Invitrogen). The fragments encoding mature SUMO2/3 and RanGAP1C were extracted by Sal/NotI digestion and inserted into PCRII-CyPet or PCRII-YPet plasmids which was linearized by SalI/NotI. After sequences were confirmed, the cDNA encoding CyPet-SUMO2/3 were cloned into the NheI/NotI sites of pET28(b) vector with a 6x-His tag engineered on N-terminus (Novagen); the cDNA encoding YPet-RanGAP1C was cloned into the EcoRI/NotI sites of pGEX4T-1 vector with a GST-tag engineered on N-terminus (GE Healthcare).

The open reading frames of Aos1, Uba2 and Ubc9 were amplified by PCR and the PCR products were cloned into PCRII-TOPO vector (Invitrogen). After the sequences were confirmed, the cDNA encoding Aos1, Uba2 and Ubc9 were cloned into the SalI/NotI sites of pET28(b) vector with a 6x-His tag engineered on N-terminus (Novagen).

The mothods of other DNA constructs used in this chapter, which encoding CyPet-(pre-SUMO1/2/3)-YPet, CyPet-SUMO1, YPet, SENP1/2/5/6/7C were described in the Material and Methods part in Chapter I (page 49-50).

Recombinant protein expression and purification

BL21 (*DE3*) *Escherchia coli* (*E. coli*) cells were transformed with pGEX4T-1 vector encoding YPet-RanGAP1C. The transformed bacteria were plated on LB agar plates containing 100 µg/ml ampicilline and single colony was picked up and inoculated in 2xYT medium to an optical density at 600nm of 0.4-0.5 by induction with 100 µM IPTG (isopropyl β-D-thiogalactoside) for 16hr at 25℃. Bacterial cells were spinned down at 6000 rpm 10 min, and resuspended in binding buffer (50 mM Tris-HCl, 150 mM NaCl, pH 7.4) and sonicated with an ultrasonic liquid processor (Misonix). Cell lysate containing recombinant proteins was cleared by centrifugation at 35000 g 30 min. The recombinant proteins were then bound to glutathione agarose beads (Thermo) followed by washing buffer (50 mM Tris-HCl, 150 mM NaCl, pH 7.4) twice, eluted by elution buffer (50 mM Tris-HCl, 150 mM NaCl, 10 mM reduced glutathione, pH 7.4) and dialyzed overnight in dialysis buffer (20 mM Tris-HCl, 50 mM NaCl, 1mM DTT, pH 7.4).

Recombinant proteins, used in this chapter, CyPet-(pre-SUMO1/2/3)-YPet, CyPet-SUMO1/2/3, YPet, SENP1/2/5/6/7C, Aos1, Uba2 and Ubc9 were expressed and purified by Ni-NTA affinity chromatography followed the procedure described in Chapter I (page 51).

The purity of the proteins was confirmed by SDS-PAGE and Coomassie blue staining. Concentrations of protein were determined by Coomassie Plus Protein

Assay (Thermo) with known quantities of bovine serum albumin as standards. Aliquots of final products were stored in -80℃.

Preparation of SUMOylated RanGAP1C Substrate

7.2 mg GST-YPet-RanGAP1C was conjugated to 4 mg His-CyPet-SUMO1/2 in 30 ml reactions with 0.5 mg Aos1, 1mg Uba2, 5 mg Ubc9 in the buffer containing 50 mM Tris-HCl, 150 mM NaCl, 5 mM $MgCl_2$, 5 mM DTT, 0.1% BSA and 5 mM ATP. The reactions were performed in 37°C up to 2hr.

The SUMOylated RanGAP1C was then purified by glutathione-GST affinity chromatography (see detailed procedure above), followed by nickel-6xHis affinity chromatography (see detailed in chapter I, page 50), and dialyzed over night in dialysis buffer (20 mM Tris-HCl, 50 mM NaCl, 1mM DTT, pH 7.4).

The purity of the proteins was confirmed by SDS-PAGE and Coomassie blue staining. Concentrations of protein were determined by Coomassie Plus Protein Assay (Thermo) with known quantities of bovine serum albumin as standards. Aliquots of final products were stored in -80℃.

Protease assay to study the specificities

FRET-based SUMO deconjugation assays were conducted by measuring the emission intensity of CyPet at 475 nm and YPet at 530 nm with an excitation wavelength of 414nm in a fluorescence multiwall plate reader FlexStation II^{384} (Molecular Devices, Sunnyvale, CA).

To test the substrate specificities, CyPet-SUMO1/2-RanGAP1C-YPet-GST were incubated with SENP1/2/5/6/7C (1:1 molar ratio) at 37℃ in low salt reaction buffer and transferred into a 384-well plate (glass bottom, Greiner). The final concentration of reacted proteins was 100 nM. Reactions were stopped at 1 hr and were analyzed by fluorometer. Three samples were repeated in each condition. The results were reported as mean ± SD.

To study the differences of endopeptidase and isopeptidase activities of SENP1, CyPet-(pre-SUMO1/2)-YPet and CyPet-SUMO1/2-RanGAP1C-YPet-GST were incubated with SENP1C separately at 37℃ in low salt reaction buffer and transferred into a 384-well plate. The final concentration of substrates and enzymes were 100 nM and 0.5 nM respectively. Reactions were tested within original 5 min with 10 sec intervals. Initial velocities were derived by the developed method. Five samples were repeated in each concentration.

Protease kinetics assay

FRET-based SUMO processing and SUMO deconjugation assays were conducted by measuring the emission intensity of CyPet at 475 nm and of YPet at 530 nm with an excitation wavelength of 414 nm in a fluorescence multi-well plate reader (Molecular Devices, Flexstation II^{384}).

For the kinetics study, CyPet-(pre-SUMO1/2/3)-YPet or CyPet-SUMO1-RanGAP1C-YPet was incubated with SENP1 at 37℃ in low salt reaction buffer to a total volume of 80μl and transferred into a 384-well plate. The final

concentration of SENP was fixed, and the final concentrations of substrate were varied, see the details in table 6.

SENP1C (nM)	**CyPet-(pre-SUMO1)-YPet (μM)**
0.15	0.02, 0.04, 0.06, 0.08, 0.12, 0.15, 0.2, 0.25, 0.3, 0.4, 0.5
SENP1C (nM)	**CyPet-(pre-SUMO2)-YPet (μM)**
0.15	0.02, 0.04, 0.06, 0.08, 0.12, 0.15, 0.2, 0.25, 0.3, 0.4, 0.5
SENP1C (nM)	**CyPet-(pre-SUMO3)-YPet (μM)**
4	0.4, 0.8, 1.2, 1.6, 2.4, 3
SENP2C (nM)	**CyPet-(pre-SUMO1)-YPet (μM)**
6	0.8, 1.2, 1.8, 2.4, 3.6, 4.5, 6, 7.5, 9
SENP2C (nM)	**CyPet-(pre-SUMO2)-YPet (μM)**
0.15	0.016, 0.032, 0.048, 0.064, 0.096, 0.12, 0.16, 0.24, 0.32, 0.4, 0.48
SENP2C (nM)	**CyPet-(pre-SUMO3)-YPet (μM)**
7.5	0.75, 1.5, 2.25, 3, 4.5, 7.5, 9.375, 11.25
SENP1C (nM)	**CyPet-SUMO1-RanGAP1C-YPet (μM)**
0.267	0.04, 0.08, 0.12, 0.16, 0.24, 0.3, 0.4, 0.5, 0.6, 0.8, 1

Table 6. Concentration of protein samples in kinetics studies.

Reactions were tested within original 5 min with 10 sec intervals. One phase association model was used to fit the exponential increased reaction velocity. Data were analyzed by the developed method and plotted in GraphPad Prism V

software fitting the Michaelis–Menten equation. Five samples were repeated in each concentration. The results were reported as mean ± SD.

Determination of K_M and k_{cat} from $[\overline{S}]$ and $\overline{v}$

The medium velocities were determined by linear relationship to fit the curve of digested substrate concentration (or product concentration) versus processing time in the middle of any chosen time range.

The derived medium velocities and remaining substrate at the middle point of the chosen time range were analyzed by the developed method and plotted in GraphPad Prism V software fitting the Michaelis–Menten equation.

Standard curve establishment

CyPet-(pre-SUMO1/2/3)-YPet was incubated at 37°C in low salt reaction buffer to a total volume of 80 µl and added to each well of a 384-well plate. The emission signals at 475nm were collected after excitation at 414nm. The concentration was varied from 0.02 to 0.6 µM or 0.4 to 3 µM.

CyPet-SUMO1/2/3 and YPet were incubated at 37°C in low salt reaction buffer to a total volume of 80 µl with 1:1 molar ratio and added to each well of a 384-well plate. The emission signals at 475nm were collected after excitation at 414nm. The concentration of CyPet-SUMO1/2/3 was varied from 0.01 to 0.2 µM or 0.15 to 0.5 µM.

Results

Quantitative FRET analysis in internal calibration fluorescence detection

In the previous chapter, pre-SUMO1 and SENP1C was used as an example to describe the quantitative FRET analysis in protease kinetics study. The direct emission of donor (CyPet) was derived from the pre-established standard curves of CyPet-(pre-SUMO1)-YPet and CyPet-SUMO1 with YPet (1:1 mixture) as:

$$\alpha I'_{d475/414} = \alpha(I'_{d475/414-csy} + I'_{d475/414-cs}) = \alpha[k(C - x) + jx] \quad \text{[Eq. 17]}$$

The standard curves were plot as the fluorescent reading detected by fluorometer versus the related protein concentration. The slops were derived as the linear fitting the fluorescent reading (RFU) to the protein concentration (μM) (Fig. 18).

k is slope of the standard curve for $I_{d475/414-csy}$ to concentration of CyPet-(pre-SUMO1/2/3)-YPet (μM) (k is 230800 for SUMO1, 238000 for SUMO2 and 188700 for SUMO3 fusion proteins). j is slope of the standard curve for $I_{d475/414-cs}$ to concentration of CyPet-SUMO1/2/3 (μM) (j is 326700 for SUMO1, 349000 for SUMO2 and 244200 for SUMO3 fused with CyPet).

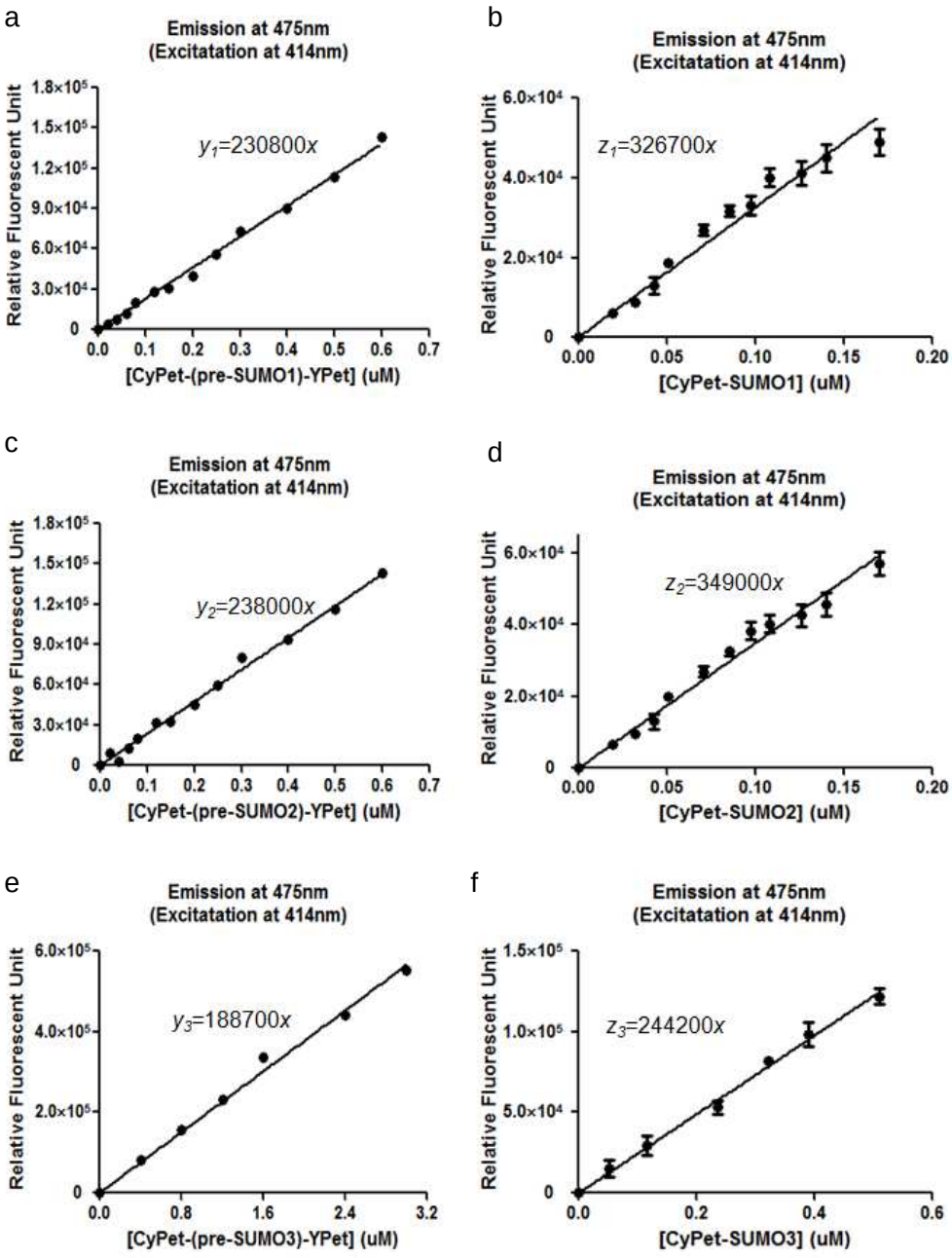

Figure 18 Pre-established standard curves of fluorescent emission at 475nm to related protein concentration. CyPet-(pre-SUMO1/2/3)-YPet (a, c, e) and CyPet-SUMO1/2/3 with YPet (1:1 molar ratio) (b, d, f). Excitation wavelength was 414nm.

However, the emission of CyPet at 475nm can be obtained directly by the fluorometer in the study as $I'_{d475/414}$, in that way, the [Eq. 9] can be modified as:

$$FL'_{530/414} = \frac{C-x}{C} \times \left(FL_{530/414} - \alpha I_{d475/414} - \beta I_{a530/475}\right) + \alpha I'_{d475/414} + \beta I_{a530/475} \quad \text{[Eq. 18]}$$

or rearranged as:

$$\frac{C-x}{C} = \frac{FL'_{530/414} - \alpha I'_{d475/414} - \beta I'_{a530/475}}{FL_{530/414} - \alpha I_{d475/414} - \beta I_{a530/475}} = \frac{FL'_{FRET}}{FL_{FRET}} \quad \text{[Eq. 19]}$$

During the pre-SUMO's maturation process, the increase of CyPet's direct emission and the decrease of FRET-induced acceptor's emission were due to the disruption of energy transfer. The detected total fluorescent emission at 530 nm, CyPet and YPet direct emission as well as the FRET-induced YPet's emission analyzed by the quantitative analysis in internal calibration and standard curve-dependent detections were compared in Fig. 19. The fluorescent emission detected at 530 nm was not equal to the FRET-induced YPet's emission, which is always considered the same in the ratiometric analysis.

The cross-talk ratio to characterize the direct emission of CyPet (α) and YPet (β) were defined in Chapter I and the values of α were 0.332, 0.278, and 0.265 for CyPet-SUMO1/2/3 individually, the value of β was 0.026.

a

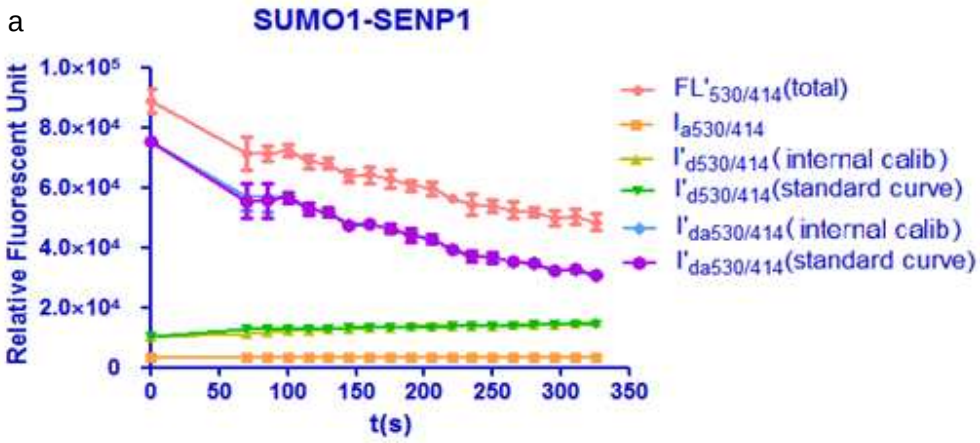
SUMO1-SENP1
Relative Fluorescent Unit
1.0×10⁵
8.0×10⁴
6.0×10⁴
4.0×10⁴
2.0×10⁴
0
0
50
100
150
200
250
300
350
t(s)
FL'530/414(total)
Ia530/414
I'd530/414(internal calib)
I'd530/414(standard curve)
I'da530/414(internal calib)
I'da530/414(standard curve)

b

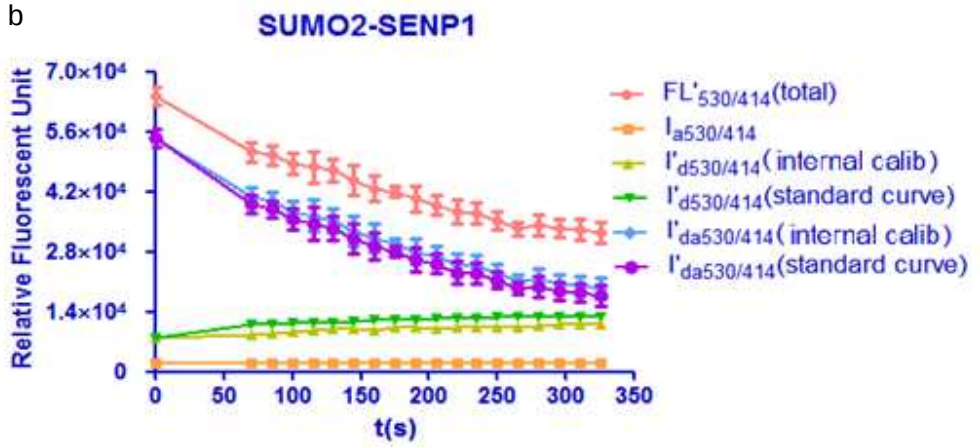
SUMO2-SENP1
Relative Fluorescent Unit
7.0×10⁴
5.6×10⁴
4.2×10⁴
2.8×10⁴
1.4×10⁴
0
0
50
100
150
200
250
300
350
t(s)
FL'530/414(total)
Ia530/414
I'd530/414(internal calib)
I'd530/414(standard curve)
I'da530/414(internal calib)
I'da530/414(standard curve)

c

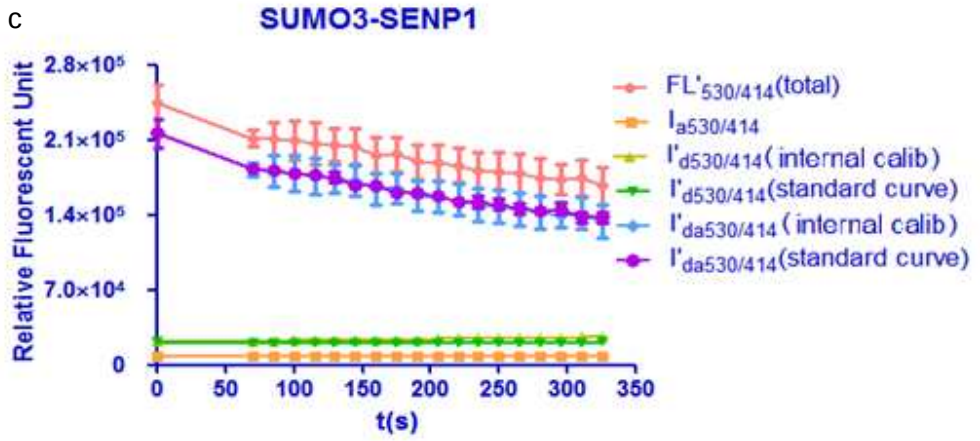
SUMO3-SENP1
Relative Fluorescent Unit
2.8×10⁵
2.1×10⁵
1.4×10⁵
7.0×10⁴
0
0
50
100
150
200
250
300
350
t(s)
FL'530/414(total)
Ia530/414
I'd530/414(internal calib)
I'd530/414(standard curve)
I'da530/414(internal calib)
I'da530/414(standard curve)

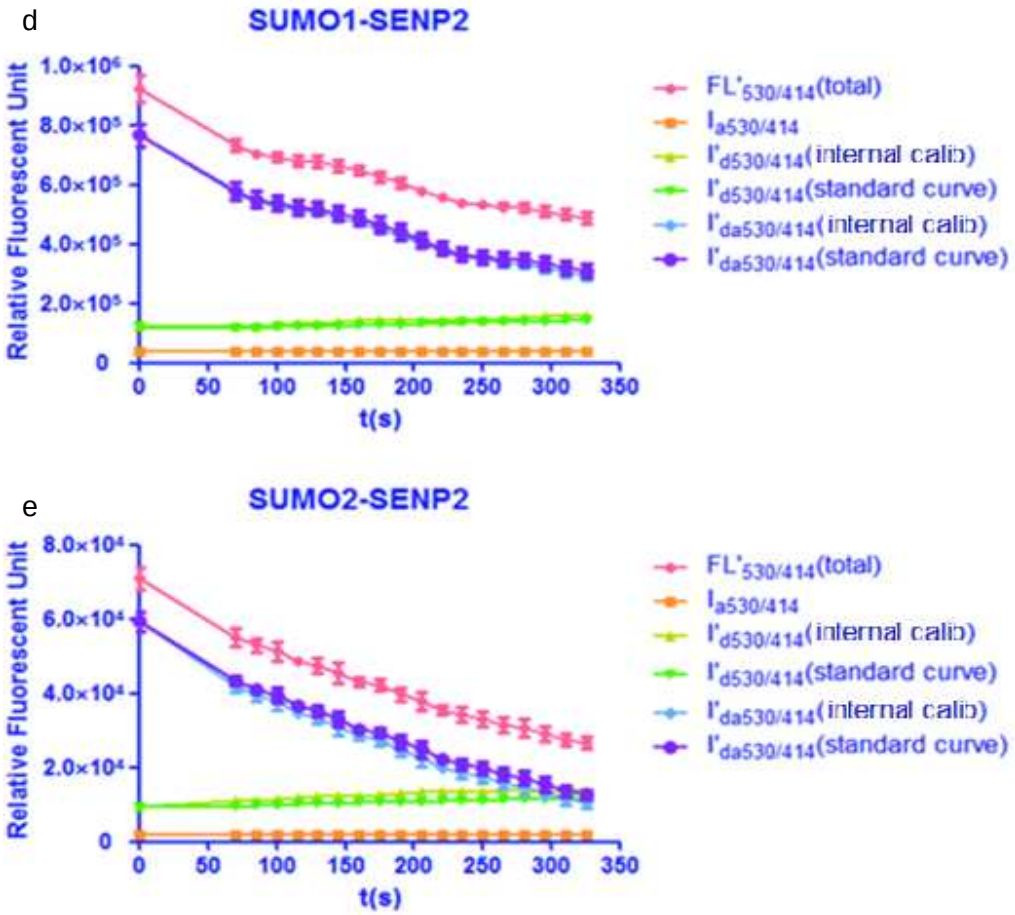

Figure 19 Time-course of fluorescence component changes during pre-SUMO maturation. Changes to fluorescence components of CyPet-(pre-SUMO1/2/3)-YPet during maturation by SENP1C (a, b, c); changes to fluorescence components of CyPet-(pre-SUMO1/2)-YPet during maturation by SENP2C (d, e). Reactions were monitored within original 5 min and 10 sec interval.

Initial velocity determination of pre-SUMO's maturation

The pre-SUMO1/2/3's maturation by SENP1/2C can be determined by monitoring the changes of fluorescent signal at 475 nm and 530 nm under excitation of 414 nm during the process. Different amounts of the fluorescent substrate were incubated with SENP1/2C (concentrations of substrate and protease were listed in Table 6). The concentration of digested substrate, x, was calculated according to the quantitative FRET analysis in internal calibration detection (described as [Eq. 18] or [Eq. 19]) (Fig. 20).

The initial velocity (v_0) of CyPet-(pre-SUMO1/2/3)-YPet's maturation by SENP1/2C was determined using methods described in Chapter I (see details in page71-72) and listed in Table 7 with quantitative FRET analysis in both internal calibration detection and standard curve-dependent method. The results displayed a good substrate does-dependent relationship as well as exhibited the tiny differences from the above two methods.

a

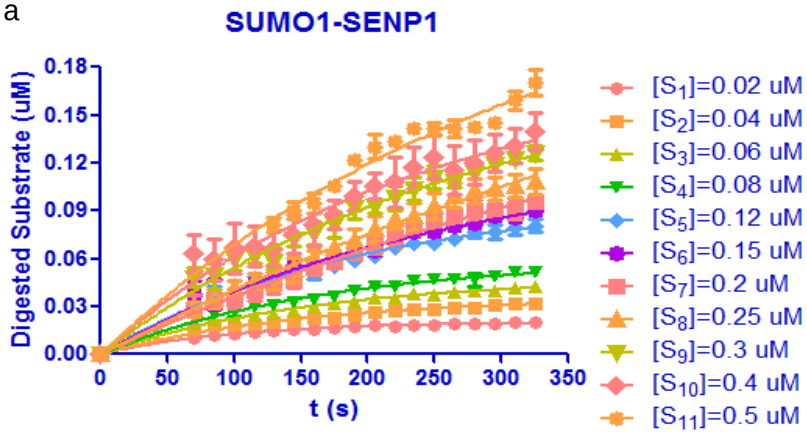
SUMO1-SENP1
Digested Substrate (uM)
0.18
0.15
0.12
0.09
0.06
0.03
0.00
0
50
100
150
200
250
300
350
t (s)
[S1]=0.02 uM
[S2]=0.04 uM
[S3]=0.06 uM
[S4]=0.08 uM
[S5]=0.12 uM
[S6]=0.15 uM
[S7]=0.2 uM
[S8]=0.25 uM
[S9]=0.3 uM
[S10]=0.4 uM
[S11]=0.5 uM

b

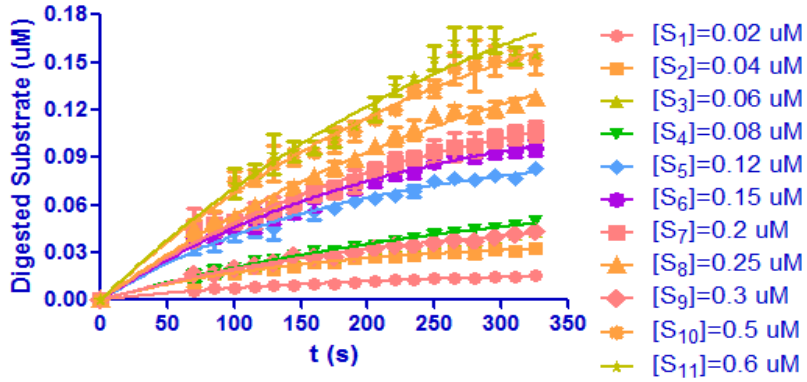
SUMO2-SENP1
Digested Substrate (uM)
0.18
0.15
0.12
0.09
0.06
0.03
0.00
0
50
100
150
200
250
300
350
t (s)
[S1]=0.02 uM
[S2]=0.04 uM
[S3]=0.06 uM
[S4]=0.08 uM
[S5]=0.12 uM
[S6]=0.15 uM
[S7]=0.2 uM
[S8]=0.25 uM
[S9]=0.3 uM
[S10]=0.5 uM
[S11]=0.6 uM

c

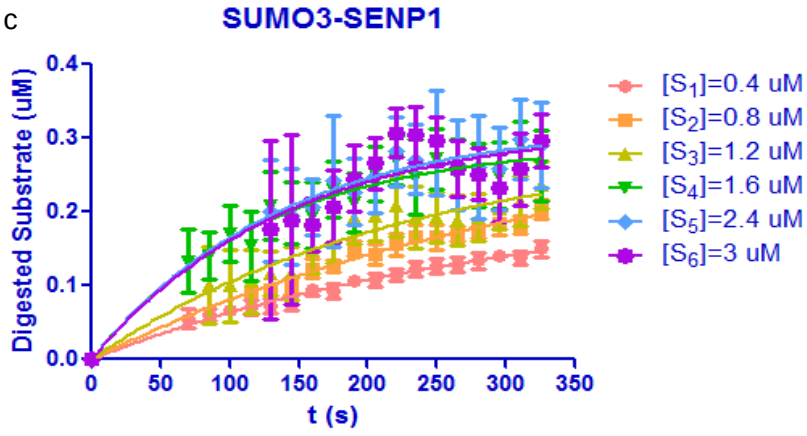
SUMO3-SENP1
Digested Substrate (uM)
0.4
0.3
0.2
0.1
0.0
0
50
100
150
200
250
300
350
t (s)
[S1]=0.4 uM
[S2]=0.8 uM
[S3]=1.2 uM
[S4]=1.6 uM
[S5]=2.4 uM
[S6]=3 uM

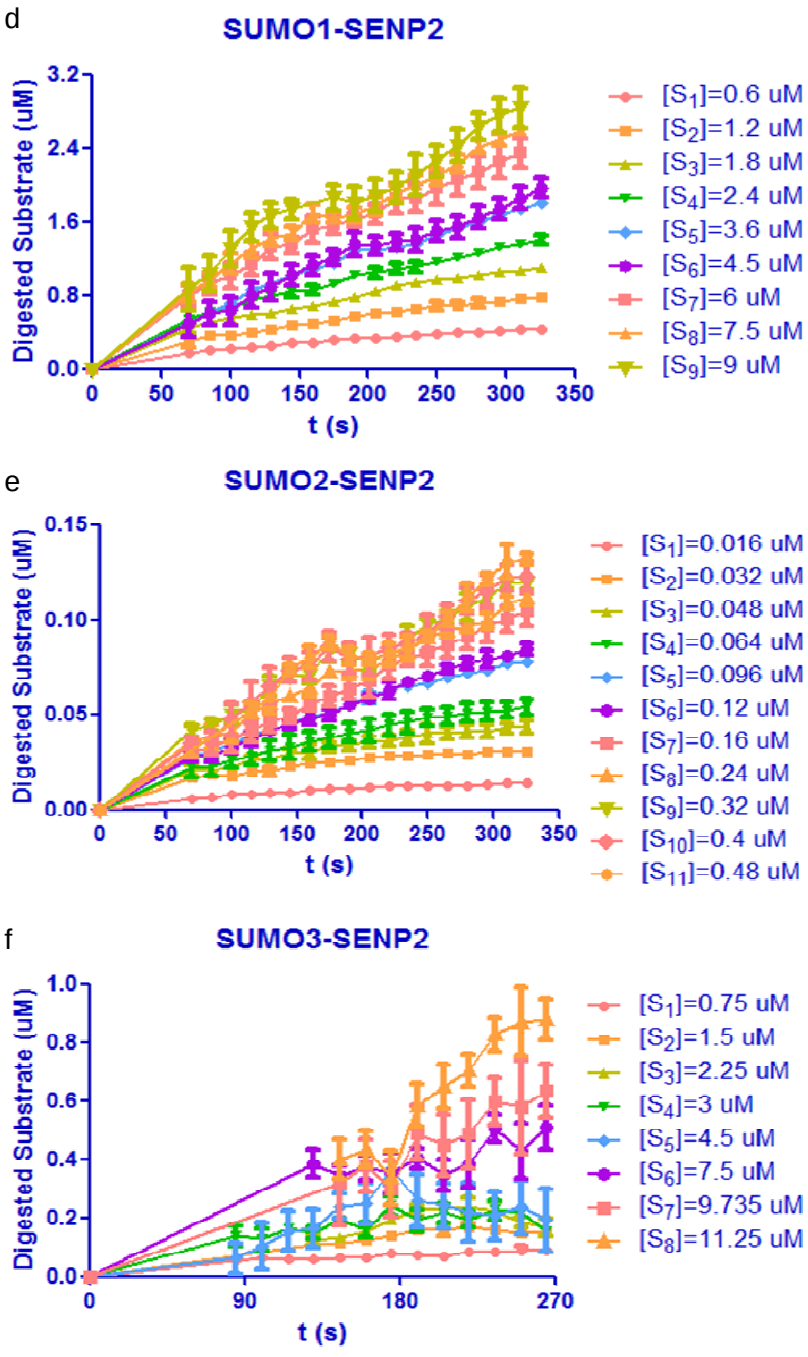

Figure 20 The concentration of digested substrate during pre-SUMO maturation process analyzed by internal calibration method. Maturation of pre-SUMO1/2/3 by SENP1C (a, b, c) and SENP2C (d, e, f). Reactions were monitored within original 5 min.

SENP1C [CyPet-(pre-SUMO1)-YPet] (μM)	v_0 (x10^{-3} μM/s)	
	Internal calibration	Standard curve-dependent
0.02	0.20 ± 0.010	0.21 ± 0.010
0.04	0.23 ± 0.014	0.26 ± 0.016
0.06	0.30 ± 0.017	0.33 ± 0.018
0.08	0.35 ± 0.029	0.35 ± 0.028
0.12	0.51 ± 0.033	0.50 ± 0.037
0.15	0.48 ± 0.044	0.48 ± 0.044
0.2	0.39 ± 0.10	0.41 ± 0.12
0.25	0.44 ± 0.13	0.42 ± 0.13
0.3	0.64 ± 0.069	0.63 ± 0.079
0.4	0.75 ± 0.13	0.84 ± 0.13
0.5	0.80 ± 0.11	0.87 ± 0.13

SENP1C [CyPet-(pre-SUMO2)-YPet] (μM)	v_0 (x10^{-3} μM/s)	
	Internal calibration	Standard curve-dependent
0.02	0.096 ± 0.007	0.065 ± 0.008
0.04	0.23 ± 0.022	0.47 ± 0.031
0.06	0.24 ± 0.020	0.26 ± 0.023
0.08	0.24 ± 0.031	0.22 ± 0.028
0.12	0.53 ± 0.043	0.50 ± 0.056
0.15	0.57 ± 0.049	0.60 ± 0.048
0.2	0.60 ± 0.068	0.64 ± 0.081
0.25	0.62 ± 0.059	0.63 ± 0.068
0.3	0.71 ± 0.088	0.71 ± 0.11
0.5	0.80 ± 0.11	0.91 ± 0.12
0.6	0.82 ± 0.13	0.90 ± 0.16

SENP1C [CyPet-(pre-SUMO3)-YPet] (μM)	v_0 (x10^{-3} μM/s)	
	Internal calibration	Standard curve-dependent
0.4	0.75 ± 0.094	0.68 ± 0.10
0.8	0.93 ± 0.16	0.91 ± 0.17
1.2	1.30 ± 0.33	1.33 ± 0.37
1.6	2.37 ± 0.34	2.31 ± 0.38
2.4	2.33 ± 0.62	2.70 ± 0.73
3	2.26 ± 0.80	2.67 ± 0.95

SENP2C [CyPet-(pre-SUMO1)-YPet] (μM)	v_0 (x10^{-3} μM/s)	
	Internal calibration	Standard curve-dependent
0.6	2.88 ± 0.095	2.43 ± 0.099
1.2	4.62 ± 0.39	4.82 ± 0.48
1.8	6.56 ± 0.40	6.31 ± 0.52
2.4	8.17 ± 0.50	7.30 ± 0.54
3.6	8.46 ± 0.56	7.96 ± 0.77
4.5	9.15 ± 1.74	9.01 ± 2.15
6	12.58 ± 1.01	14.36 ± 1.05
7.5	12.81 ± 1.40	14.33 ± 1.57
9	14.89 ± 2.40	18.72 ± 2.81

SENP2C [CyPet-(pre-SUMO2)-YPet] (μM)	v_0 (x10^{-3} μM/s)	
	Internal calibration	Standard curve-dependent
0.016	0.11 ± 0.009	0.08 ± 0.012
0.032	0.29 ± 0.014	0.29 ± 0.016
0.048	0.32 ± 0.028	0.32 ± 0.024
0.064	0.33 ± 0.043	0.32 ± 0.049
0.096	0.42 ± 0.019	0.38 ± 0.025
0.12	0.37 ± 0.042	0.38 ± 0.046
0.16	0.39 ± 0.129	0.40 ± 0.122
0.24	0.49 ± 0.059	0.48 ± 0.069
0.32	0.58 ± 0.065	0.67 ± 0.066
0.4	0.55 ± 0.110	0.68 ± 0.104
0.48	0.50 ± 0.216	0.57 ± 0.209

SENP2C [CyPet-(pre-SUMO3)-YPet] (μM)	v_0 (x10^{-3} μM/s)	
	Internal calibration	Standard curve-dependent
0.75	0.75 ± 0.01	
1.5	1.57 ± 0.23	
2.25	2.27 ± 0.60	
3	2.40 ± 0.38	
4.5	1.74 ± 1.02	
7.5	4.69 ± 1.02	
9.375	4.46 ± 1.64	
11.25	5.51 ± 2.31	

Table 7. The initial velocities (v_0) of pre-SUMO's maturation by SENP1/2C derived by quantitative FRET analysis in both internal calibration and standard curve-dependent method. The initial velocities of pre-SUMO3's maturation by SENP2 were not listed since the variation were too large cannot fitted into Michaelis-Menten equation.

Enzyme kinetics parameters determination by Michaelis-Menten analysis

The values of K_M and V_{max} can be obtained from the Michaelis–Menten equation by plotting the various velocities of SENP1/2C digestion versus the related substrates in different concentrations. The obtained initial velocities in Table 7 were plotted in Michaelis-Menten equation (Fig. 21). k_{cat}, K_M, and the k_{cat}/K_M ratio were obtained by both the quantitative FRET analysis of internal calibration and standard curve-dependent method (Table 8).

Again, the values of k_{cat}/K_M from the quantitative FRET analysis were close to those derived from ratiometric FRET analysis in one of the previous SENP1 endopeptidase function studies [61], but not the individual k_{cat} and K_M. The study of SENP indicated the same conclusion that the key step for pre-SUMOs maturation is binding (different K_M) not catalysis (close k_{cat}) although the individual K_M, k_{cat} and their ratios were quite different [63]. Also, the k_{cat}/K_M ratio was in agreement with the preference of SENP2 to pre-SUMO's maturation is pre-SUMO2>pre-SUMO1>pre-SUMO3 [60].

As expected, the derived kinetic parameters from the internal calibration method and standard curve-dependent method were close to each other, but the standard errors in standard curve-dependent method were larger than those in internal calibration method, especially for pre-SUMO3, which were so large that the derived initial velocities cannot fit into the Michaelis-Menten equation.

a

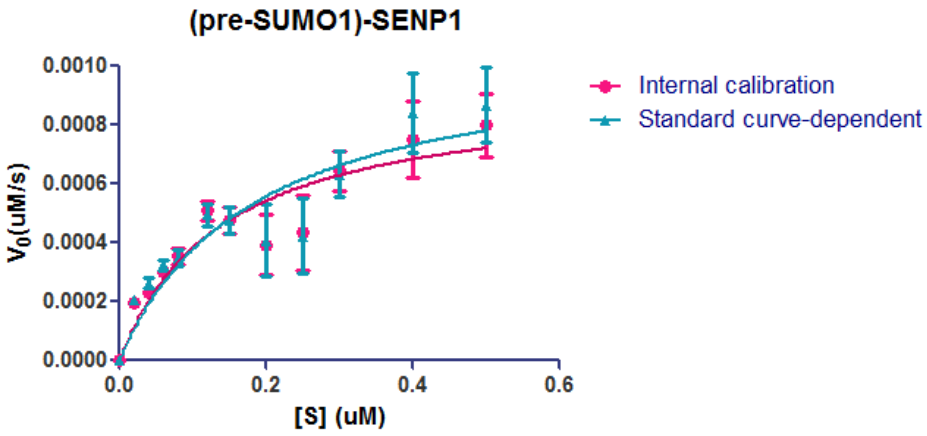
(pre-SUMO1)-SENP1
0.0010
0.0008
0.0006
0.0004
0.0002
0.0000
V0(uM/s)
0.0
0.2
0.4
0.6
[S] (uM)
Internal calibration
Standard curve-dependent

b

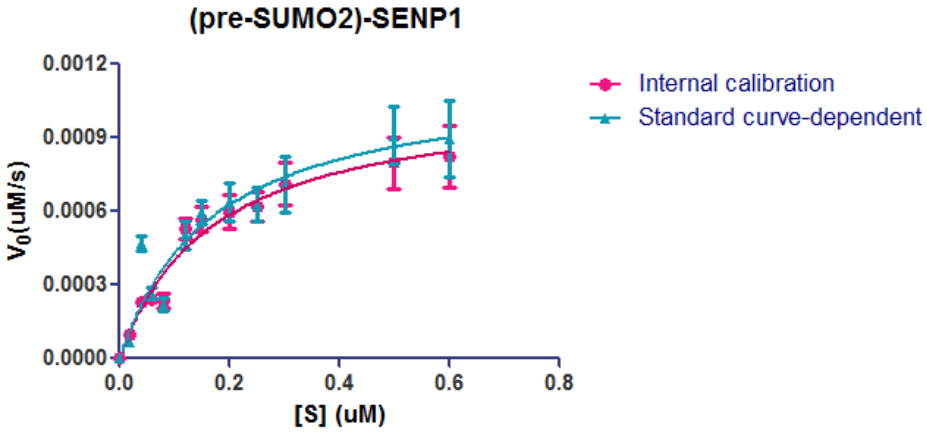
(pre-SUMO2)-SENP1
0.0012
0.0009
0.0006
0.0003
0.0000
V0(uM/s)
0.0
0.2
0.4
0.6
0.8
[S] (uM)
Internal calibration
Standard curve-dependent

c

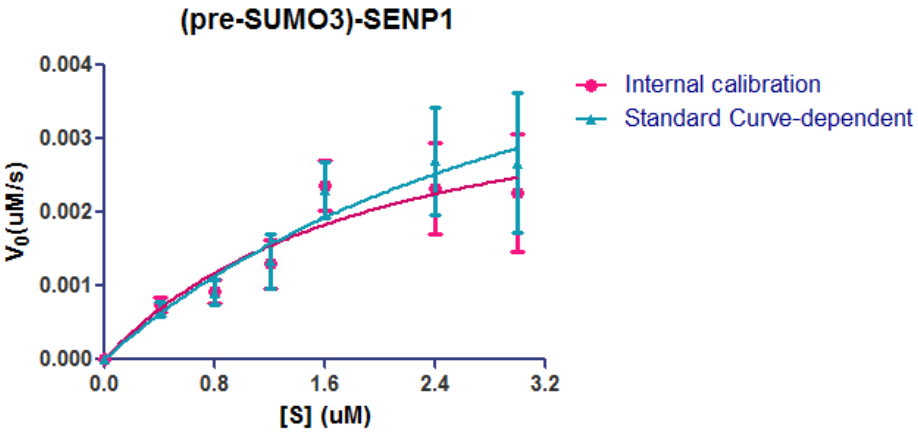
(pre-SUMO3)-SENP1
0.004
0.003
0.002
0.001
0.000
V0(uM/s)
0.0
0.8
1.6
2.4
3.2
[S] (uM)
Internal calibration
Standard Curve-dependent

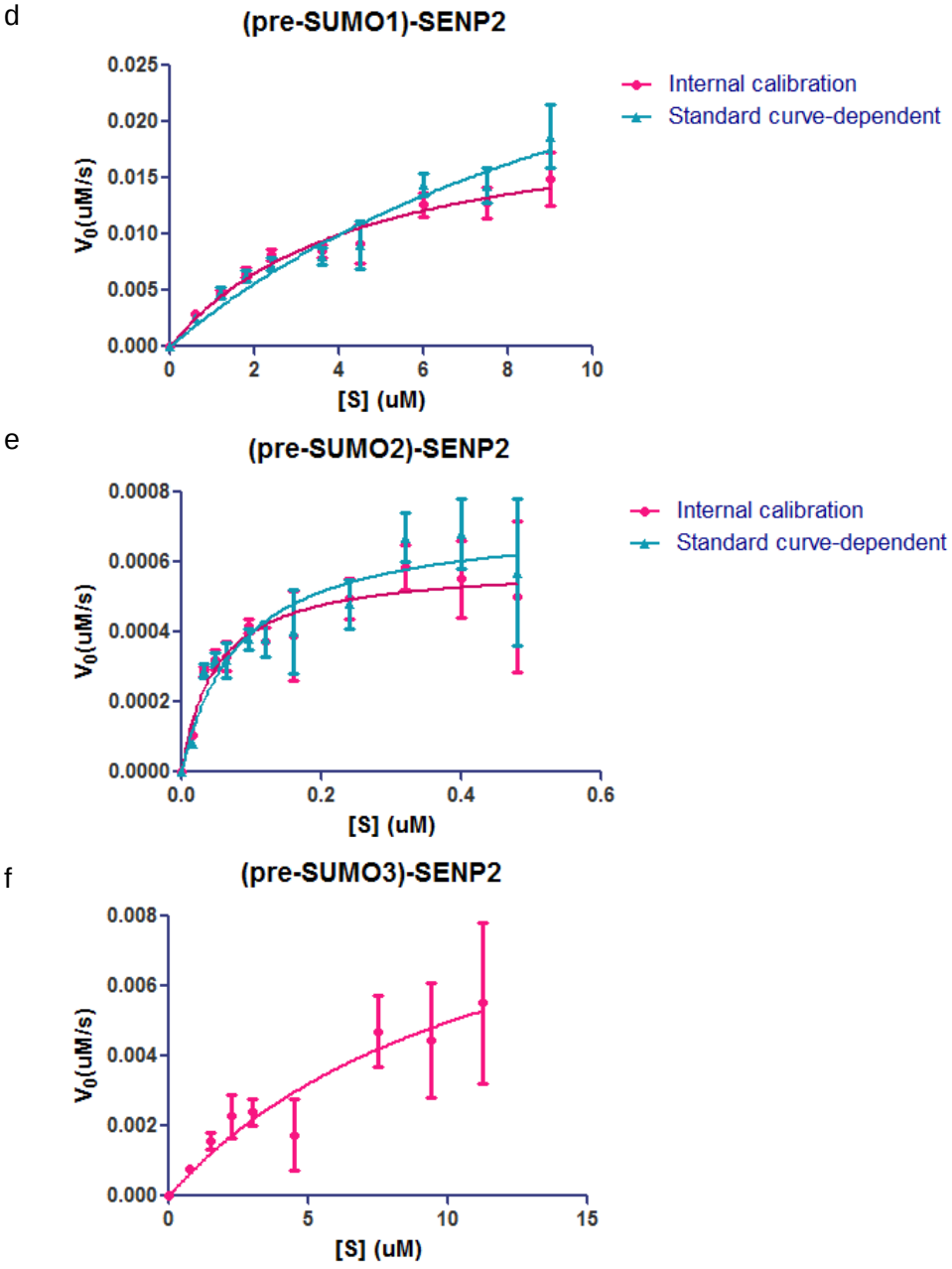

Figure 21 Michaelis–Menten graphical analysis of pre-SUMO's maturation by SENP. Pre-SUMO1/2/3's maturation by SENP1C (a, b, c), pre-SUMO1/2/3's maturation by SENP2C (d, e, f). Data were plotted and analyzed by GraphPad Prism 5 in nonlinear regression (Michaelis-Menten model).

SENP1 Substrate	Analysis Method	K_M (µM)	k_{cat} (s^{-1})	k_{cat}/K_M (x 10^6 $M^{-1}{\cdot}s^{-1}$)
pre-SUMO1	IC	0.14 ± 0.051	6.14 ± 0.89	44.1 ± 17.4
	SC	0.18 ± 0.078	7.07 ± 1.33	39.2 ± 18.5
	Ref. [61]	0.098	3.73	38.06
pre-SUMO2	IC	0.17 ± 0.0031	7.17 ± 0.54	42.8 ± 8.3
	SC	0.17 ± 0.0055	7.66 ± 1.04	46 ± 16.6
pre-SUMO3	IC	1.99 ± 1.25	1.03 ± 0.33	0.52 ± 0.365
	SC	3.75 ± 2.22	1.61 ± 0.62	0.43 ± 0.304
	Ref. [61]	0.126	0.075	0.595

SENP2 Substrate	Analysis Method	K_M (µM)	k_{cat} (s^{-1})	k_{cat}/K_M (x 10^6 $M^{-1}{\cdot}s^{-1}$)
pre-SUMO1	IC	4.49 ± 0.99	3.52 ± 0.37	0.78 ± 0.19
	SC	13.96 ± 6.74	7.44 ± 2.49	0.53 ± 0.31
	Ref. [63]	27.9 ± 3.7	0.72 ± 1.5	0.026
pre-SUMO2	IC	0.048 ± 0.011	3.93 ± 0.23	82 ± 18.7
	SC	0.081 ± 0.023	4.83 ± 0.45	59.3 ± 17.8
	Ref. [63]	2.0 ± 0.6	0.77 ± 0.07	0.38
pre-SUMO3	IC	12.06 ± 7.46	1.46 ± 0.55	0.12 ± 0.088
	Ref. [63]	2.2 ± 0.3	0.11 ± 0.01	0.05

Table 8. Kinetic parameters of CyPet-(pre-SUMO1/2/3)-YPet's maturation by SENP1/2C determined by quantitative FRET analysis in internal calibration (IC), standard curve-dependent (SC) method, and compared to references (Ref.).

Determination of K_M and k_{cat} from $[\overline{S}]$ and $\bar{v}$

The substrate digestion at the very beginning of the process cannot be obtained due to the sensitivity of the fluorometer. In that way, the initial velocities determined as the derivative at $t = 0$ according to the fitted one phase association model were not accurate enough.

The medium velocities were determined by linear relationship to fit the curve of digested substrate concentration (or product concentration) versus processing time in the middle of any chosen time range. In the time range t_1 to t_2, the detected product concentration can be fitted in the linear relationship to provide the velocity $\bar{v}$, which is the slop of the linear curve fitting. The product concentration at the middle point of the time range, $t = \frac{t_1+t_2}{2}$, can be derived from the calculated velocity as:

$$[P]_{t_m} = \bar{v} \times \frac{t_1 + t_2}{2} \qquad \text{[Eq. 20]}$$

The remaining substrate concentration can be derived as:

$$\overline{[S]} = [S]_O - [P]_{t_m} \qquad \text{[Eq. 21]}$$

As the initial velocity is the reaction velocity at $t = 0$, at which time point no product is created, the remaining substrate concentration is the total substrate concentration. In that way, the previous method of using initial velocity and total substrate concentration for enzyme kinetics determination is the special case for the utilization of medium velocity and remaining substrate concentration.

However, this method cannot provide accurate kinetic parameters with the consideration of product inhibition.

The process of SENP1C maturing CyPet-(pre-SUMO1)-YPet was used to demonstrate this method, two time range 70-205 sec and 145-325 sec were selected, the reaction velocities in each time range were derived by linear curve fitting (under different total substrate concentration) and listed in Table 8-a. The digested substrate concentrations were analyzed by internal calibration method. The product concentrations as well as the remaining substrate concentrations at medium time point (137.5 sec and 235 sec) were also calculated according to the reaction velocities (listed in Table 8-b). The determined kinetic parameters, K_M and k_{cat}, were calculated by using the data in Table 8-b in Michaelis-Menten equation and listed in Table 8-c. The two sets of data were plot into Michaelis-Menten equation in Fig. 22.

a

Total [CyPet-(pre-SUMO1)-YPet] (μM)	v **(x10^{-3} μM/s)**	
	70-205 sec	145-325 sec
0.02	0.051 ± 0.00375	0.025 ± 0.00291
0.04	0.080 ± 0.00551	0.061± 0.00293
0.06	0.11 ± 0.00714	0.080± 0.00421
0.08	0.13 ± 0.00969	0.10 ± 0.00819
0.12	0.21 ± 0.0130	0.17 ± 0.00817
0.15	0.23 ± 0.0169	0.21 ± 0.00659
0.2	0.30 ± 0.0219	0.27 ± 0.0140
0.25	0.36 ± 0.0213	0.31 ± 0.0178
0.3	0.35 ± 0.0242	0.30 ± 0.0137
0.4	0.33 ± 0.0426	0.33 ± 0.0294

b

Total [CyPet-(pre-SUMO1)-YPet] (μM)	Remaining [CyPet-(pre-SUMO1)-YPet] (μM)	
	137.5 sec in 70-205 sec time range	235 sec in 145-325 sec time range
0.02	0.0055 ± 0.00106	0.065 ± 0.008
0.04	0.020 ± 0.00155	0.47 ± 0.031
0.06	0.033 ± 0.00201	0.26 ± 0.023
0.08	0.048 ± 0.00273	0.22 ± 0.028
0.12	0.071 ± 0.00366	0.50 ± 0.056
0.15	0.10± 0.00476	0.60 ± 0.048
0.2	0.15 ± 0.00616	0.64 ± 0.081
0.25	0.20 ± 0.00601	0.63 ± 0.068
0.3	0.23 ± 0.00682	0.91 ± 0.12
0.4	0.32 ± 0.0120	0.90 ± 0.16

c

Time range	K_M (μM)	k_{cat} (s^{-1})	k_{cat}/K_M (x 10^6 $M^{-1}{\cdot}s^{-1}$)
70-205 sec	0.10 ± 0.0216	3.23 ± 0.282	32.3 ± 7.53
145-325 sec	0.095 ± 0.0154	3.05 ± 0.208	32.1 ± 5.65
Whole range (original initial velocity method)	0.14 ± 0.051	6.14 ± 0.89	44.1 ± 17.4

Table 9. Determination of K_M and k_{cat} from $[\bar{S}]$ and $\bar{v}$. (a) The velocities in 70-205 sec and 145-325 sec time range at under different total substrate concentration; (b) remaining substrate concentration at medium point (137.5 sec in 70-205 sec time range and 235 sec in 145-325 sec time range); (c) comparison of kinetics parameters in different time range and previous initial velocity method.

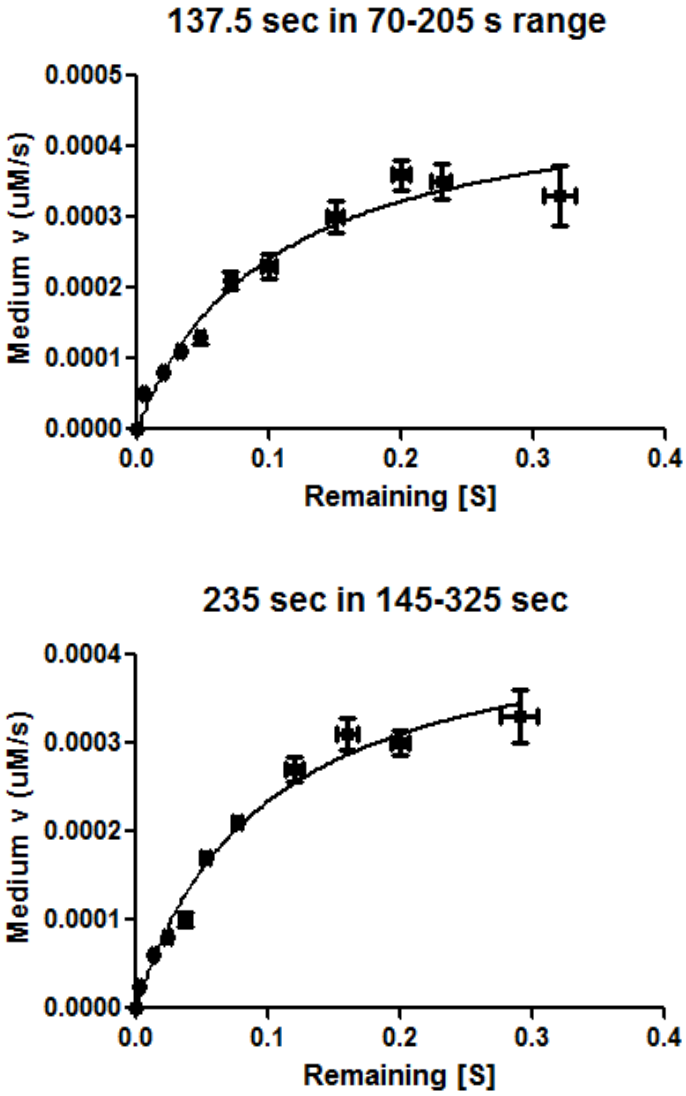

Figure 22. Velocities in time range 70-205 sec or 145-325 sec were plotted versus remaining substrate concentration at the medium point (137.5 sec in 70-205 sec time range or 235 sec in 145-325 sec time range) in Michaelis-Menten equation.

Compare to previous method, which applied the initial velocity to derive the kinetics parameters, the method using medium remaining substrate concentration and the velocities in specific time provided similar K_M but smaller k_{cat}. The initial velocity is the reaction velocity at the very beginning of the process, which should hold the maximal value compared to the velocities in any other time point during the reaction. However, these two methods provided similar results in kinetics determination. The medium method can be used to replace the initial velocity method especially the facility is not accurate enough to generate kinetics parameters.

Similarly, the kinetics parameters determined by medium remaining substrate concentration and velocities (fluorescent reading analyzed by internal calibration method) were also analyzed for other (pre-SUMO)-SENP pairs and listed in Table 10.

SENP1 **Total [CyPet-(pre-SUMO2)-YPet] (μM)**	**v in 160-280 sec time range (x10^{-3} μM/s)**	**Remaining $[S]$ at 220 sec (μM)**
0.02	0.033 ± 0.00262	0.0080 ± 0.00116
0.04	0.062 ± 0.00107	0.013 ± 0.00475
0.06	0.095 ± 0.00673	0.027 ± 0.00299
0.08	0.12 ± 0.112	0.043 ± 0.00494
0.12	0.18 ± 0.142	0.051 ± 0.00780
0.15	0.23 ± 0.209	0.071 ± 0.00928
0.2	0.27 ± 0.259	0.12 ± 0.0115
0.3	0.29 ± 0.390	0.21 ± 0.0166
0.4	0.39 ± 0.542	0.28 ± 0.0240
0.5	0.47 ± 0.337	0.38 ± 0.0149

SENP1 Total [CyPet-(pre-SUMO3)-YPet] (μM)	v in 160-280 sec time range (x10^{-3} μM/s)	Remaining $[S]$ at 220 sec (μM)
0.4	0.36 ± 0.0341	0.29 ± 0.0151
0.8	0.43 ± 0.0511	0.65 ± 0.0226
1.2	0.28 ± 0.135	1.0 ± 0.0597
1.6	0.43 ± 0.164	1.4 ± 0.0725
2.4	0.48 ± 0.221	2.15 ± 0.0982
3	0.63 ± 0.230	2.74 ± 0.102

SENP2 Total [CyPet-(pre-SUMO1)-YPet] (μM)	v in 160-280 sec time range (x10^{-3} μM/s)	Remaining $[S]$ at 220 sec (μM)
0.6	0.95 ± 0.0390	0.24 ± 0.0173
1.2	2.0 ± 0.163	0.60 ± 0.0721
1.8	2.8 ± 0.153	0.92 ± 0.0678
2.4	3.2 ± 0.193	1.3 ± 0.0855
3.6	4.0 ± 0.161	2.3 ± 0.0716
6	5.7 ± 0.361	4.1 ± 0.0160
7.5	6.3 ± 0.457	5.6 ± 0.202
9	6.3 ± 0.833	6.9 ± 0.370

SENP2 Total [CyPet-(pre-SUMO2)-YPet] (μM)	v in 160-280 sec time range (x10^{-3} μM/s)	Remaining $[S]$ at 220 sec (μM)
0.016	0.022 ± 0.00344	0.011 ± 0.000757
0.032	0.042 ± 0.00448	0.023± 0.000986
0.048	0.089 ± 0.0147	0.028 ± 0.00324
0.064	0.13 ± 0.0198	0.036 ± 0.00436
0.096	0.19 ± 0.00812	0.053 ± 0.00179
0.12	0.25 ± 0.0116	0.065 ± 0.00255
0.24	0.26 ± 0.0164	0.18 ± 0.00361
0.32	0.26 ± 0.0260	0.26 ± 0.00571
0.4	0.24 ± 0.0352	0.35 ± 0.00774
0.48	0.21 ± 0.0385	0.343 ± 0.00846

SENP1 substrate	K_M (μM)	k_{cat} (s^{-1})	k_{cat}/K_M (x 10^6 $M^{-1}\cdot s^{-1}$)
pre-SUMO2	0.14 ± 0.0324	3.93 ± 0.411	28.1 ± 7.13
pre-SUMO3	0.25 ± 0.24	0.14 ± 0.0272	0.56 ± 0.548

SENP2 substrate	K_M (μM)	k_{cat} (s^{-1})	k_{cat}/K_M (x 10^6 $M^{-1}\cdot s^{-1}$)
pre-SUMO1	2.03 ± 0.247	1.38 ± 0.0650	0.680 ± 0.0887
pre-SUMO2	0.043 ± 0.0183	1.92 ± 0.243	44.65 ± 19.83

Table 10. Determination of K_M and k_{cat} from $[\bar{S}]$ and $\bar{v}$ for pre-SUMO2/3 processed by SENP1C and pre-SUMO1/2 processed by SENP2C. pre-SUMO3's maturation by SENP2C cannot be derived due to large variations.

SUMOylation of RanGAP1 and Design of FRET-based protease assay to study isopeptidase activity of SENPs

RanGAP1 is the first identified SUMO target, and its SUMOylation cycle mediates the constant shuttling between the cytoplasm and nuclear [13]. The formation of an isopeptide bond between SUMO and Lys526 of RanGAP1 *in vitro* occurs in the presence of E1, E2 enzyme and ATP, and this reaction does not require E3 ligase RanBP2 [13] (RanBP2 may coordinate the SUMO-Ubc9 thioester in an optimal conformation for catalysis without directly contacting the RanGAP to enhance SUMOylation).

Similar as the design of the FRET-based protease assay to study the endopeptidase activity of SENPs, the FRET pair, CyPet and YPet, was applied to monitor the SUMOylation of RanGAP1 and deconjugation SUMO from the SUMO-RanGAP substrate by SENPs.

CyPet and YPet were genetically tagged to the N-terminus of SUMO1/2 and RanGAP1C respectively. With the existence of SUMO E1 (Aos1/Uba2), E2 enzyme (Ubc9) and ATP, CyPet-SUMO1/2 will be covalently linked to YPet-RanGAP1C. The excitation of CyPet will transfer energy to YPet in close proximity, the quenching of donor and increased emission of acceptor can be observed (Fig. 23a).

CyPet-SUMO1/2 and YPet-RanGAP1C proteins were first mixed with Aos1, Uba2 and Ubc9 proteins in the low-salt Tris buffer (50 mM Tris-HCl, 150 mM

NaCl, 5 mM $MgCl_2$, 5 mM DTT, 0.1% BSA) without ATP. ATP was added at time point 0 and the fluorescent emission at 475nm and 530nm as well as the emission ratio (FL_{530}/FL_{475}) of the protein mixture were monitored every 2 min. Compared with the negative control sample which did not have ATP, the sample with ATP presented significant decrease of fluorescent emission at 475nm and increase of fluorescent emission at 530nm. The emission ratios (FL_{530}/FL_{475}) were also dramatically increased and reached the plateau in 30 min (Fig. 23b&c).

The multiple Lys residues in the N-terminal extensions of SUMO2 and SUMO3 can form polySUMO chains but SUMO1 does not have [17]. SENP6 and SENP7 have been discovered to have the ability to edit polySUMO tail [65]. The molar ratio of CyPet-SUMO2 to YPet-RanGAP1C used in the SUMOylation assay was about 1:1, which was expected to modify every RanGAP1C by SUMO and avoid polySUMO tail on RanGAP1C. As all the SUMO2 were genetically tagged with CyPet, the formation of polySUMO2 will lead to the multiple SUMO2 on one RanGAP1C, or in other words, multiple CyPet with one YPet. The detected fluorescent emission of 475nm and increased fluorescent emission of 530nm should not be the same as the emissions for one donor coupled one acceptor in the FRET system. The fluorescent emission change at 475nm and 530nm as well as the emission ratio of SUMO2-RanGAP1C conjugation were the same as those of SUMO1-RanGAP1C conjugation, which denoted that there was no formation of polySUMO2 on RanGAP1C in the protein assay with current condition (Fig. 23b&c).

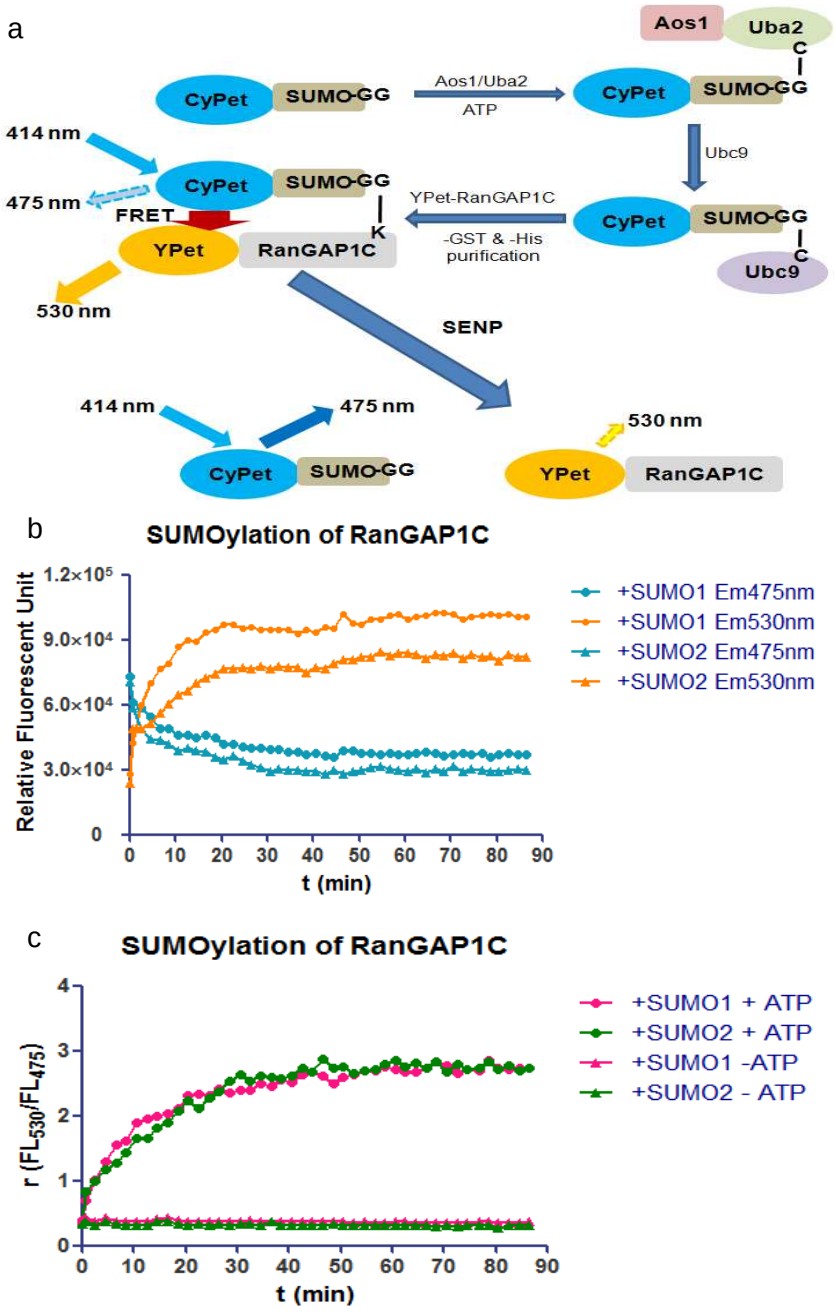

Figure 23. FRET-based protein assay to monitor the SUMO-RanGAP1C conjugation and deconjucation *in vitro*. (a) principle of FRET-based protein assay; (b) fluorescent emission at 475nm and 530nm can be used to monitor SUMO1/2 conjugation under the excitation of 414nm (with ATP); (c) fluorescent emission ratio (FL_{530}/FL_{475}) of SUMO1/2 conjugation under the excitation of 414nm (with/without ATP).

To obtain the pure substrate in the next step of protease kinetics study, different tag affinity purification methods were used: 6xHis-Ni and GST (glutathione S-transferase) –glutathione.

The GST sequence was incorporated into the bacterial expression vector (pGEX4T-1, GE-Healthcare) alongside the gene sequence encoding YPet-RanGAP1C. Induction of protein expression from the tac promoter resulted in expression of a fusion protein: GST-YPet-RanGAP1C. The GST tag has the size of 220 amino acids (~26kDa), which, compared to other tags like the myc- or the FLAG-tag, is quite big. Agargose beads coated with glutathione, the GST substrate, can bind to GST-fused YPet-RanGAP1C. The free reduced glutathione added to agarose beads could release the GST-YPet-RanGAP1C.

All the recombinant proteins were tagged with 6xHis, except YPet-RanGAP1C. The reaction system of SUMOylation included CyPe-SUMO1/2, Aos1, Uba2, Ubc9 and YPet-RanGAP1C. After SUMOylation, the reaction system was firstly flow through agarose beads coated with glutathione to bind CyPet-SUMO1/2-RanGAP1C-YPet and unSUMOylated YPet-RanGAP1C, get rid of the SUMO E1, E2 enzyme as well as the unused CyPet-SUMO1/2. The eluted proteins were then flow through Ni-NTA agarose beads to bind the CyPet-SUMO1/2-RanGAP1C-YPet, get rid of the unSUMOylated YPet-RanGAP1C. The SUMOylated RanGAP1C was eluted by imidazole and dialyed over night to remove the extra salt. The same size of CyPet-SUMO1-RanGAP1C-YPet-GST and CyPet-SUMO2-RanGAPC-YPet-GST shown on the polyacrylamide gel

confirmed that there was no polySUMO2 conjugated to RanGAP1C derived from the performed SUMOylation (Fig. 24).

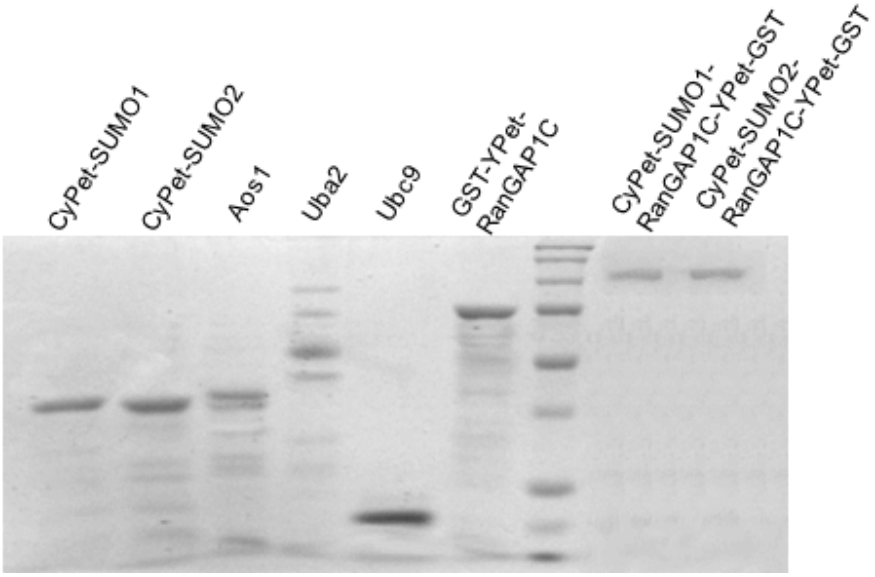

Fig. 24 Coomassie staining of purified proteins in SUMO conjugation assay. From left to right: CyPet-SUMO1 (~40 kD) CyPet-SUMO2 (~40 kD), Aos1 (~38 kD), Uba2 (~65 kD), Ubc9 (~ 22 kD), GST-YPet-RanGAP1C (~ 75 kD), protein marker, CyPet-SUMO1-RanGAP1C-YPet-GST (~113 kD) and CyPet-SUMO2-RanGAP1C-YPet-GST (~113 kD).

The SUMOylated RanGAP1C were then incubated with different SENPs in 1:1 molar ratio at 37℃ for 1 hr. The fluorescent e mission ratio (FL_{530}/FL_{475}) under the excitation of 414nm was used to characterize the changes of FRET signals. The results indicated that different SENPs exhibit various specificities towards SUMO deconjugation: both SENP1C and SENP2C can deconjugate SUMO1 and SUMO2 from target substrate (RanGAP1C); SENP5, SENP6 and SENP7 prefer SUMO2 in SUMO deconjugation (isopeptidase activity), and

exhibit poor activities toward SUMO1 deconjugation. The observations were in the agreement with previous studies [54, 60-65]. Here, as mature form of SUMO2 and SUMO3 are 95% similarity, only SUMO1 and SUMO2 deconjugation were compared by different SENP paralogs (Fig. 25).

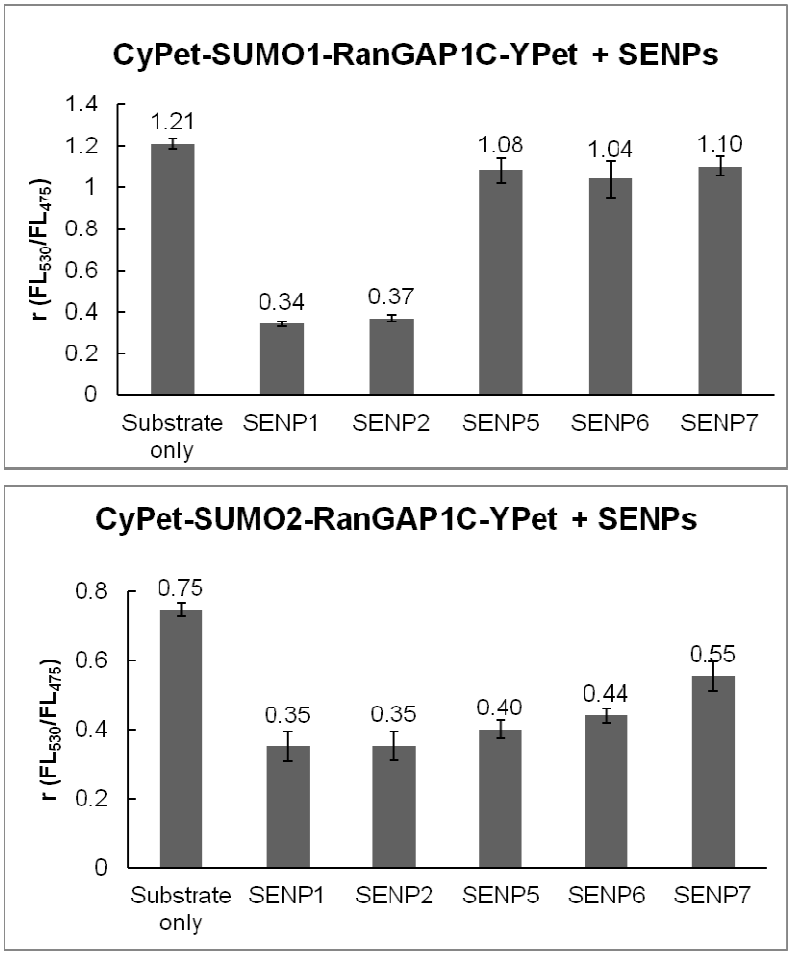

Figure 25. Characterization of SUMO1/2 deconjugation from RanGAP1C by SENP1/2/5/6/7C in developed FRET-based protease assay.

Quantitative FRET analysis in protease kinetic study of SUMO deconjugation

SENP can function as endopeptide to mature SUMO precursor or as isopeptide to deconjugate SUMO from its target protein. As both SENP1C and SENP2C can mature pre-SUMO1/2/3 or deconjugate SUMO1/2 from RanGAP1C in long-term hydrolysis study (Fig. 11& Fig. 24), the kinetics of the two processes have to be studied to compare the different activities of SENPs.

To study the differences of endo- and iso-peptidase activities of SENP1C, the same concentration (100 nM) of CyPet-(pre-SUMO1/2)-YPet and CyPet-SUMO1/2-RanGAP1C-YPet-GST were incubated with SENP1C (0.5 nM) as 200:1 molar ratio respectively. The digestions of substrates were monitored within 5 min with 10 sec interval (Fig. 26) and the initial velocities under ($[S] = 100\,nM$) were derived by the quantitative FRET analysis in internal calibration method (Table 9). The results indicated that SENP1 exhibited higher activity toward SUMO deconjucation than pre-SUMO maturation (especially for SUMO2). Interestingly, the preferences were different for the same SUMO-SENP pair. In pre-SUMO maturation, SENP1 preferred pre-SUMO1 than pre-SUMO2, but in the process of SUMO deconjugation, SUMO2 was preferred by SENP1 than SUMO1.

.

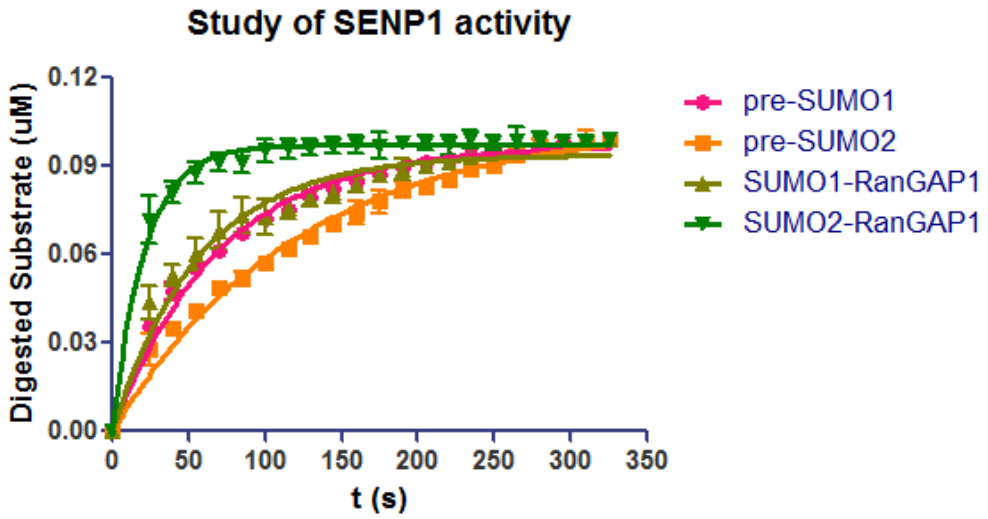

Figure 26. Quantitative FRET analysis to compare SENP1C's endo- and iso-peptidase activities. 0.1 µM Substrate CyPet-(pre-SUMO1)-YPet, CyPet-(pre-SUMO2)-YPet, CyPet-SUMO1-RanGAP1C-YPet-GST and CyPet-SUMO2-RanGAP1C-YPet-GST were incubated with 0.5 nM SENP1C in low salt Tris buffer at 37°C. Reactions were monitored as the fluorescent emission at 475 nm and 530 nm (under the excitation of 414 nm) for every 10 seconds in the first 5 minutes. The digested substrate concentrations were calculated based on the developed quantitative FRET analysis in internal calibration method. Data were plotted in GraphPad Prism 5 and nonlinear regression.

SENP1 Substrate	**Pre-SUMO1**	**Pre-SUMO2**	**SUMO1-RanGAP1**	**SUMO2-RanGAP1**
v_0 **(x10^{-3} µM/s)**	1.39 ± 0.03	0.89 ± 0.03	1.65 ± 0.07	4.60 ± 0.03

Table 11. The initial velocity (v_0) of pre-SUMO1/2 maturation and SUMO1/2-RanGAP1C deconjugation by SENP1C derived by quantitative FRET analysis in internal calibration method (substrate concentration was 0.1 µM).

CyPet-SUMO1-RanGAP1C-YPet and SENP1C were used as an example here to demonstrate the quantitative FRET analysis in protease kinetic study of SUMO deconjugation.

As analyzed above, the change of fluorescent emission of 475 nm and 530 nm (under the excitation of 414 nm) can be used to characterize the kinetic process of SENP1C hydrolysis toward its substrate (CyPet-SUMO1-RanGAP1C-YPet-GST).

Internal calibration method of quantitative FRET analysis was used here to derive the initial velocities under different substrate concentrations (Fig. 27a and listed in Table 12-a). The kinetic constants were derived by plotting the initial velocities versus substrate concentration in Michaelis-Menten equation (Fig. 27b) and listed in Table 13. The values of derived kinetic constants were close to the previous studies [61].

Similarly, the kinetics parameters determined by medium remaining substrate concentration and velocities (fluorescent reading analyzed by internal calibration method) were also analyzed for other (pre-SUMO)-SENP pairs and listed in Table 12-b and Table 13.

a

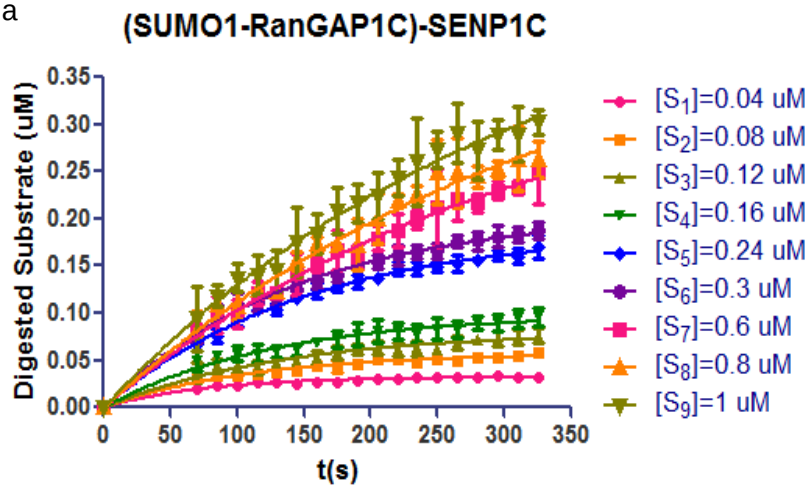

b

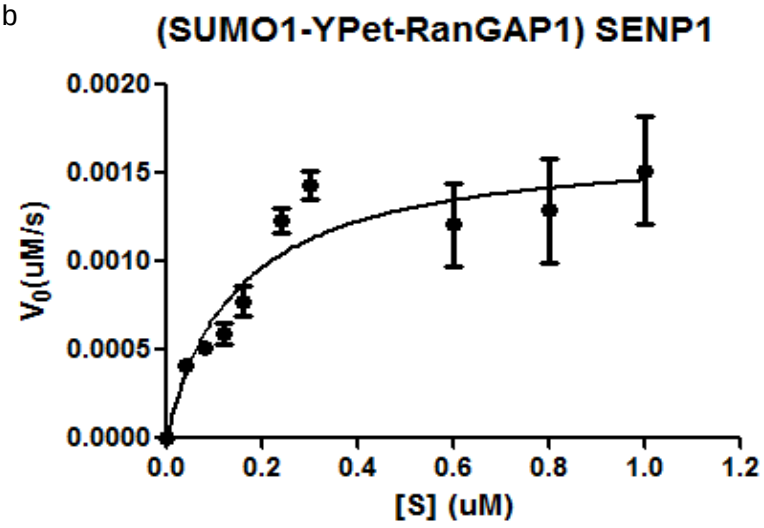

Figure 27 Quantitative FRET analysis in study the protease kinetics of SUMO1-RanGAP1C deconjugation by SENP1C. (a) Initial velocities determinations under different substrate concentrations; (b) Michaelis–Menten graphical analysis. Data were plotted and analyzed by GraphPad Prism 5 and nonlinear regression (one phase association model for (a) and Michaelis-Menten model for (b)).

a

[CyPet-SUMO1-RanGAP1C-GST] (μM)	v_0 (x10^{-3} μM/s)
0.04	0.41 ± 0.032
0.08	0.51 ± 0.038
0.12	0.59 ± 0.060
0.16	0.78 ± 0.081
0.24	1.23 ± 0.070
0.3	1.43 ± 0.081
0.6	1.21 ± 0.232
0.8	1.29 ± 0.295
1	1.52 ± 0.305

b

SENP1 Total [CyPet-(pre-SUMO2)-YPet] (μM)	v in 160-280 sec time range (x10^{-3} μM/s)	Remaining $[S]$ at 220 sec (μM)
0.04	0.045 ± 0.0114	0.030 ± 0.00250
0.08	0.072 ± 0.0173	0.064 ± 0.00380
0.12	0.12 ± 0.0257	0.093 ± 0.00565
0.16	0.14 ± 0.0384	0.13 ± 0.00845
0.24	0.27 ± 0.0286	0.18 ± 0.00628
0.3	0.35 ± 0.0319	0.22 ± 0.00701
0.4	0.37 ± 0.0573	0.32 ± 0.0126
0.5	0.53 ± 0.0819	0.38 ± 0.0180
0.6	0.67 ± 0.0794	0.45 ± 0.0175
0.8	0.77 ± 0.0911	0.63 ± 0.0200
1	0.91 ± 0.110	0.80 ± 0.0242

Table 12. The initial velocity (v_0) of SUMO1-RanGAP1C deconjugation by SENP1C derived by quantitative FRET analysis in internal calibration in initial velocity versus total substrate concentration (a) and medium velocity versus medium remaining substrate concentration method (b).

Analysis Method	K_M **(μM)**	k_{cat} **(s^{-1})**	k_{cat}/K_M **(x 10^6 $M^{-1}\cdot s^{-1}$)**
Quantitative FRET analysis (original velocity and total substrate concentration)	0.14 ± 0.046	6.26 ± 0.63	43.47 ± 14.57
Quantitative FRET analysis (medium velocity and substrate concentration)	2.18 ± 0.93	12.89 ± 4.39	5.91 ± 3.226
Ratiometric FRET analysis [61]	0.15 ± 0.015	8.27 ± 0.26	55.13 ± 5.78

Table 13. Kinetic parameters of SUMO1-RanGAP1C deconjugation by SENP1C determined by quantitative FRET analysis and compared to those derived from ratiometric FRET analysis [61].

.

Discussion

Förster resonance energy transfer (FRET) technology has been widely used in biological and biomedical research, and it is a very powerful tool for elucidating protein interactions in either dynamic or steady state. A variety of FRET-based protease assays were developed to study the DUBs or SENPs, including the Lanthanide assay combined with TR-FRET technology and the genetically tagged ECFP-YFP on interested SENP substrate[61, 166, 167, 170, 171, 180]. Most of the previous studies use two-channel ratiometric analysis to quantify the FRET signals.

The accurate determinations of kinetics parameters are critical for estimating enzymatic activity, specificity and drug candidate evaluation. In Chapter I, I developed a quantitative FRET analysis in protease kinetic study to relate the fluorescent signal change at 530 nm to digested substrate concentration during the pre-SUMO1's maturation process. Compare to the ratiometric FRET analysis, the developed quantitative FRET analysis considered the direct emissions of donor and acceptor at acceptor's emission wavelength. The pre-established standard curve can correlate the concentrations of substrate and product to detected fluorescent signals.

In this chapter, the standard curve-dependent quantitative FRET analysis was improved to internal calibration method to quantify the FRET signal. The emission of CyPet can be directly obtained by the spectrometer, which still can

be divided into two parts: undigested CyPet-(pre-SUMOs)-YPet and digested CyPet-SUMOs, instead of calculated from the pre-established standard curves. The fluorescent signal were in linear curve to fit the protein concentrations in the standard curves establishment, the values of slope were derived to fit the linear relationship of fluorescent readings versus protein concentrations. The variations of slopes cannot be avoided, and thus brings the inaccuracy to the kinetic constants determination. Moreover, the different batches of protein sample prepare for standard curve establishment have variations in fluorescent emissions resulting from pipetting variations, impure constitutes of protein samples, maturation level of fluorescent proteins and variations from protein concentration determination based on the Beer's Law in application of Bradford assay. Except to the variations of protein samples, it has to be noted that the variations from fluorometer cannot be ignored in the study to protease kinetics. According to the review of quantitative FRET analysis [172], the value of FRET efficiency was not repeatable for the detection of FRET signal in only one channel (donor with or without the existence of acceptor), more accurate and robust results can be obtained by observing multiple channels instead of only one channel. The comparisons between the previous standard curve-dependent and the improved internal calibration method detected quantitative FRET analysis (Table 8) indicated that the standard errors of standard curve-dependent method were larger than those of the internal calibration method. The initial velocities of pre-SUMO3's maturation derived from standard curve-dependent

method even cannot fit the Michaelis-Menten equation due to the large variations. The improved internal calibration method for quantitative FRET analysis in protease kinetic study not only simplified the operation as no steps for establishment of standard curve, but also helped to minimize the errors in kinetic constants determination.

The crystal structures of pre-SUMO1/3-SENP1 (C603A) [59, 61, 186], pre-SUMO1-SENP1 (C603S) [185] have been characterized before. The crystal structures showed that the scissile bound has the *cis* arrangements of the amide nitrogen, which is an important feature of the proteolytic mechanism of SENP1 [61]. The C-terminal five residues (tail) of pre-SUMO1 adopt an elongated strand structure that fits into a central cleft in SENP1. The strand is stabilized by the hydrogen bond between His98 (SUMO1) and Gly600 of SENP1 (Fig. 28). The di-Gly motif at the C-terminus of pre-SUMO1 is capped by Trp465 of SENP1, effectively enclosing the C terminus inside a tunnel. The SUMO3's (referred as SUMO2 in ref. [61]) Pro95 position has a negative effect due to its rigid structure having an inhibitory effect on orientation of the scissile peptide bond. In addition, another mutation of C603S of SENP1 indicated that the C-terminal peptides of pre-SUMOs might not be the only factor to change the SUMO precursor's maturation efficiency [186]. An observed specific binding groove generated from the backbone oxygen Asn599, as well as the Trp465, His529 and Trp534 in the catalytic triad of SENP1, may also contribute to affect the maturation efficiency.

SENP1's pre-SUMO1 maturation has been studied by gel-based analysis and FRET-based protease assay [59, 61, 62, 164]. The proteolytic efficiency of pre-SUMO1 is the highest followed by pre-SUMO2 and then pre-SUMO3. The C-terminal fragment after the di-Gly is essential for efficient maturation as the preference could be reversed by swapping SUMO tails between respective SUMO isoforms [62]. However, the SUMO2 used in ref. [59] was tagged another 9 amino acids of pre-SUMO3's tail after SUMO2's VY tail, which cannot show the intrinsic maturation of pre-SUMO2 from the results. The SUMO2 referred in ref. [61] was actually SUMO3 as they followed another definition of SUMO2/3. Due to the limitation of gel-based technology, the quantitative kinetics of the maturation process cannot be provided. According to our results, the preference of SENP1 to pre-SUMO1 and pre-SUMO2 were almost the same, both in the binding step and the catalysis step, and the maturation was much more efficient than pre-SUMO3, which was comparable to the previous studies as pre-SUMO1>pre-SUMO3. The initial velocity of pre-SUMO2's maturation by SENP1 was slightly smaller than that of pre-SUMO1's maturation (Fig. 26 & Table 11) under the condition of same substrate concentration, which indicated that pre-SUMO1 is a little bit more preferred by SENP1 in pre-SUMO maturation. As the derived value of K_M and k_{cat} were quite close to each other, the pre-SUMO's maturation preferences was not obvious.

Referred to ref. [61], the value of K_M of pre-SUMO3'smaturation by SENP1C was close to that of pre-SUMO1's maturation by SENP1, but the values of k_{cat}

differed by 50-fold. The conclusion from their results was the ability of SENP1 to differentially cleave SUMO-1 over SUMO-3 is not a consequence of preferential binding of substrate but is based on more efficient catalysis. Even though we obtained the similar value of K_M/k_{cat} compared to their results, the values of individual K_M and k_{cat} were quite different: the values of K_M upon pre-SUMO1 and pre-SUMO3'S maturation by SENP1 differed by 10-fold and the values of k_{cat} differed by 5-fold (Table 8). Based on the structure analysis in their study, the obtained crystal structure of pre-SUMO3-SENP1 complex was in the form of non-productive with the mutation of C603A. The rigid structure of Pro95 of pre-SUMO3 could inhibit the binding of SENP1 to pre-SUMO3 and thus affect the value of K_M. In that way, the ability of SENP1 to prefer pre-SUMO1 than pre-SUMO3 in maturation is the consequence of preferential binding and catalysis. The consideration of donor and acceptor's direct emission in FRET signal quantification provided more accurate and consistent determinations of kinetic constants. As stated before, the overestimations of FRET signal might not greatly affect the final k_{cat}/K_M kinetic ratio, but the effect is more obvious when studying the individual parameters, K_M and k_{cat}, which are important in determining the rate-limiting step and inhibitor potency of enzymes.

It was observed with little appreciable difference between structure complex pre-SUMO1-SENP1 (C603A) and SENP1 (C603A)-RanGAP1-SUMO1 with the exception that the side chain of His533 (part of the catalytic triad) has an altered conformation [61]. The activities of SENP1 to mature pre-SUMO1 or deconjugate

SUMO1 from RanGAP1 were very similar as the value of initial velocity under the same substrate concentration, K_M and k_{cat} were close to each other (Fig. 26, Table 8 and Table 11).

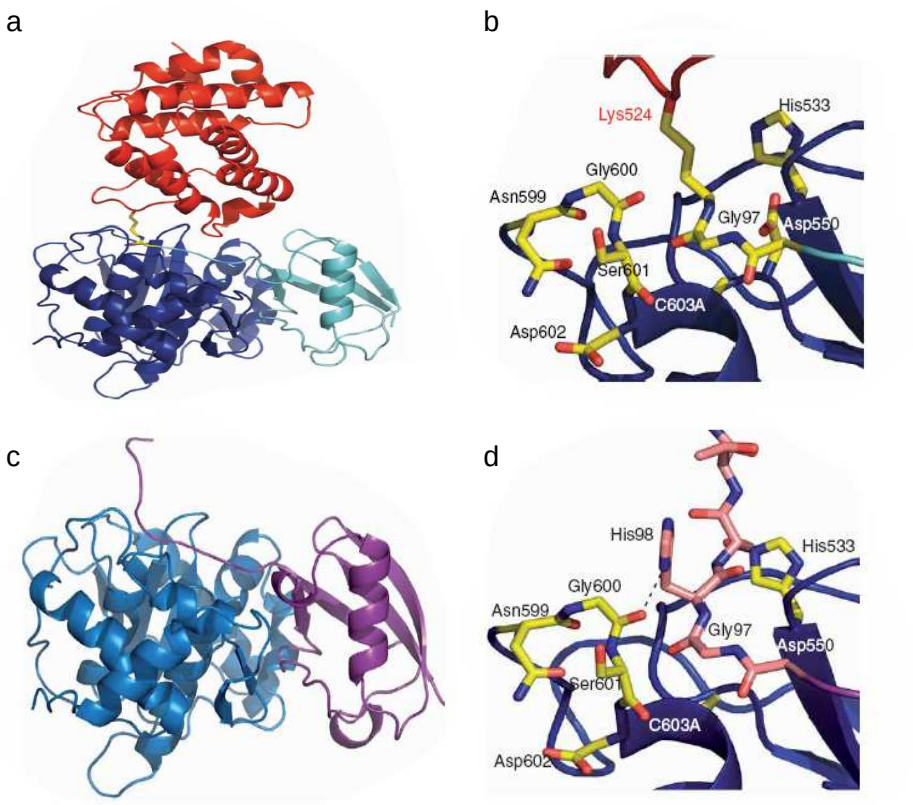

Figure 28 Structure of the complex of SENP1 C603A bound to SUMO1–modified RanGAP1 (a, b) and full-length SUMO-1 (c, d) [61]. (a) Overall structure of the complex. RanGAP1 is shown in red ribbon, SENP1 C603A in blue and SUMO-1 in turquoise. Isopeptide bond between Lys524 of RanGAP1 and Gly97 of SUMO1 is shown as sticks with carbon yellow, nitrogen blue and oxygen red; (b) Details of the complex in (a); (c) SENP1(C603A)–SUMO1-FL complex. Cyan, SENP1; purple, SUMO1-FL; (d) Detail of the complex in (c), with SENP1 in dark blue and carbons of SUMO-1-FL in pink.

Previous studies of SENP2 indicated that the pre-SUMO2 (shortest tail, 2 amino acid) was processed more efficiently than pre-SUMO1 (medium tail, 5 amino acids), and pre-SUMO1 was processed more efficiently than pre-SUMO3 (longest tail, 11 amino acids). The preference could be reversed by swapping SUMO tails between respective SUMO isoforms [60]. The crystal structures of nonproductive complex SENP2 with pre-SUMO1/2/3 have been elucidated previously [60, 63] which can explain the SENP2's maturation preference. As a cysteine protease, there is a covalent thiohemiacetal bond between Cys548 of SENP2 to Gly97 of pre-SUMO1or Gly93 of pre-SUMO2/3. Cys548, His475 and Asp495 residues form the catalytic triad of SENP2. Residues Trp410 is involved in forming a constricted hydrophobic tunnel which di-Gly motif of pre-SUMOs has to pass through. The highest preference of pre-SUMO2 by SENP2 dues to the kinking position Gly92 which directs SENP2's Trp410 rotated nearly 180° around its Cβ carbon from the position observed in (pre-SUMO1)-SENP2 complex. More complicated SENP2-(pre-SUMO3) structures suggested that the extended SUMO3's tail makes fewer contacts to the SENP2 surface and is positioned away from Cys548. Trp410 is rotated away from the active site. These effects make the lowest preference of pre-SUMO3 by SENP2 (Fig. 29).

However, the previous studies applied gel-based western blot method of SENP2 cannot provide accurate kinetics properties. According to their results [63], the K_M was similar for pre-SUMO2 (2.0 ± 0.6 μM) and pre-SUMO3 (2.2 ± 0.3 μM) with SENP2, and was much smaller than the value of pre-SUMO1 (27.9 ± 3.7

μM). The K_M value of the bind step is not consistent to the discovery of the nonproductive crystal structures of SENP2-(pre-SUMO1/2/3). Moreover, the k_{cat}/K_M ratio obtained by western-blot analysis was SENP2 preferred pre-SUMO2 (3.8 x 10^5 $M^{-1}{\cdot}s^{-1}$)>pre-SUMO3 (5.0 x 10^4 $M^{-1}{\cdot}s^{-1}$)>pre-SUMO1 (2.6 x 10^4 $M^{-1}{\cdot}s^{-1}$). The results were also not in agreement with other studies [60, 164]. However, the values of kinetic constants derived from the developed quantitative FRET-based protease assay followed the previous discoveries as SENP2 preferred pre-SUMO2 (8.2 x 10^6 $M^{-1}{\cdot}s^{-1}$)>pre-SUMO1 (7.8 x 10^5 $M^{-1}{\cdot}s^{-1}$)>pre-SUMO3 (1.2 x 10^5 $M^{-1}{\cdot}s^{-1}$). Also, the values of derived K_M indicated the difficulties of SENP2 binding to pre-SUMO2 (0.048 μM) <pre-SUMO1 (4.49 μM) <pre-SUMO3 (12.06 μM), or in other words, (pre-SUMO2)-SENP2 complex was tighter than (pre-SUMO1)-SENP2, then (pre-SUMO3)-SENP2. Compare to the value of individual K_M and k_{cat}, the preference of pre-SUMO1/2/3's maturation by SENP2 was mainly affected by the binding step rather than the catalytic step.

In the study of SENP2's endopeptidase activities, compare to biochemistry western-blot assay, the developed quantitative FRET-based assay can provide more accurate and convincible results of kinetic constants determination.

It has to be noted that FRET signal can only provide the relative change of distance between the protein pairs, which may result from the conformational change or due to the protein pair dissociation or association. The conformational change of substrate has to be studied in the future to quantify the effect in detected FRET signal change. Nevertheless, the effects like conformational

change and electrostatic change result from the tagged proteins, CyPet, YPet and GST, have to be elucidated in the future to obtain more accurate and convincible kinetic studies (even though it was discovered the tagged fluorescent proteins did not affect protein activities [167]).

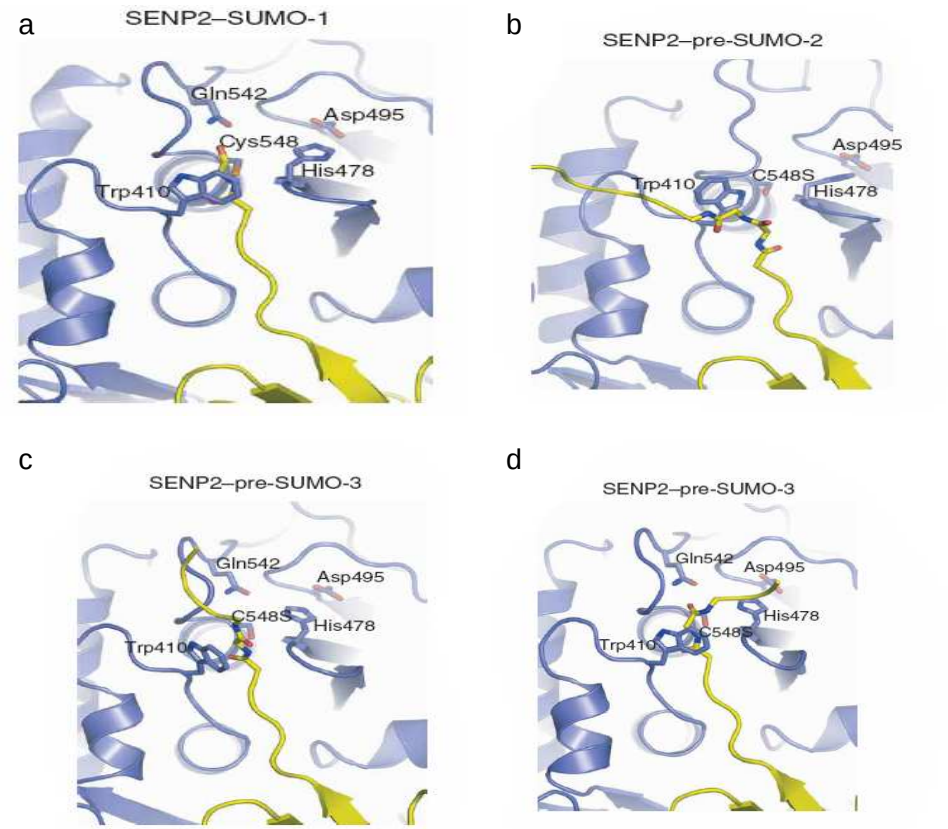

Figure 29 Structure of the SENP2–SUMO precursor complexes [63]. (a–d) Ribbon representations of SENP2 (blue) complexes with indicated SUMO molecules (yellow): transition-state complex with SUMO-1 (a; PDB 1TGZ) [60]; complex with pre-SUMO-2, including the C-terminal 6xHis tag (b); and nonproductive (c) and productive (d) complexes with pre-SUMO-3. Catalytic residues are shown in bond representation.

CHAPTER III: Expanded Application of Developed FRET-based Protease Assay in Enzymatic Studies

Abstract

SUMO4, the latest discovered SUMO paralog, has been discovered in regulation a series of signaling pathway in carcinoma genesis, inflammation and type I diabetes. The biological mechanism of pre-SUMO4 maturation is still unclear as no SENP displays endopeptidase activity toward pre-SUMO4. Different mutations were generated to reverse pre-SUMO4 to pre-SUMO2, which is preferred by SENP in maturation, based on electrostatic perturbative design. The effects of different mutations were studied in the developed FRET-based protease assay, the quantified in the methodology described before.

Product inhibition is a very essential negative feedback in controlling metabolic pathway. Quantitative FRET analysis was used to derive the product (SUMO1)-enzyme (SENP1) binding affinity K_d as well as product inhibition IC_{50} in pre-SUMO1 maturation process. The obtained real K_M was less than 50% of the apparent K_M from Michaelis-Menten analysis. More importantly, the study of product inhibition of quantitative FRET analysis indicated the possibility of characterization of selected chemical compound inhibitors from HTS assay.

The application of quantitative FRET analysis in protease kinetics study was expanded to study the biological mechanism of pre-SUMO4's maturation and product inhibition.

Introduction

Proteases, also known as proteolytic enzymes, are enzymes that catalyze the breakdown of proteins by hydrolysis of peptide bonds. Proteases are extremely important signaling molecules that are involved in numerous vital processes, including proliferation and apoptosis, cellular signal transductions, protein maturation and trafficking, and represent potential drug targets for diseases ranging cardiovascular disorders, autoimmune diseases, metabolic diseases to cancers [174, 175, 187]. Kinetic analysis of enzyme-catalyzed reactions is the most commonly used means of elucidating enzyme mechanism and, especially when coupled with protein engineering, identifying catalytically relevant structural components.

SUMOylation is a reversible post-translational modification that targets a variety of proteins in control of diverse cellular mechanisms such as subcellular localization, protein-protein interactions, cell cycle, cell survival, or transcription factor activity. The human genome encodes four distinct SUMO proteins: SUMO1-SUMO4. SUMO1-SUMO3 are ubiquitously expressed, whereas SUMO4 seems to have a tissue- or organ-dependent distribution, and only be found to express mainly in the kidney, lymph node and spleen [188]. Recent studies also demonstrated high levels of SUMO4 expression in dendritic cells (DCs) and moderate levels of SUMO4 expression in the pancreatic islets [189]. The characterization of SUMO4 expression in immune cells and pancreatic islets

provides a foundation for the demonstration of its role in the pathogenesis of Type 1 diabetes (T1D).

Nuclear factor κB (NFκB) is a family of transcription factors that is associated with immune response, inflammation, cell survival and apoptosis. In most cell type, NFκB complexes are usually sequestered in the cytoplasm in an inactive form via a non-covalent interaction with inhibitory proteins known as IκBs. In response to multiple stimuli such as cytokines, viral and bacterial pathogens and stress-inducing agents, the NFκB /IκB complex become dissociated via phosphorylation of the conserved serine residues in the N-terminal portion of IκB, thereby leading to the nuclear translocation of NFκB, which then activates the transcription for immune responsive genes. Dysregulation of the NFκB signaling pathway has long been shown to be involved in the pathogenesis of a number of human autoimmune diseases as well as T1D [190]. SUMO4 was characterized to interact with IκB [188], and thus could be a negative feedback regulator for the NFκB signaling pathway. JAK/STAT signaling pathway is a typical pathway in regulating numerous aspects of immune response. STAT comprises a family of several transcription factors that are activated by a variety of cytokines, hormones and growth factors. They are activated through tyrosine phosphorylation, mainly by JAK kinases, which lead to their dimerization, nuclear translocation and regulation of target gene expression. The JAK/STAT signaling pathway is tightly controlled by multiple negative regulatory mechanisms including the PIAS family (repression of STAT DNA binding activity). PIAS were

found to be SUMO E3 ligases that stimulate the attachment of SUMO to its target proteins. SUMO4 can suppresses STAT1 DNA binding activity by direct SUMOylation [189], and result in a down regulation of STAT transcriptional activity. Activator Protein-1 (AP-1) regulates transcriptions for a broad array of genes implicated in many of the major physiological processes, such as cell proliferation, differentiation, organogenesis, apoptosis and response to stress [191]. More importantly, it is also a necessary effecter in a wide variety of pathological situations, such as tumor genesis and autoimmune pathogenesis [192, 193]. SUMO4 can repress AP-1 transcriptional activity by directly SUMOylation or indirect inhibition of the AP-1 upstream activators [194-196]. However, the role of SUMO4 remains enigmatic, as it is presently unclear whether it can be processed to its mature conjugation-competent form *in vivo* [188, 197].

Charge plays a significant role in biological structure, dynamics, interactions and function. Charge and the electrostatic properties of biomolecules are significant for protein stability, the recognition and binding of proteins and ligands in protein-protein or protein-ligand interactions, and in enzymatic catalysis [198-201].

SUMO4 and SUMO2 precursors exhibit very high sequence similarity, which only 14 amino acids different out of the total 95. Most importantly, pre-SUMO4 and pre-SUMO2 share the same SUMO tail (-VY) after di-Gly SUMO active motif (Fig. 30). One notable difference between pre-SUMO2 and pre-SUMO4 is the net charge: the net charge of pre-SUMO2 is -3 while the net charge of pre-SUMO4 is 0. Based on this observation, one hypothesis was proposed in the study that the

differences in the electrostatic character of pre-SUMO4 prevent the formation of the stable bound complex with SENP as well as the prevention of the following catalysis. The collaborated work was performed by me and Dr. Chris Kieslich in Dr. Dimitrios Morikis' group (Department of Bioengineering, University of California-Riverside). The aim of the collaborated work was to identify a minimum set of pre-SUMO4 mutations necessary to regain catalytic ability, at least the SUMO-SENP binding ability, based on electrostatic pertubative design.

According to the analysis in Chapter II, pre-SUMO2 is highly preferred by SENP2 in maturation, and the binding between (pre-SUMO2)-SENP2 is the tightest due to the smallest value of K_M. In that way, SENP2 was selected in the study as the functional protease. The mutations were generated based on electrostatic on the model of (pre-SUMO4)-SENP2 complex.

```
SUMO-2      MADEKPKEGVKTENNDHINLKVAGQDGSVVQFKIKRHTPLSKLMKAYCERQGLSMRQIRF
SUMO-4      MANEKPTEEVKTENNNHINLKVAGQDGSVVQFKIKRQTPLSKLMKAYCEPRGLSVKQIRF

SUMO-2      RFDGQPINETDTPAQLEMEDEDTIDVFQQQTGGVY 95
SUMO-4      RFGGQPISGTDKPAQLEMEDEDTIDVFQQPTGGVY 95
```

Figure 30. Sequence alignment for pre-SUMO2 and pre-SUMO4. Positions with differing amino acids are shown in red. Residues 94-95 are pre-SUMO tail, which is cleaved by SENP in the maturation.

Any substance that reduces the velocity of an enzyme-catalyzed reaction can be considered to be an "inhibitor". The inhibition of enzyme activity is one of the

major regulatory devices of living cells, and one of the most important diagnostic procedures of the enzymologist. The activity of an enzyme can be blocked in a number of ways. Inhibitors can act by irreversibly binding to an enzyme and rendering it inactive. This typically occurs through the formation of a covalent bond between some group on the enzyme molecule and the inhibitor. Some inhibitors can bind so tightly to the enzyme that they are for all practical purposes permanently bound. These inhibitors form a special class known as tight binding inhibitors. In the most commonly encountered form, inhibitors, which are known as classical reversible inhibitors, are molecules that bind reversibly to enzymes with rapid association and dissociation rates.

To understand the molecular basis of reversible inhibition, it is useful to reflect upon the equilibria between the enzyme, its substrate, and the inhibitor that can occur in solution. Fig. 31 provides a generalized scheme for the potential interactions between these molecules. In the scheme, K_s is the equilibrium constant for dissociation of the ES complex to the free enzyme and the free substrate, K_i is the dissociation constant for the EI complex, and k_p is the forward rate constant for product formation from the ES or ESI complexes. The factor α reflects the effect of inhibitor on the affinity of the enzyme for its substrate, and likewise the effect of the substrate on the affinity of the enzyme for the inhibitor. The factor β reflects the modification of the rate of product formation by the enzyme that is caused by the inhibitor. An inhibitor that completely blocks enzyme activity will have β equal to zero. An inhibitor that only partially blocks

product formation will be characterized by a value of β over 0 and 1. An enzyme activator, on the other hand, will provide a value of β greater than 1. The values of α and β provide information on the degree of modification that on ligand (substrate or inhibitor) has on the binding of the other ligand, and they define different modes of inhibitor interaction with the enzyme.

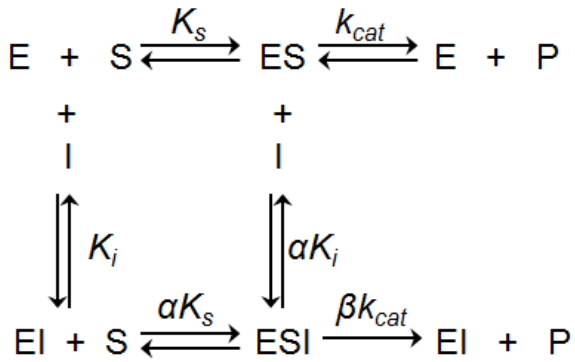

Figure 31. Equilibrium scheme for enzyme turnover in the presence and absence of an inhibitor.

According to the mechanism, there are three modes of reversible inhibition (Fig. 32). Competitive inhibition (Fig. 32-a) refers to the case of the inhibitor binding exclusively to the free enzyme and not at all to the ES binary complex. Thus, referring to the scheme in Fig. 31, complete competitive inhibition is characterized by values of $\alpha = \infty$ and $\beta = 0$. In competitive inhibition, inhibitor and substrate compete for the same enzyme form and generally bind in a mutually exclusive fashion; that is, the free enzyme finds either a molecule of inhibitor or a molecule of substrate, but not both simultaneously. Most often competitive inhibitors function by binding at the enzyme active site.

Noncompetitive (Fig. 32-b) inhibition refers to the case in which an inhibitor displays binding affinity for both the free enzyme and the enzyme-substrate binary complex. Hence, complete noncompetitive inhibition is characterized by a finite value of $\alpha = \beta = 0$. Noncompetitive inhibitors do not compete with substrate for binding to the free enzyme; hence they bind to the enzyme at a site distinct from the active site. Uncompetitive inhibitors (Fig. 32-c) bind exclusively to the ES complex, rather than to the free enzyme form. Complete uncompetitive inhibitors are characterized by $\alpha \ll 1$ and $\beta = 0$.

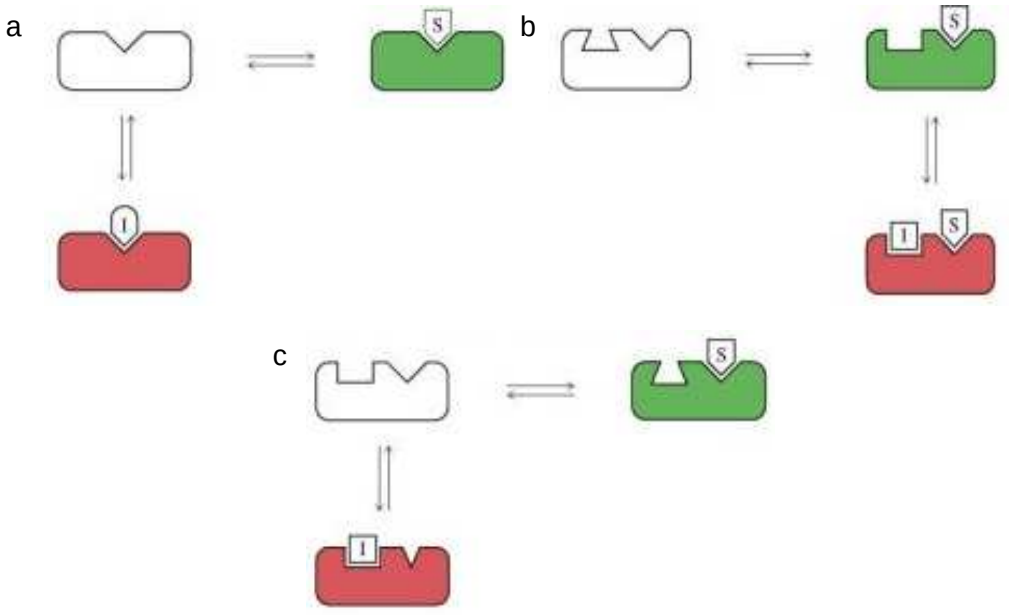

Figure 32. Representations of the three major forms of inhibitor interactions with enzymes: (a) competitive inhibition; (b) uncompetitive inhibition; (c) noncompetitive inhibition.

Product inhibition is a type of enzyme inhibition where product molecule bears some structural resemblance to the substrate and can thus bind to the active site of the enzyme. Product binding blocks the binding of further substrate molecules to inhibit the substrate's activity. Product inhibition is important in the regulation of metabolism as a form of negative feedback controlling metabolic pathways. This type of inhibition is also an important topic in biotechnology as overcoming this effect can increase the yield of a product. Since the product acts as an inhibitor to compete "occupying" the active sites of enzymes with substrate, product inhibition can be assumed to be "competitive". The dissociation constant of enzyme-inhibitor interactions, referred to as inhibitor constant K_i, is the dissociation constant K_d between the enzyme and product [202]. Considering the inhibition from the product, the apparent K_M values derived by the Michaelis-Menten analysis are larger than the value of actual K_M.

The concentration of inhibitor required to achieve a half-maximal degree of inhibition is referred to as the IC_{50} value, and the equation describing the effect of inhibitor concentration on reaction velocity is related to the Langmuir isotherm equation as follows (Fig. 33):

$$\frac{v_i}{v_0} = \frac{1}{1+\frac{[I]}{IC_{50}}} \qquad \text{[Eq. 22]}$$

where v_i is the initial velocity in the presence of inhibitor at concentration $[I]$ and v_0 is the initial velocity in the absence of inhibitor.

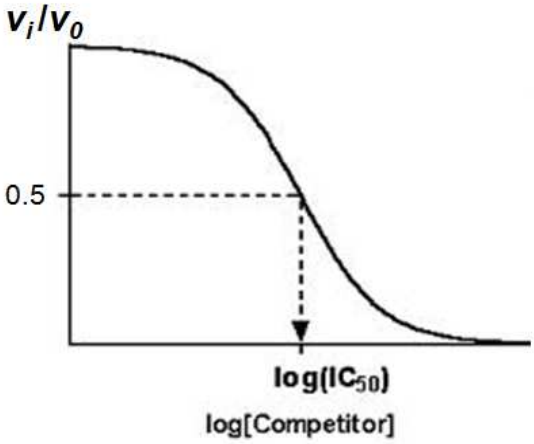

Figure 33. Dose-response plot of enzyme fractional activity as a function of inhibitor concentration. The value of the IC_{50} for the inhibitor can be determined graphically as illustrated.

The relationship between the K_i, $[S]$, K_M and IC_{50} values can be derived from the analyzed velocities and the derivations have been described in detail by Cheng and Prusoff for competitive, non-competptitive and uncompetitive inhibitors [202]. For the competitive inhibitors:

$$K_i = \frac{IC_{50}}{1+\frac{[S]}{K_M}} \qquad \text{[Eq. 23]}$$

In this chapter, I will describe the two extended applications for the developed quantitative FRET analysis in enznmatic studies in: 1) biological mechanism study and 2) product inhibition characterization.

In the first application of study the maturation of pre-SUMO4 by SENP2, 3 sets of mutations were generated on electrostatic analysis of AESOP (analysis of electrostatic similarities of proteins). The effects of mutations on SENPs

catalyzed pre-SUMO4's mutation were compared by the developed quantitative FRET analysis. The generated mutations improved the pre-SUMO4 from a "poor" substrate to a "good" substrate recognized by SENP2. The combination between the electrostatic perturbative design (performed by Dr. Chris Kieslich in Dr. Dimitrios Morikis' group) and the quantitative FRET analysis in protease kinetics study (performed by me) has led to a successful protein engineering case study.

In the second application of characterizing the product inhibition in the (pre-SUMO1)-SENP1 maturation process, the quantitative FRET analysis were used to derive the protein binding affinity (K_d, which was also the K_i) between the SUMO1-SENP1, product (inhibitor)-enzyme, and the IC_{50} value by inhibitor titration. The real K_M was derived upon [Eq. 23] and was about 1/3 of the apparent K_M derived from Michaelis-Menten analysis. Most importantly, the methodology of product inhibition characterization can be developed in the future to be a general approach to characterize reversible protease inhibitors.

Material and Methods

Electrostatic Perturbative Design

There is no available structural data for (pre-SUMO4)-SENP2 interaction as pre-SUMO4 cannot form stable complexes with any SENPs. The crystal structure of the (pre-SUMO2)-SENP2 complex (PDB Code: 2IO0) [63] was used as a template to generate an initial model of the (pre-SUMO4)-SENP2 interaction. The homology modeling software MODELLER was utilized to extend the N-terminal tail of pre-SUMO2 in the (pre-SUMO2)-SENP2 complex.

All electrostatic calculations were performed using the AESOP frame work. All alanine-scan mutations were performed using truncations by AESOP functions, while all non-alanine mutations were performed using the SCWRL4 package [203]. The PDB2PQR utility was used to prepare all structure for electrostatic calculations by incorporating atomic radii and partial charges according to the PARSE forcefield.

Molecular clone of DNA constructs

The point mutations of pre-SUMO4 were introduced by PCR using the QuikChange site-directed mutagenesis kit (Invitrogen) based on the construct CyPet-(pre-SUMO4)-YPet. P90Q mutation was achieved by replacing CCA to CAA; G63D mutation was achieved by replacing GGC to GAC; K21A mutation was achieved by replacing GCG to AAG.

The open reading frame of SENP1C was amplified by PCR and the PCR product was cloned into PCRII-TOPO vector (Invitrogen). The fragments encoding SENP1C were extracted by Sal/NotI digestion and inserted into PCRII-PCRII-YPet plasmid which was linearized by SalI/NotI. After sequences were confirmed, the cDNA encoding YPet-SENP1C was cloned into the NheI/NotI sites of pET28(b) vector with an engineered 6-His on its N-terminus (Novagen).

The open reading frame of SUMO1 was amplified by PCR and the PCR product was cloned into PCRII-TOPO vector (Invitrogen). After the sequences were confirmed, the cDNA encoding SUMO1 was cloned into the SalI/NotI sites of pET28(b) vector with an engineered 6-His on its N-terminus (Novagen).

The mothods of other DNA constructs used in this chapter, which encoding CyPet-(pre-SUMO1/2/4)-YPet, CyPet-SUMO1, SENP1/2C were described in the Material and Methods part in Chapter I (page 49-50).

Recombinant protein expression and purification

Recombinant proteins, used in this chapter, CyPet-(pre-SUMO1/2/4)-YPet, CyPet-(pre-SUMO4P90Q)-YPet; CyPet-(pre-SUMO4P90Q/G63D)-YPet; CyPet-(pre-SUMO4P90Q/G63D/K21A)-YPet; CyPet-SUMO1, YPet-SENP1C, SENP1C, SENP2C, were expressed and purified by Ni-NTA affinity chromatography followed the procedure described in Chapter I (page 51).

The purity of the proteins was confirmed by SDS-PAGE and Coomassie blue staining. Concentrations of protein were determined by Coomassie Plus Protein

Assay (Thermo) with known quantities of bovine serum albumin as standards. Aliquots of final products were stored in -80℃.

Protease assay and western-blot to study the effects of generated mutations in pre-SUMO4 mutation by SENP2

FRET-based assays were conducted by measuring the emission intensity of CyPet at 475 nm and YPet at 530 nm with an excitation wavelength of 414 nm in a fluorescence multiwall plate reader FlexStation II^{384} (Molecular Devices, Sunnyvale, CA).

To test the effects of different mutations in (pre-SUMO4)-SENP2 maturation process, CyPet-(pre-SUMO4)-YPet, CyPet-(pre-SUMO4P90Q)-YPet, CyPet-(pre-SUMO4P90Q/G63D)-YPet and CyPet-(pre-SUMO4P90Q/G63D/K21A) were incubated with SENP2C (1:1 molar ratio) at 37℃ in low salt reaction buffer and transferred into a 384-well plate (glass bottom, Greiner). The final concentration of reacted proteins was 100 nM. Reactions were stopped at 1 hr and were analyzed by fluorometer. Three samples were repeated in each concentration. The results were reported as mean ± SD.

The western blot was performed by standard procedure as described in Chapter I (page 53), except antibodies: 1^{st} antibody 1:1500 5% BSA in TBST (anti-His, Sigma) and 2^{nd} antibody 1:3000 2% milk in TBST (anti mouse, Sigma).

Protease kinetics assay

FRET-based pre-SUMO4 maturation assays were conducted by measuring the emission intensity of CyPet at 475 nm and of YPet at 530 nm with an excitation wavelength of 414 nm in a fluorescence multi-well plate reader (Molecular Devices, Flexstation II^{384}).

CyPet-(pre-SUMO2)-YPet, CyPet-(pre-SUMO4P90Q)-YPet, CyPet-(pre-SUMO4P90Q/G63D)-YPet and CyPet-(pre-SUMO4P90Q/G63D/K21A) was incubated with SENP2C at 37℃ in low salt reaction buffer to a total volume of 80µl and transferred into a 384-well plate. The final concentration of SENP was fixed, and the final concentrations of substrate were varied (Table 14).

SENP1C (nM)	**CyPet-(pre-SUMO2)-YPet (µM)**
0.08	0.01, 0.02, 0.04, 0.06, 0.075, 0.1, 0.125, 0.15, 0.2, 0.25, 0.3
SENP1C (nM)	**CyPet-(pre-SUMO4P90Q)-YPet (µM)**
22.5	2.25, 4.5, 6.75, 9, 13.5, 16.875, 22.5, 28.125,
SENP1C (nM)	**CyPet-(pre-SUMO4P90Q/G63D)-YPet (µM)**
10	1, 2, 3, 4, 6, 10, 12.5, 15, 20, 25, 30
SENP2C (nM)	**CyPet-(pre-SUMO4P90Q/G63D/K21A)-YPet (µM)**
5	0.5, 1, 1.5, 2, 3, 3.75, 5, 6.25, 7.5, 10, 12.5, 15

Table 14. Concentration of protein samples in kinetics studies.

Reactions were tested within original 5 min with 10 sec intervals. One phase association model was used to fit the exponential increased reaction velocity. Data were analyzed by the developed method and plotted in GraphPad Prism V software fitting the Michaelis–Menten equation. Five samples were repeated in each concentration. The results were reported as mean ± SD.

Quantitative FRET analysis in determine the binding affinity (K_d) of product-enzyme interactions

Recombinant proteins CyPet-SUMO1 and YPet-SENP1C were diluted with buffer containing 20 mM Tris-HCl (pH=7.4) and 50 mM NaCl, and mixed in a 384-well plate to 100 µL in each well. The final concentrations of CyPet-SUMO1 in six mixture groups were 0.1 µM, 0.2 µM, 0.35 µM, 0.5 µM, 0.75 µM and 1 µM respectively. In each group YPet-SENP1C was added in increment up to 4.3 µM. The fluorescence emission spectrum of each well was determined by a fluorescence multi-well plate reader FlexstationII^{384} (Molecular Devices, Sunnyvale, CA). The emission intensities at 475 nm and 530 nm were measured at the excitation wavelength of 414 nm with a cutoff filter of 455 nm, and the emission intensity at 530 nm was measured at the excitation wavelength of 475 nm with a cutoff filter of 495 nm. The experiments were repeated three times and the average value of fluorescence intensity was calculated for each specific condition.

Surface plasmon resonance (SPR) assay

All analyses of interaction between SUMO1 and SENP1C were performed on BIACORE X100 system equipped with NTA sensor chips (BIACORE AB, Uppsala, Sweden) at a flow rate of 30 µL/min. For immobilization of proteins, the chip was treated with 500 µM $NiCl_2$ for 1 min before 1 µg/mL purified SENP1C was injected for 120 s and stabilized for 120 s. Then 60-150 µg/mL thrombin-digested SUMO1 was injected for 120 sec and disassociated for 10 min. In order to continuously monitor the non-specific background binding of samples to the NTA surface, SUMO1 was injected into a control flow cell without treatment of $NiCl_2$ and SENP1C. All measurements were performed at 25°C in a buffer containing 10mM HEPES (pH=7.4), 150 mM NaCl, 50 µM EDTA and 0.005% Tween-20. The value of K_d was derived by BIACORE X100 evaluation software ver.1.0 (BIACORE).

Protease assay to characterize product inhibition

IC_{50} value for inhibition of SENP1C by SUMO1 in (pre-SUMO1)-SENP1 maturation was determined with CyPet-(pre-SUMO1)-YPet at 1.5 µM, SENP1C at 3 nM plus SUMO1 titrated from 15 nM to 60 µM. The value of IC_{50} was derived from dose-response plot, which had the form of a Langmuir isotherm, of calculated initial velocities under different concentrations of titrated SUMO1. The initial velocities were derived from the developed quantitative FRET analysis as

described before. The value of real K_M was derived from [Eq. 23] by K_i (K_d) and IC_{50}.

Five samples were repeated for each concentration, nonlinear regression was used to fit the measured cleavage rates at each SUMO1 concentration to the "onsite competition" model (Prism V, Graphpad Software) to give IIC_{50} value.

Results

Mutagenesis of pre-SUMO4 based on electrostatic

The crystal structure of the (pre-SUMO2)-SENP2 complex (PDB Code: 2IO0) [63] was used as a template to generate an initial model of the (pre-SUMO4)-SENP2 interaction (Fig. 34).

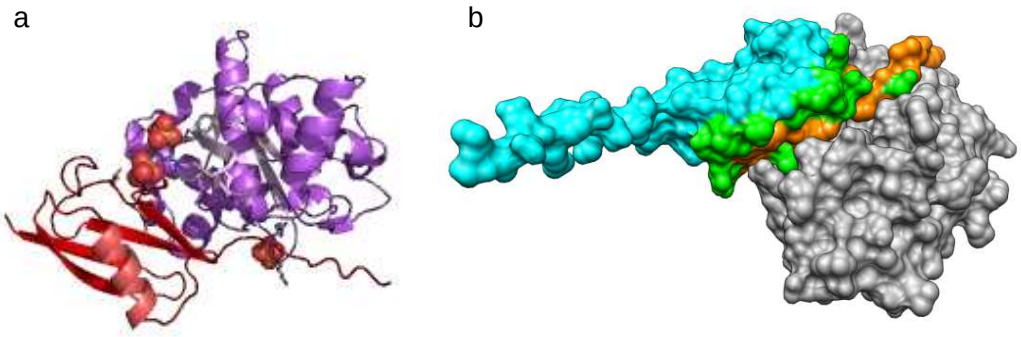

Figure. 34 Crystal structure of (pre-SUM2)-SENP2 (a) and (pre-SUMO4)-SENP2 (b). (a) Purple: catalytic domain of SENP2, red: pre-SUMO2; (b) pre-SUMO4 and SENP2 are represented by a molecular surface with SENP2 in gray, while pre-SUMO4 residues are colored based on their distance from SENP2: orange, < 3.5 Å; green, > 3.5 Å and < 8 Å; cyan, > 8 Å.

The first generated mutation P90Q was not related to electrostatic character. The rigid structure of proline at position 90 of pre-SUMO4 was found to introduce a kink in the C-terminal tail of pre-SUMO4 preventing SENP binding and maturation. The replacement of proline to glutamine at position 90 produced a pre-SUMO4 mutant which was capable of being matured by SENP2C [197]. Moreover, the glutamine residue was conserved in other three SUMO paralogs.

The residues glutamine and threonine before di-Gly were required for SENP recognition [168], the P90Q mutation was generated to remove the effect of proline and made pre-SUMO4 more similar to the other three SUMO prologs.

To identify the electrostatic differences between pre-SUMO2 and pre-SUMO4, each position in pre-SUMO4 was replaced, which is different from pre-SUMO2, to the corresponding pre-SUMO2 amino acid, one at a time. The effects of these mutations were quantified using electrostatic clustering and salvation free energies of association as shown in Fig. 35-a. Of these 13 mutations (except P90Q), only the mutation of pre-SUMO4 residue 63 from glycine to aspartic acid had a noticeable effect on the predicted binding ability, which favorable decreased the salvation free energy of association.

After introducing the G63D mutation, the difference of net charge between pre-SUMO4 to pre-SUMO2 becomes 3 to 2. The alanine-scan mutagenesis, in which each charged residue is replaced with alanine, one at a time, was performed to elucidate the role of each charged residue of pre-SUMO4 in association (Fig. 35-b). K21A was predicted to be the most favorable according to its free energy value. The replacement of lysine to alanine at position 21 reduced the net change of pre-SUMO4 to -2.

The work of the electrostatic pertubative design was performed by Dr. Chris Kieslich in Dr. Dimitrios Morikis' group.

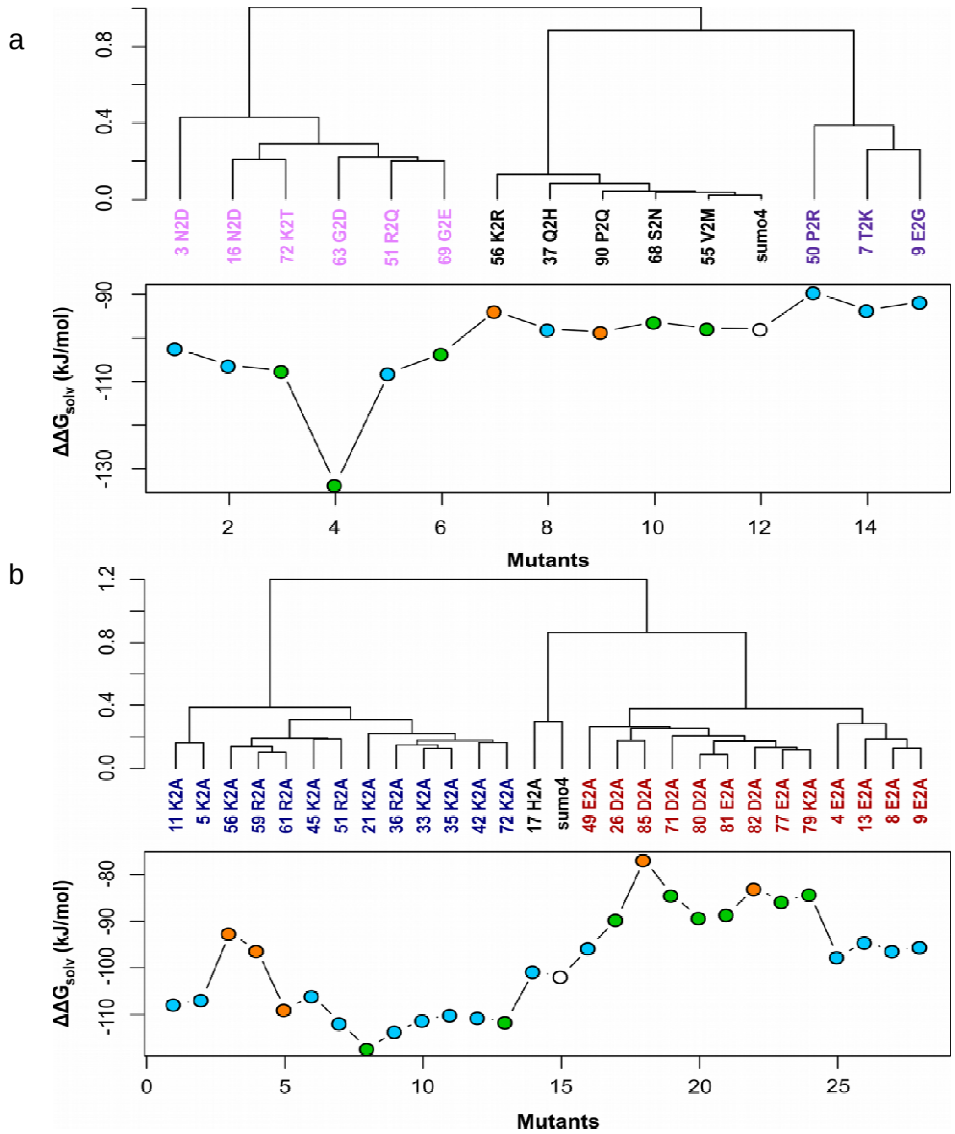

Figure 35 Electrostatic clustering and free energies of association for pre-SUMO2 based mutations of pre-SUMO4 (a) and pre-SUMO4 alanine-scan (b). Electrostatic clustering is illustrated as a dendrogram tree (top) with label color indicating: (a) the net charge of the resulting analog: pink, - 1; black, 0; purple, +1; (b) the type of amino acid being replace by alanine: red, acidic; blue, basic. The color of the free energy data points indicates the distance of the mutated residue from SENP2 as illustrated by Figure 33: orange, < 3.5 Å; green, > 3.5 Å and < 8 Å; cyan, > 8 Å (white point represents parent structure). (Note: This design was performed and kindly provided by Dr. Chris Kieslich and Professor Dimitrios Morikis, Department of Bioengineering, University of California-Riverside)

FRET-based protease assay to characterize the effects of generated pre-SUMO4 mutants

SUMO4 has been discovered in regulation of several important signaling pathway, but the mechanism of how SUMO4 be matured *in vivo* is still unclear. As the pre-SUMO maturation by SENP is the first step in SUMOylation pathway, it is significant to understand the mechanism of pre-SUMO4's maturation. The aim of the collaborated work was to identify a minimum set of pre-SUMO4 mutations necessary to regain catalytic ability, at least the SUMO-SENP binding ability, based on electrostatic pertubative design.

To test the effects of generated mutations of pre-SUMO4 in the SENP2 maturation, CyPet and YPet tagged wild type CyPet-(pre-SUMO4)-YPet as well as the other 3 pre-SUMO4 mutants (P90Q, P90Q/G63D, P90Q/G63D/K21A) were incubated with SENP2C (1:1 molar ratio, 100 nM each) at 37°C for 1 hr. The fluorescent emission spectra under the excitation of 414nm were detected.

The results indicated that different mutants presented different effects to improve pre-SUMO4's maturation by SENP2: wild type pre-SUMO4 cannot be processed at all and pre-SUMO4 P90Q/G63D mutants were the most favorable substrate for SENP2 (Fig. 36-a), the results were also confirmed by the biochemistry western-blot assay in parallel (Fig. 36-b).

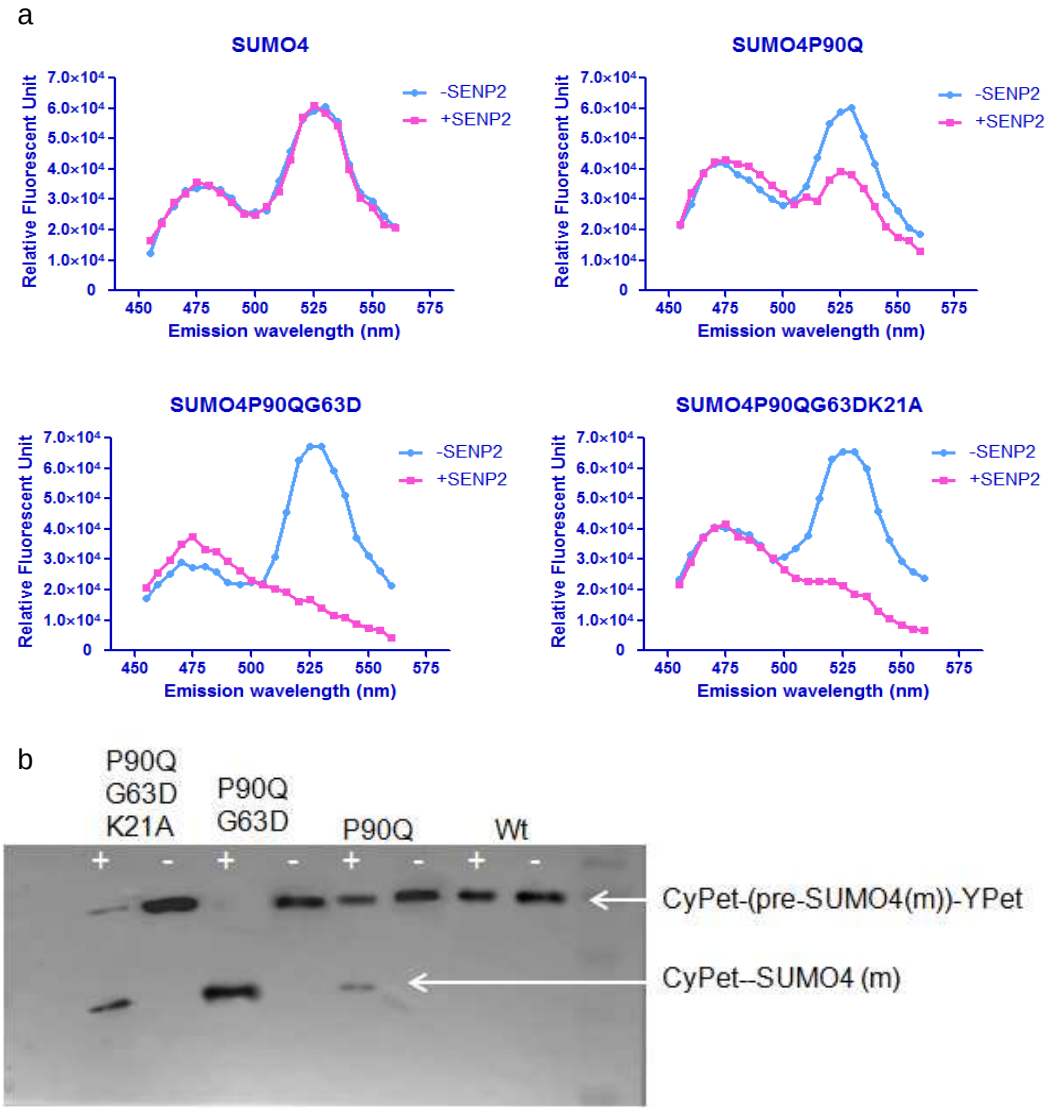

Figure 36 Characterization of CyPet-(pre-SUMO4 wt)-YPet, CyPet-(pre-SUMO4P90Q)-YPet, CyPet-(pre-SUMO4P90Q/G63D)-YPet, CyPet-(pre-SUMO4P90Q/G63D/K21a)-YPet maturation by SENP2C by developed FRET-based protease assay (a) and biochemistry western-blot analysis (b). Reactions were incubated in low salt reaction buffer at 37℃ for 1 hr. Final concentration of pro teins was 100 nM.

Kinetic analysis of protease-catalyzed reactions can identify catalytically relevant structural components in protein engineering. The developed FRET-based protease assay and the methodology of quantitative FRET analysis in determination of protease kinetic constants (internal calibration method) were applied to quantify the effects of different mutations in pre-SUMO4 mutants' maturation by SENP2C. The kinetic of (pre-SUMO2)-SENP2 was also studied as a control to comparison (Fig. 37, Fig. 38 and Table 15, Table 16).

The results of the protease kinetics analysis indicated the different effects of mutants in (pre-SUMO4)-SENP2 mutation process. As the mutations were generated based on the model of non-productive (pre-SUMO4)-SENP2 binding complex, the effects of mutants were mainly on the binding step rather than the catalysis step. The values of k_{cat} were close to each other, but the values of K_M varied a lot. The replacement of glycin to aspartic acid at position 63 of pre-SUM4 had a great impact upon forming the stable binding complex with SENP2C as the K_M was only 1.63 μM. However, out of the exception, the replacement of lysine to alanine at position 21 of pre-SUMO4 brought slightly negative effect on the binding of (pre-SUMO4)-SENP2 as the related K_M was 5.45 μM, larger than the value of the G63D mutants.

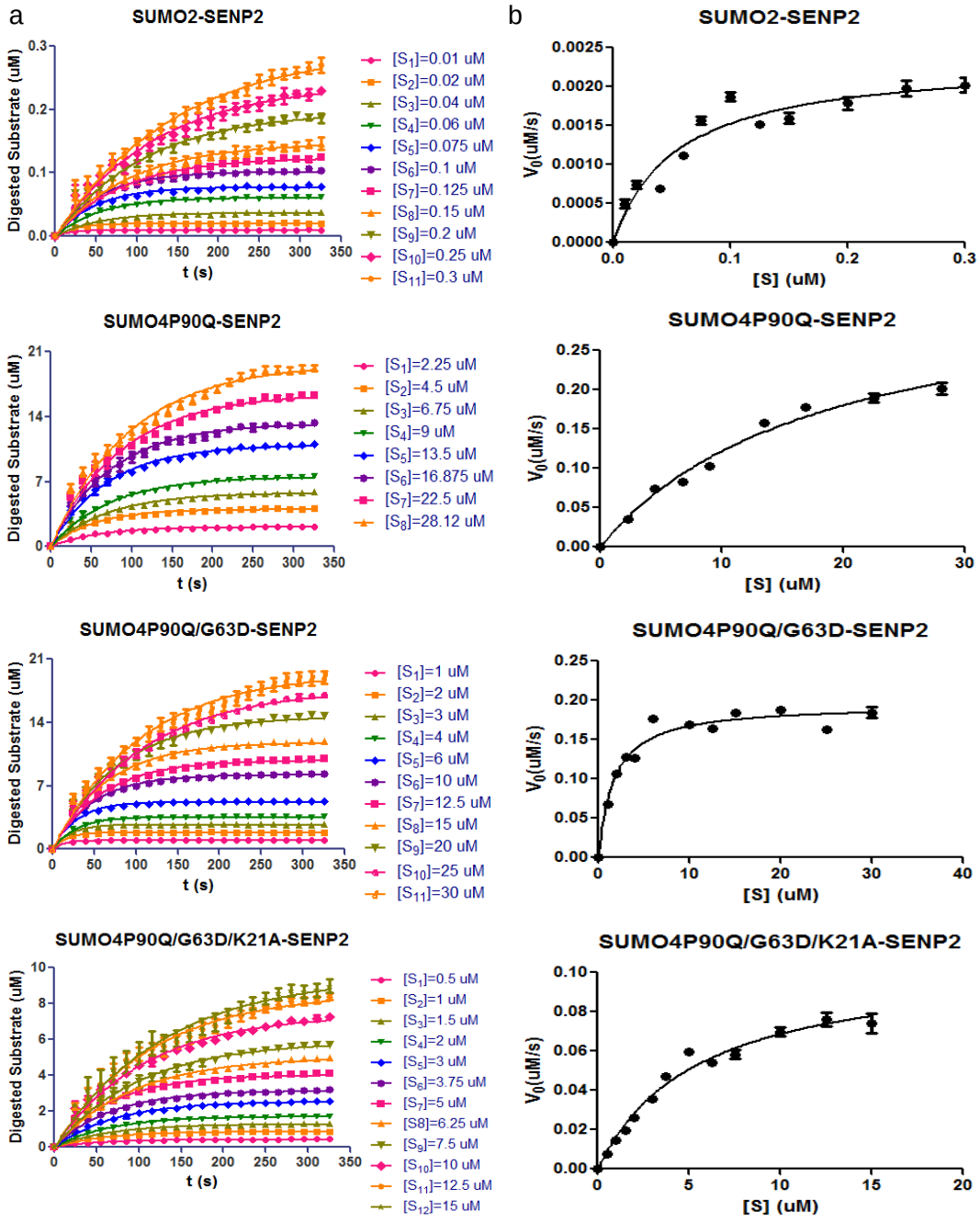

Figure 37. Quantitative FRET analysis in study the protease kinetics of pre-SUMO2, pre-SUMO4s (m)' maturation by SENP2C. (a) The concentration of digestion substrate in the maturation process and (b) Michaelis–Menten graphical analysis.

[CyPet-(pre-SUMO2)-YPet] (μM)	v_0 (x10^{-3} μM/s)
0.01	0.49 ± 0.058
0.02	0.74 ± 0.050
0.04	0.69 ± 0.036
0.06	1.12 ± 0.037
0.075	1.56 ± 0.050
0.1	1.87 ± 0.056
0.125	1.51 ± 0.047
0.15	1.59 ± 0.070
0.2	1.78 ± 0.084
0.25	1.98 ± 0.101
0.3	2.02 ± 0.095

[CyPet-(pre-SUMO4P90Q)-YPet] (μM)	v_0 (x10^{-3} μM/s)
2.25	35.49 ± 0.88
4.5	74.50 ± 2.23
6.75	82.25 ± 2.59
9	103.01 ± 2.45
13.5	157.19 ± 3.36
16.875	178.21 ± 4.67
22.5	189.18 ± 5.50
28.125	201.44 ± 7.33

[CyPet-(pre-SUMO4P90Q/G63D)-YPet] (μM)	v_0 (x10^{-3} μM/s)
1	68.17 ± 1.23
2	106.22 ± 2.00
3	127.36 ± 1.73
4	126.58 ± 2.86
6	176.40 ± 2.86
10	169.00 ± 2.62
12.5	163.92 ± 3.27
15	183.46 ± 3.10
20	187.69 ± 4.77
25	163.13 ± 4.02
30	184.26 ± 7.17

[CyPet-(pre-SUMO4P90Q/G63D/K21A)-YPet] (μM)	v_0 (x10^{-3} μM/s)
0.5	7.41 ± 0.226
1	14.51 ± 0.312
1.5	19.62 ± 0.460
2	25.95 ± 0.468
3	35.44 ± 1.024
3.75	47.31 ± 1.011
5	59.52 ± 1.506
6.25	54.29 ± 1.316
7.5	58.21 ± 2.246
10	69.81 ± 2.041
12.5	76.11 ± 3.575
15	74.13 ± 5.010

Table 15. The initial velocities of pre-SUMO2 and pre-SUMO4s (m)' maturation by SENP2C derived by quantitative FRET analysis in internal calibration method.

SENP2 Substrate	K_M (μM)	k_{cat}(s^{-1})	k_{cat}/K_M(M^{-1}·s^{-1})
SUMO2	0.054 ± 0.0149	29.33 ± 2.571	(5.45 ± 1.590) x10^{8}
SUMO4P90Q	18.3 ± 3.67	15.34 ± 1.613	(8.38 ± 1.896) x10^{5}
SUMO4P90Q/G63D	1.63 ± 0.287	19.43 ± 0.69	(1.19 ± 0. 214) x10^{7}
SUMO4P90Q/G63D/K21A	5.45 ± 0.837	21.2 ± 1.413	(3.89 ± 0.648) x10^{6}

Table 16. Kinetic constants of pre-SUMO2 and pre-SUMO4s (m)' maturation by SENP2C.

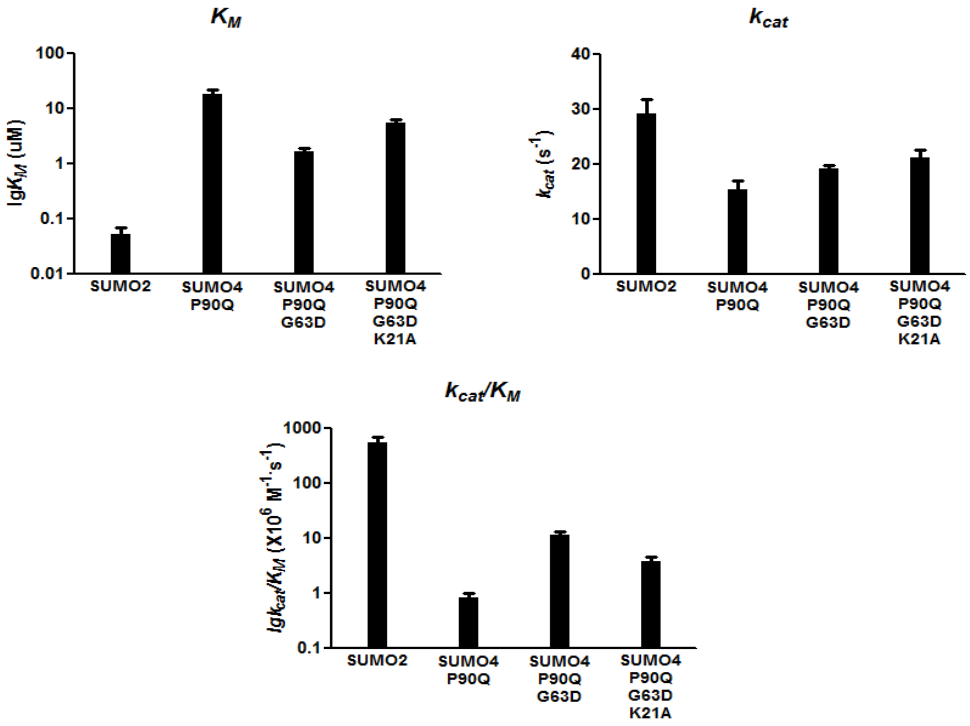

Figure 38. Kinetics constants' comparison of pre-SUMO2 and pre-SUMO4s' (m) maturation by SENP2C in bar presentation.

Quantitative FRET analysis in determination of binding affinity (K_d)

Binding affinity (K_d) is an important parameter to characterize protein-protein interactions. Compared with surface plasmon resonance (SPR) technique to measure K_d, FRET has unique advantages such as no requirement of immobilize ligand to solid surface, which can maintain the bioactivities of the interacted proteins in aqueous phase.

Our group has developed quantitative FRET analysis in protein-protein interaction study and the binding affinity determination [204]. The basic idea is to quantify the concentration of proteins in binding or non-binding by the quantitative FRET analysis in:

$$Em_{FRET} = Em_{FRETmax}\left(1 - \frac{2K_d}{X-a+K_d+\sqrt{(X-a-K_d)^2+4K_dX}}\right) \quad \text{[Eq. 24]}$$

where Em_{FRET} is the FRET-induced acceptor's emission derived from the similar analysis as [Eq. 1] , a is the total concentration of donor-tagged protein, X is the total concentration of acceptor-tagged protein. Maximum FRET-induced acceptor's emission ($Em_{FRETmax}$) and binding affinity (K_d) were derived simultaneously.

In the competitive inhibition, the bond-tightness (K_i) between enzyme and the corresponding enzyme inhibitor is the binding affinity (K_d) between the enzyme inhibitor. In the case of product inhibition, K_i is the binding affinity between the enzyme and the product.

The quantitative FRET-based protein assay was performed to study the interaction between CyPet-SUMO1 and YPet-SENP1C. Our previous studied has proved that the fluorescent protein tag does not affect the binding affinity between the interested protein pair [204]. Six concentration of CyPet-SUMO1 were used in the test, and in each fixed concentration of CyPet-SUMO1, YPet-SENP1C was titrated from 0 to 4.3 µM. The value of K_d was derived according to [Eq. 24], and confirmed with SPR assay for non-tagged SUMO1-SENP1C pair (Fig. 39 and Table 17). The value of K_d derived from quantitative FRET analysis was 0.152 ± 0.014 µM, from SPR assay was 0.124 µM.

[CyPet-SUMO1] (µM)	**K_d (µM)**
0.1	0.064 ± 0.026
0.2	0.071 ± 0.021
0.35	0.119 ± 0.024
0.5	0.171 ± 0.036
0.75	0.283 ± 0.054
1	0.204 ± 0.039

Table 17. Summary of K_d derived in the quantitative FRET protein assay upon six concentrations of CyPet-SUMO1.

a

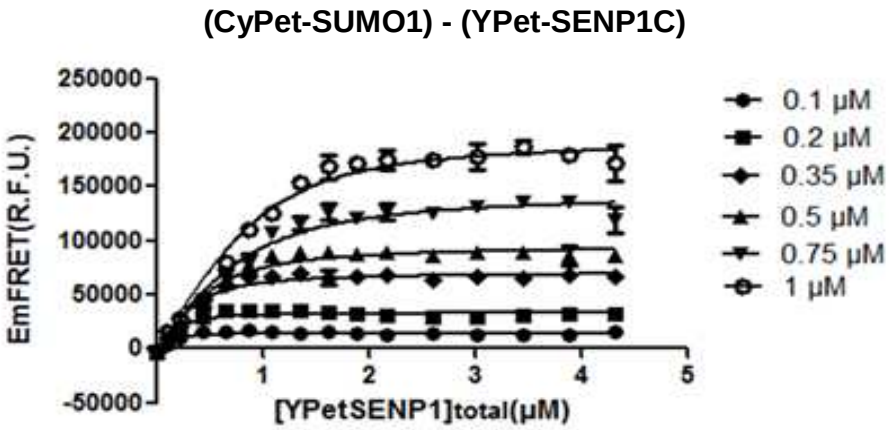

b

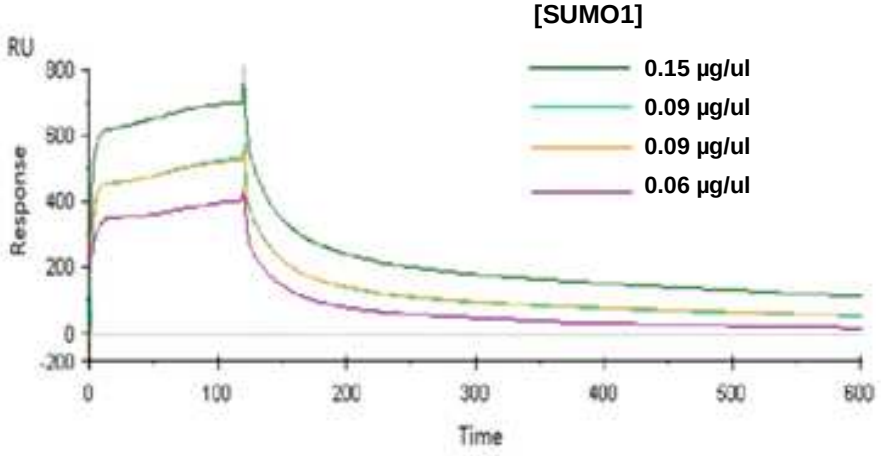

Figure 39. Determination of binding affinity K_d between SUMO1-SENP1C. (a) Fitting Em_{FRET} and [YPet-SENP1]$_{total}$ with the developed algorithm according to quantitative FRET analysis; (b) surface plasmon resonance assay.

Product inhibition characterization

In many biological assays one can measure a specific signal as a function of the concentration of some exogenous substance. A plot of the signal obtained as a function of the concentration of exogenous substance is referred to as a *dose-response* plot. The dose-response plots are very widely used to comparing the relative inhibitor potencies of multiple compounds for the same enzyme, under well-controlled conditions. The method is popular because it permits analysts to determine the IC_{50} by making measurements over a broad range of inhibitor concentrations at a single, fixed substrate concentration.

In the study of product inhibition, untagged mature form SUMO1 (15 nM to 60 μM) was titrated in the reaction system of the fixed concentration of substrate (CyPet-(pre-SUMO1)-YPet, 1.5 μM) and protease (SENP1C, 3 nM). The initial velocities derived from quantitative FRET analysis decreased with the increment of product/inhibitor concentration (Fig. 40 and Table 18). The value of IC_{50} was 3.80 ± 0.956 μM.

a

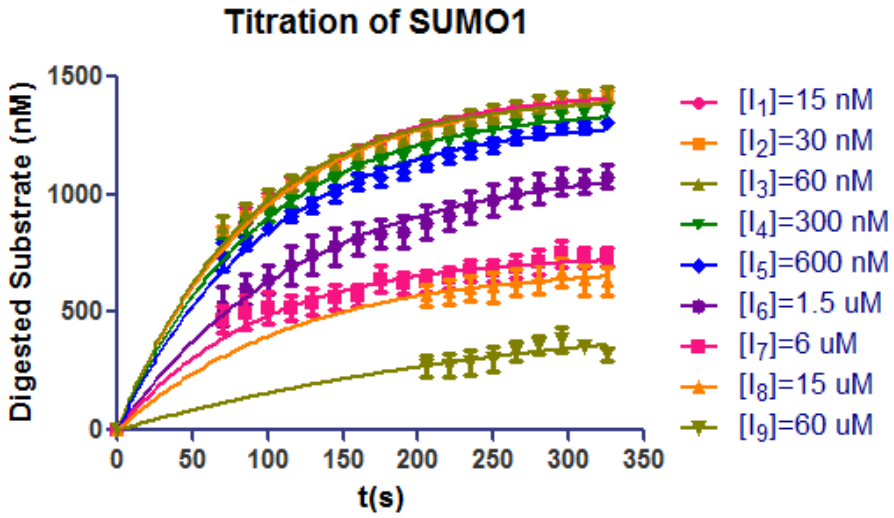

b

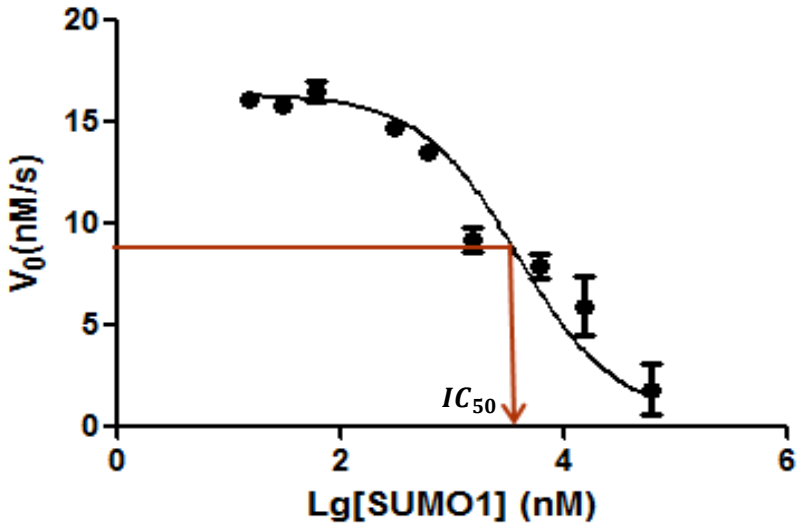

Figure 40. Effect of product inhibition on pre-SUMO1 maturation by SENP1C. (a) Changes of substrate concentration in maturation process with the titration of inhibitor SUMO1; and (b) dose-response plot of IC_{50} determination. FRET-based SENP1 protease assays had a fixed concentration of the CyPet-(pre-SUMO1)-YPet substrate (1500 nM) and SENP1C enzyme (3 nM) with inhibitor active SUMO1 from 15 nM to 6 µM.

[SUMO1] (nM)	Lg [SUMO1] (nM)	v_0 (nM/s)
15	1.176	16.10 ± 0.25
30	1.477	15.82 ± 0.33
60	1.778	16.51 ± 0.48
300	2.477	14.76 ± 0.34
600	2.778	13.47 ± 0.36
1500	3.176	9.21 ± 0.58
6000	3.778	7.89 ± 0.58
15000	4.176	5.94 ± 1.45
60000	4.778	1.86 ± 1.29

Table 18. Initial velocities in product inhibition study characterization from quantitative FRET analysis.

For the competitive inhibitors, the relationship between IC_{50} and K_i was characterized by [Eq. 23], as $K_i = K_d$, the real K_M can be obtained as:

$$K_M = \frac{[S]}{\frac{IC_{50}}{K_d} - 1} \qquad \text{[Eq. 25]}$$

The value of derived real K_M was 0.063 ± 0.017 µM, the apparent K_M derived from Michaelis-Menten equation was 0.14 ± 0.051 µM (Chapter II, table 8), which was more than twice of the real K_M.

Discussion

Previous biological studies indicate a functional role of SUMO4 in heat shock and NF-κB transcription factor expression [12, 188], however, the SUMO4 proteins studied were made from expression vectors that over-express the SUMO4 and these proteins were made to end in the C-terminal di-Gly residues. These studies appear not to be biologically relevant, since native SUMO4 appears not be processed to mature active form.

Electrostatic contributes significantly to protein function by forming the inter/intra-molecular interactions, driving recognition leading to protein-protein binding and facilitating pH-dependent phenomena, such as enzymatic catalysis and conformational switching [205]. It is expected that proteins with similar spatial distributions of electrostatic potential are likely to have similar functions. The net charge difference between pre-SUMO2 and pre-SUMO4 expected to play an essential role in pre-SUMO's maturation by SENPs.

The AESOP framework is centered on the idea of electrostatic similarity. According to the computational model by AESOP, the net charge of pre-SUMO4 turned into -1 and -2 after introducing the point mutation of G63D and then K21A. The replacement of Gly to Asp at position 63 achieved big improvement upon SENP2C binding, but the K21A mutant displayed a decreased binding ability toward SENP2. To get further understanding into the protease kinetics results for the pre-SUMO4 mutants, the inter/interamolecular coulombic interactions, which

may contribute to improve and weaken the association of the generated mutants were analyzed on structure complex.

The replaced aspartic acid at position 63 can form a strong bifurcated intramolecular salt bridge between the two basic amino acid residues Arg456 and Lys459 (Fig. 41-a). Further analysis indicated that a negative charged amino acid is conserved in all SUMO paralogs at position 63 [60]. Nevertheless, the sequence alignment of SENP family also shows the positive charge at position 456 and 459 is highly conserved. In that way, the introduced mutation G63D, upon the P90Q mutation, not only turned pre-SUMO4 be preferred by SENP2, but also was a good substrate for SENP1, 3 and 5.

The replacement of Lys to Ala at position 21 removed intermolecular Coulombic interactions among Lys21-Glu-81-Asp-82, which was expected to stabilize the local structure (Fig. 41-b). However, we were not clear about whether the effect of structure change was more obvious than the effect of changes in electrostatic. Also, the computational model for mutagenesis was based on the native form of pre-SUMO4, which was not tagged with any fluorescent proteins, the effects of either the conformational or electrostatic change from the tagged CyPet and YPet of pre-SUMO4 need to be studied in the future.

In addition, other mutations were also generated by Dr. Chris Kieslich, like K21E, K21A/R36A and G69E/K72A based on P90Q/G63D pre-SUMO4 mutants.

There mutations add one more negative charge of pre-SUMO4, which equals to the net charge -3 of pre-SUMO2. The effects of these mutations need to be studied in the future to see whether they can improve the pre-SUMO4's maturation by SENP2 more effectively.

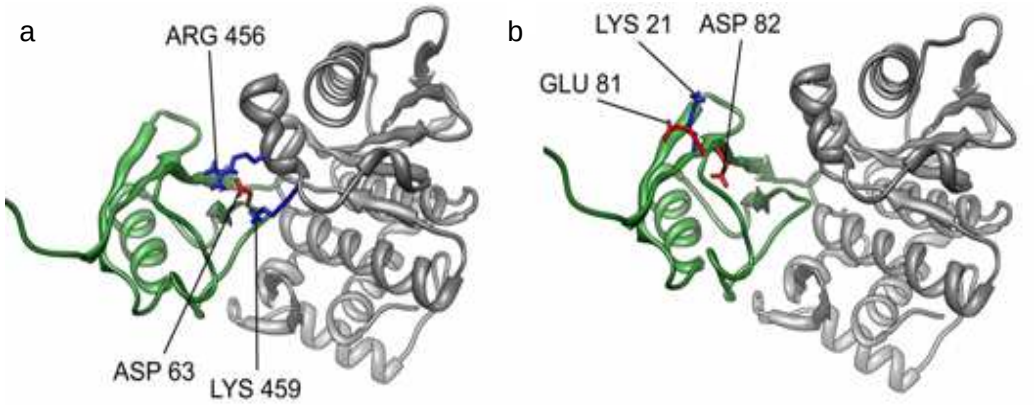

Figure 41. Molecular graphic of pre-SUMO4 mutants. Ribbon models are used to represent pre-SUMO4 (green) and SENP2 (gray). Charged residues of interest are in stick representation: red, negative; blue, positive.

The product inhibition is the inhibition from product during the process as the product has a high affinity for the enzyme. The dissociation constants (K_d) of SENP1 (C603A) between SUMO1 precursor and active form of SUMO1 were analyzed before by isothermal titration calorimetry (ITC) assay [61]. ITC is a thermodynamic technique that directly measures the heat released or absorbed during a biomolecular binding event. The K_d value of (pre-SUMO1)-SENP1C603A was ~787 nM, but the K_d value of SUMO1-SENP1C603A was only ~6.22 nM, which indicated the active SUMO1 has a very strong binding to

SENP1, and thus the active form SUMO could act as an inhibitor of the pre-SUMO's maturation. However, it has to be noted that the binding affinity in their study was different from ours as the SENP1 in their study had a mutation at position 603. The cysteine at position 603 is the key amino acid residue to SENP1 as providing the nucleophilic cysteine thiol in the catalytic dyad. For the cysteine proteases, a thioester intermediate links the carbosy-terminus of the substrate (which has to release with an amine terminus) to the cysteine thiol. The replacement of cysteine to alanine at position 603 changed the binding of substrate-enzyme thioester binding to a much tighter binding complex and never dissociate again. The binding of SUMO1 between wild type SENP1 should be much weaker than that of SUMO1 between SENP1C603A mutant. In that case, the K_d between SUMO1-SENP1 should be larger than that between SUMO1-SENP1C603A. The value of K_d between SUMO1-SENP1 derived from quantitative FRET analysis was ~ 152 nM, very close to the value derived from SPR assay, which was ~ 124 nM. In that way, the difference between real K_M and apparent K_M should not be so large as they studied, which the real $K_M$was ~50 times smaller than the apparent K_M. The apparent K_M was only 2.2 times larger than the real K_M from our analysis.

The analysis of product inhibition in pre-SUMO's maturation indicated the concentration of product, here active SUMO, is an important negative feedback to control the SUMOylation signaling pathway. As the pre-SUMO's maturation is the first step in the whole SUMOylation, the amount of mature SUMO determines

the level of SUMOylation *in vivo*. Enhanced or reduced level, out of the balance, of the SUMOylation will lead to serious consequences, like up-regulation or down-regulation the gene transcription related to carcinoma genesis or neuron-degenerative disease.

The quantitative FRET analysis was used to study the binding between product and enzyme and the substrate catalysis by enzyme. The product inhibition can be quantified from the developed method described in this chapter. The previous studies have to utilize more than one technology to characterize the product inhibition. It is not easy to standardize the results, including the standard errors in different methods. Here, the protein-protein binding and substrate hydrolysis can be derived by the same technology – quantitative FRET, which not only simplified the procedure, but also provided more accurate and reliable results. Most importantly, the study of product inhibition by quantitative FRET analysis denoted the possibility of the methodology for small chemical compound inhibitors characterization. The K_M and IC_{50} can be obtained from Michaelis-Menten analysis and dose-responsive plot separately. The important inhibition constant K_i can be determined upon the inhibition types [202]. The potential application of using quantitative FRET analysis is very essential in the future studies, especially to characterize the potency from high-throughput screening (HTS) assay developed in next chapter.

As discussed in the previous two chapters, the two-channel ratiometric FRET analysis may give close values of k_{cat}/K_M to the ones derived from

quantitative FRET analysis, but not the same case to the individual k_{cat} and K_M. The individual k_{cat} and K_M are important in studying the substrate-enzyme binding ability and rate-limiting step, as the studies in the comparison of different mutations to (pre-SUMO4)-SENP2 maturation. Upon the same theory, the initial velocities derived from ratiometric FRET analysis were not accurate since the direct fluorescent emissions of donor and acceptor are included in the FRET signal. The accuracy of initial velocity determination is significant in the study of inhibitor's IC_{50}.

In this chapter, the application of quantitative FRET analysis in protease kinetics study was expanded to study the biological mechanism of pre-SUMO4's maturation and product inhibition, not only in comparison of substrate specificities as previous two chapters. The methodology of quantitative FRET analysis can provide accurate and reliable results of individual kinetics constant K_M and initial velocity v_0. More importantly, the quantitative FRET analysis can be used in the future to characterize selected chemical compounds in the HTS assay.

CHAPTER IV: Development of *in vitro* High Sensitive FRET-based High-throughput Screening Assay for SENP Inhibitors in SUMOylation Pathway

Abstract

Ubiquitin or ubiquitin-like proteins (ULPs), such as SUMO (small ubiquitin-related modifier), play important roles in diverse cellular processes. The conjugation of SUMO to its target proteins is achieved by a cascade of protein-protein interaction. SUMO is processed into mature form from its precursor, pre-SUMO, by its specific protease SENPs. Conjugated SUMO is then removed from the substrate by SENPs to re-start the SUMOylation cascade.

A highly sensitive *in vitro* FRET-based high-throughput screening (HTS) assay was development to look for small chemical SENP1 inhibitor. This assay was based on steady state and high efficiency of fluorescent energy transfer between CyPet and YPet fused pre-SUMO1. The screening conditions of the HTS assay were optimized and validated by general cysteine inhibitors. 55,000 compounds were screened by the developed FRET-based HTS assay without finding any potential inhibitors. However, the developed FRET-based HTS assay provided a powerful tool for large-scale and high-throughput applications. In addition, the robust and reproducible FRET-based HTS assay can be expanded to other protease inhibitor discoveries.

Introduction

The conjugation of ubiquitin or ubiquitin-like proteins is an important regulatory mechanism that is widespread in many biological processes. SUMO conjugates with protein including androgen receptor, IκBα, c-Jun, histone deacetylases, and regulate cellular activities such as transcription, DNA repair, signal transduction and cell cycle [31, 206]. SUMOylation of target proteins is regulated by dedicated enzyme machinery, including a family of SUMO-specific proteases (SENPs). SENPs play two primary roles in SUMO regulation: they process pre-SUMOs to reveal a C-terminal di-glycine before conjugation, and cleave the isopeptide bond between the C-terminal glycine of SUMO and the lysine side chain of a target protein.

It has been difficult to draw conclusion about SUMO-specific target recognition, selectivity and the mechanisms connecting SUMO modification to downstream phenotypes as the SUMOylation process is highly dynamic and reversible. Therefore, there has been much interest in the development of tools to globally characterize SUMOylation events using biochemical methods. However, it has remained difficult to globally assess the temporal aspects of SUMOylation in the regulation of basic biological processes. Small chemical compound inhibitors not only provide spatial and temporal control to the biosignaling pathway, but also can investigate the function when gene knockout is not feasible.

Pathological and biochemical studies suggest that over expression of SENP1 can stimulate androgen receptor-mediated transcription, may promote prostate cancer development, and stabilize H1F1α during hypoxia in angiogenesis. SENP1 is over expressed in more than 50% of the high-grade precancerous prostate tissues and in a large number of prostate cancer cases. Correlation between SENP1 and increased prostate epithelial cell proliferation and precancerous structure formation was demonstrated in transgenic mice [70, 80, 207, 208]. As SENP1 represents a novel target for anti-cancer drug action, several effectors have been taken to try to discovery potent and specific small molecular inhibitors of SENPs without much success except identifications of low affinity covalent inhibitors, including full-length or truncated forms for SUMO containing a vinyl sulfone (VS) or vinyl methyl ester (VME) reactive group at the C-terminal glycine residue [106, 110, 209]; a series of synthesized benzodiazepine-based inhibitors in design from the structure-activity relationship [111]; a lead compound JCP666 contained a reactive aza-epoxide eletrophile linked to an extended, nonnatural peptide backbone structure yielded from a library screen of cystene protease inhibitors in lysates of the human parasite pathogen *Plasmodium falciparum* [112] and a class of synthesized compound contains the acryloxymethyl ketone (AOMK) reactive group with retained structure of JCP666 [113].

Accompanying with these efforts, several biochemical assays and high-throughput screening have been developed. The commercial available SUMO (full length or truncated tetrapeptide QTGG form)-AMC, Lanthascreen and

ALPHAscrenn SUMO substrate have been used in HTS assay to look for SENP specific inhibitors [112, 113, 166, 170, 171, 180]. However, the excitation wavelength is in the UV range, which is known to result in false positive rates as high as 20% in HTS [210, 211]. Nevertheless, additional steps are required for conjugation of reactive group AMC, lanthanide chelate or reactive beads to SUMO. The conjugation efficiency and side effects may lead to false positive or true negative. The reporter assays, SUMO-PLA_2 (phospholipase A_2) [212-214], SUMO-EK_L (enterokinase light chain) and SUMO-GZMB (granzyme B) [215] have been also used to characterize SENP isopeptidase activity and look for small chemical inhibitors as a high-throughput screening platform. In the reporter assay, SUMO was genetically fused to the N-terminus of PLA_2, EK_L and GZMB. The cleavage of SENP toward SUMO can be detected by the interaction of fluorogenic substrates and correlated enzymes. The combination of the assay in a multiplex format allows rapidly determination of substrate or inhibitor specificities. However, the inhibition between the reporter enzyme and correlated substrate may bring to the false positive hints for the SUMO-SENP hydrolysis. A FRET strategy was used to determine SENP activity and potential application for inhibitors' high-throughput screening [167]. The precursor of SUMO1 was flanked by a FRET pair, ECFP and YFP. The cleavage of the pre-SUMO1 by SENPs led to a loss of FRET signal. However, the low energy transfer efficiency of the FRET pair, ECFP and YFP, lead to low signal as well as low signal-to-noise ratio in HTS

assay (see the comparison of energy transfer of CyPet-YPet and ECFP-YFP in Chapter I).

In the previous chapters, a FRET-based protease assay to study the SENP activities in pre-SUMO maturation and SUMO-target substrate deconjugation. In the developed protease assay, the fluorescent protein CyPet and YPet were genetically tagged to the N- and C-terminus of pre-SUMO or active SUMO and its target substrate RanGAP1C respectively. The cleavage of SENP upon pre-SUMO or SUMO-RanGAP1C complex can be observed by monitoring the increased emission at 475 nm and the decreased emission at 530 nm, as shown in Fig. 9a and 23a.

In this chapter I will describe the work to convert the FRET-based protease assay into high-throughput screening platform, in which the disruption of SENP towards pre-SUMO's maturation by small chemical inhibitors was captured by a fluorescence reader in multi-well plate manner, which readily allows repeated study and large scale application. The conditions were optimized and the assay was validated by the inhibition of general cysteine inhibitors. More than fifty thousand compounds were screened by the developed HTS assay. The developed HTS assay will hopefully provide new tools to study the mechanism and function of SENP. This assay platform can be easily adapted to other protease HTS assay and industrial applications.

Material and Methods

Molecular clone of DNA constructs

The mothods of DNA constructs used in this chapter, which encoding CyPet-(pre-SUMO1)-YPet, and SENP1C were described in the Material and Methods part in Chapter I (page 49-50).

Recombinant protein expression and purification

Recombinant proteins, used in this chapter, CyPet-(pre-SUMO1)-YPet and SENP1C, were expressed and purified by Ni-NTA affinity chromatography followed the procedure described in Chapter I (page 51).

The purity of the proteins was confirmed by SDS-PAGE and Coomassie blue staining. Concentrations of protein were determined by Coomassie Plus Protein Assay (Thermo) with known quantities of bovine serum albumin as standards. Aliquots of final products were stored in -80℃.

Fluorescence measurement and analysis

The fluorescent emission of CyPet-(pre-SUMO1)-YPet was determined by the fluorescent plate reader FlexStation II ^{384} (Molecular Device, Sunnyvale, CA) in 384-well plates at the excitation wavelength of 414 nm with emission at 475 nm and 530 nm respectively. The readings were later corrected by subtracting the background fluorescence of the plate to get the emission intensities of the

fluorescent proteins. The emission ratio of each well was then calculated by dividing the emission intensity at 530 nm by that at 475 nm.

Optimization of high-throughput screening conditions

To determine the ratio of substrate and protease in the screening assay, recombinant protein CyPet-(pre-SUMO1)-YPet was dispensed by a liquid handler (Molecular Devices, AquaMax DW4) into 384-well plate in buffer containing 20 mM Tris-HCl (pH 7.4), 50 mM NaCl, 1 mM DTT and 0.1% (v/v) Tween-20. Then, SENP1C was dispensed into desired well in a total volume of 60 µl. The final concentration of CyPet-(pre-SUMO1)-YPet was fixed as 100 nM and final concentration of SENP1C was varied as 250 pM, 100 pM and 50 pM. Reactions were incubated at 37°C for at most 35 minutes. The fluorescence emissions were determined by fluorescence plate reader FlexStation II ^{384} (Molecular Devices) for every three minutes. After the emission ratios of each condition were determined, Z' factor was calculated as:

$$Z' = 1 - \frac{3(\sigma_{c+} + \sigma_{c-})}{|\mu_{c+} - \mu_{c-}|} \qquad \text{[Eq. 26]}$$

where μ_{c+}, μ_{c-}, σ_{c+}, σ_{c-}, are the mean values and standard derivations of the fluorescent emission ratio of CyPet-(pre-SUMO1)-YPet in the absence and presence of SENP1C, respectively.

Assay validation by FRET analysis and confirmation of western-blot

To determine the dose-dependent activities of potential positive compound hits, general cysteine inhibitor N-Ethylmaleimide (NEM) was used to inhibit the hydrolysis of SENP1C towards pre-SUMO1. The concentration of CyPet-(pre-SUMO1)-YPet and catalytic domain of SENP1C were fixed at 100 nM and 100 pM in a total of 60 µl buffer in the presence of NEM with concentration varied from 10 µM to 50 mM. At each NEM concentration, the emission ratio of the mixture of CyPet-(pre-SUMO1)-YPet and SENP1C was measured and compared with the emission of CyPet-(pre-SUMO1)-YPet alone. The digestion of substrate CyPet-(pre-SUMO1)-YPet by SENP1 in the presence or absence of NEM was also analyzed by the western-blot using anti-SUMO1 antibody.

Screening of small chemical compounds that disrupt the pre-SUMO1's maturation by SENP1C

55,000 compounds obtained from the compound collects at UCR Genomic Institute were dissolved in Dimethyl sulfoxide (DMSO) to 10 mM and stored in 384-well plate. The compounds of every four stock plates were combined into the corresponding wells in a single screening 384-well plate. 22 µl low-salt Tris buffer was dispensed into each well of the screening plates and four compounds of 0.5 µl each were added using Biomek FX workstation (Beckman Coulter). Overall 44 screening plates were prepared from 172 stock plates. In the screening, the recombinant protein SENP1C was aliquoted into 384-well plate containing

compounds by the liquid handler Aquamax4 (Molecular Devices) and incubated with compounds for 10 minutes before CyPet-(pre-SUMO1)-YPet was dispensed. The concentration of CyPet-(pre-SUMO1)-YPet and SENP1C were fixed at 100 nM and 100 pM in a total of 60 µl buffer. After incubated at 37°C for 30 minutes, the fluorescent emission intensities at 475 nm and 530 nm at the excitation wavelength of 414 nm were determined by FlexStation II ^{384} (Molecular Devices) to calculate the emission ratios. The positive hints were picked and confirmed by western-blot using anti-SUMO1 antibody (Fig. 42).

Data Analysis

All data were processed by Prism 5 (GraphPad) and reported in the format of mean ± SD.

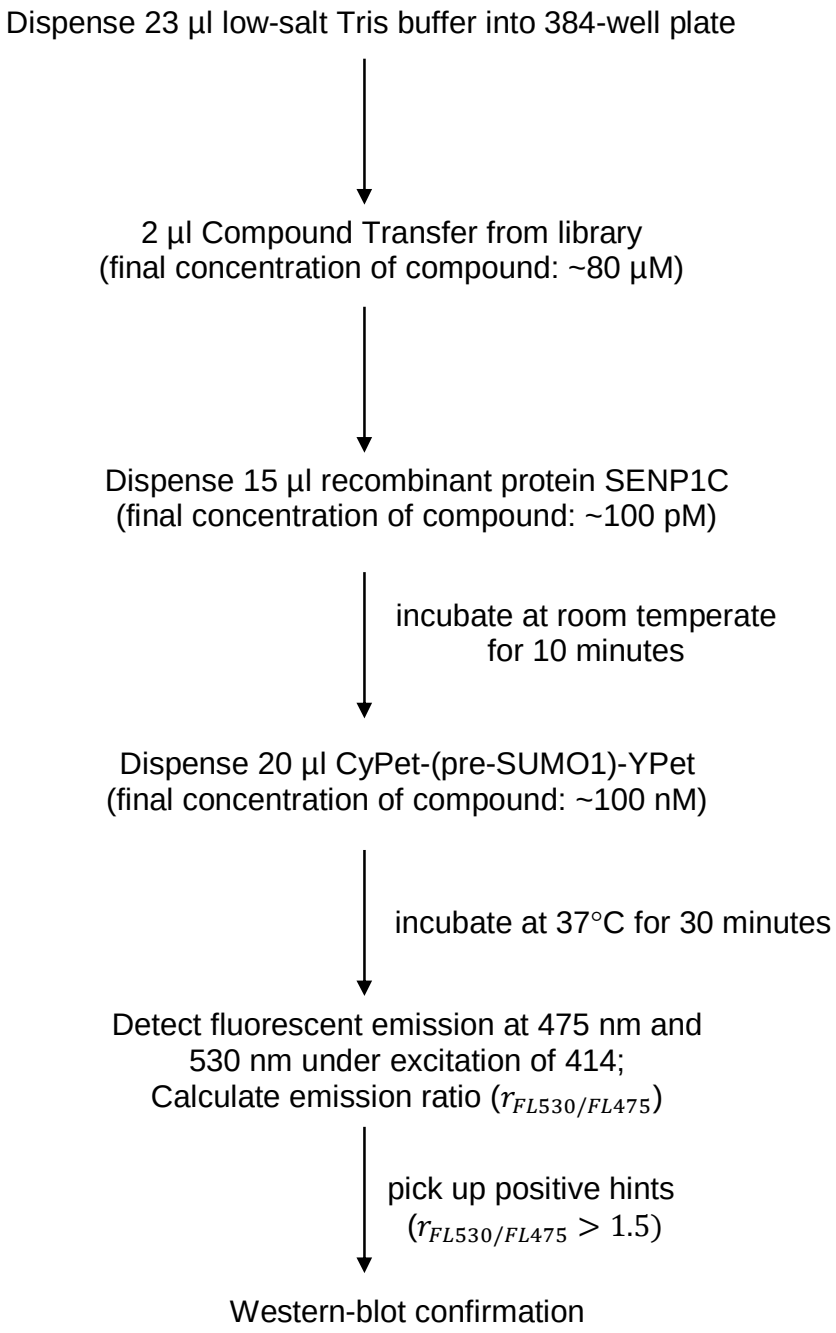

Fig. 42. Procedure of FRET-based HTS assay for SENP inhibitors.

Results

Design of a high-sensitive FRET-based high-throughput screening assay

A general strategy for a high-sensitive FRET-based high-throughput screening assay for SENP was designed based on the engineered high efficient FRET pair CyPet and YPet. This FRET pair was chosen because of the improved energy transfer efficiency by protein engineering from CFP and YFP, respectively to achieve high dynamic range and sensitivity of FRET assay [173]. In this strategy, SUMO1 precursor was genetically tagged by CyPet and YPet on its N- and C- terminus. When CyPet was excited at 414 nm, the energy transfer occured from CyPet to YPet, and thus led to a quenching of CyPet and an increased emission of YPet. When the substrate was mixed with the SENP1C, the pre-SUMO1 was cleaved after Gly-Gly motif and released the products: CyPet-SUMO1 and YPet-SUMO1 tail. The disrupted FRET pair resulted in the increase of CyPet's emission and decrease of YPet's emission when CyPet was excited. When the SENP1 is inhibited by a chemical compound, the decrease of FRET signal YPet will not take place.

Optimization of FRET-based high-throughput screening assay

A high-quality HTS assay should have good reproducibility, a high signal-to-noise ratio and low cost. Based on the guidance of enzyme assay provided by National Institute of Health Chemical Genomics Center, the substrate concentration in the assay should be around or below the K_M as using substrate

concentrations higher than the K_M will make the identification of competitive inhibitors more difficult. Here in the developed HTS assay for SENP inhibitors, the concentration of substrate CyPet-(pre-SUMO1)-YPet was fixed at 0.1 µM (the value of calculated K_M was ~0.14 µM, Chapter II, table 8). Different molar ratios of the substrate to protease and the related Z' factor of the HTS assay were tested to determine the quality of the FRET-based protease assay and optimize the screening conditions. The concept of Z' factor was introduced to estimate the quality of a high-throughput screening assay [216]. Typically, the quality of an HTS assay can be considered excellent when the Z' factor is between 0.5 and 1.

In the study of screening condition optimization, concentration of substrate was fixed at 100 nM, concentration of protease was varied as 250 pM, 100 pM and 50 pM. The substrate and protease were mixed in a final volume of 60 µl and incubated at 37°C. The fluorescent emissions at 475 nm and 530 nm were detected every three minutes under the excitation of 414 nm. After the emissions of all mixtures at different time point were determined, the mean values and standard deviations of each group were calculated (Fig. 43-a), the Z' factors were also determined (Fig. 43-b).

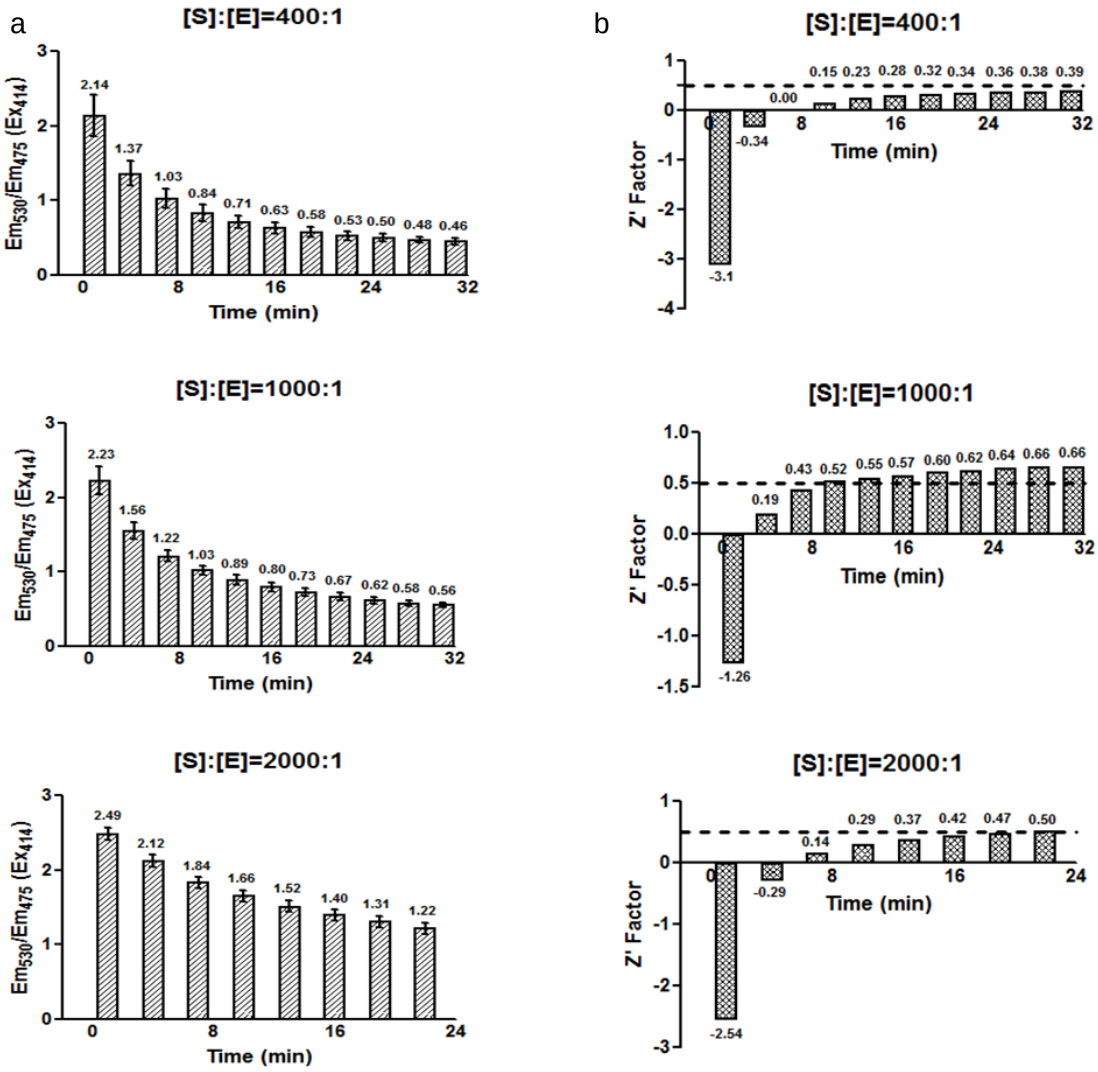

Fig. 43 Optimization of the FRET-based HTS assay. (a) Substrate-enzyme molar ratio optimization; (b) related Z' factor determination. The concentration of substrate fixed at 100 nM, the protease concentration varied at 250 pM, 100 pM and 50 pM, the ratio of substrate to protease was 400:1, 1000:1 and 2000:1. Positive control was only substrate; negative control was substrate with enzyme in different ratio as listed.

At the three different concentration ratios of substrate to protease (400:1, 1000:1, 2000:1), the fluorescent emission ratio at 530 nm to 475 nm gradually decreased and the related Z' factor gradually increased during the pre-SUMO maturation process with the increment of time. The value of Z' factor should be at least > 0.5 and the change of fluorescent emission ratio should be obvious to detect the positive hints. Compared all the conditions test in the HTS assay, the optimized condition was picked as the concentration ratio of substrate to protease at 1000:1 and incubation time at 25-30 minutes. At this condition, the Z' factor was about 0.66 and the change of fluorescent emission ratio was nearly four-fold, from 2.23 decreased to 0.56. For the condition of protease concentration was 250 pM, the value of Z' factor cannot reach to 0.5 in 30 minutes. For the condition of protease concentration was 50 pM, the value of Z' factor was just ~0.5 at 30 minutes, but the change of fluorescent emission ratio was less than 2-fold, from 2.49 to 1.22.

Validation of FRET-based HTS assay using non-specific SENP inhibitor

N-Ethylmaleimide (NEM) (Fig. 44-a) is an organic compound that is derived from maleic acid and has been widely used to probe the functional role of thiol groups in enzymology. NEM is an irreversible inhibitor of all cysteine peptidases, including SENPs. The dose-dependent effect of NEM to inhibit SENPs' activities was studied by using the developed FRET-based HTS assay.

The concentration of substrate CyPet-(pre-SUMO1)-YPet and protease SENP1C was fixed as 100 nM and 100 pM respectively as optimized. The inhibitor NEM was mixed with substrate and protease in low-salt Tris buffer, and its concentration varies from 10 µM to 50 mM. The mixtures were incubated at 37°C for 30 minutes, and then transferred to 384-well plate. The emission at 475 nm and 530 nm were detected under excitation of 414 nm. The ratio of fluorescent emission at 530nm to 475nm was used to characterize energy transfer signals. The NEM can inhibit the activity of SENP1C in pre-SUMO1's maturation from the concentration of 500 µM and above (Fig. 44-b). The results were confirmed by the western-blot (Fig. 44-c). This test exhibited a concentration-dependent inhibition of SENP1 activity by NEM and demonstrates a good correlation between FRET-based assay and biochemical western blot assay. The high-sensitive FRET-based HTS assay can then be applied to screenings to look for SENP1 inhibitors.

a

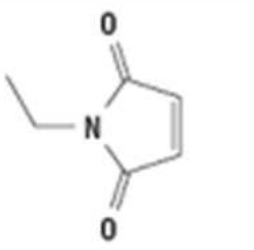

N-Ethylmaleimide
M.W. 125.13

b

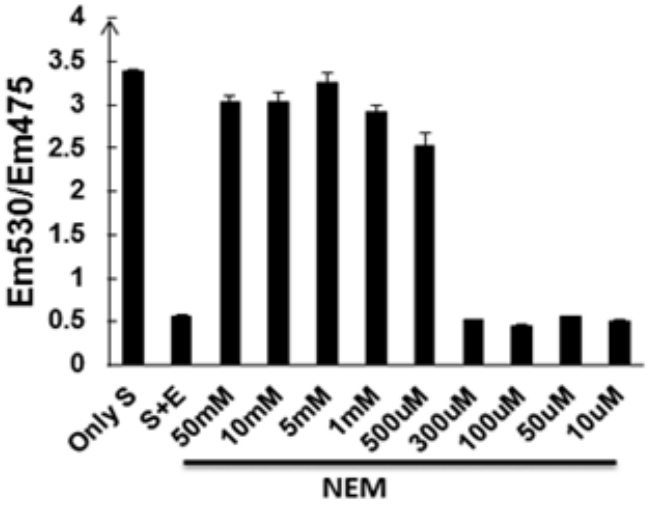

c

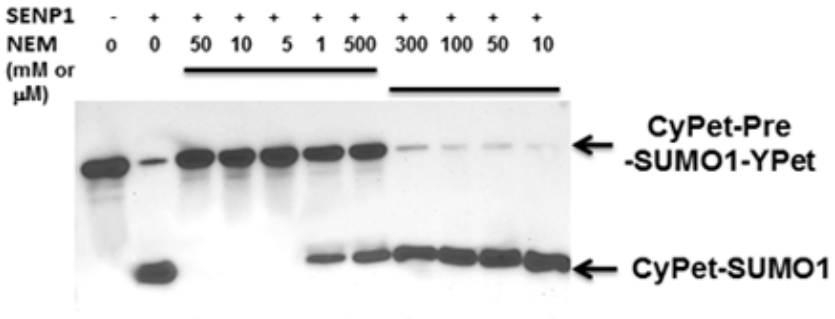

Fig. 44 HTS assay validation by studying the CyPet-(pre-SUMO1)-YPet maturation by SENP1C with NEM inhibition. (a) Structure of NEM; detection of substrate digestion by FRET-based assay (b) and western-blot (c).

Screening for SENP inhibitions

55,000 compounds were screened by using the developed FRET-based HTS assay for SENP inhibitors. In order to save proteins and plates, I combined every four stock 384-well plates into one screening plate, screened the compound mixtures at a concentration of 80 μM, and picked up corresponding positive compounds for further characterization.

In the compound stock plates, the two columns on the left and right respectively were empty, without any compounds, only DMSO. In the screening, the left two columns, as the positive control, were dispensed with only substrate. The other twenty-two columns were dispensed with substrate and protease. The right two columns were used as the negative control (Fig. 45).

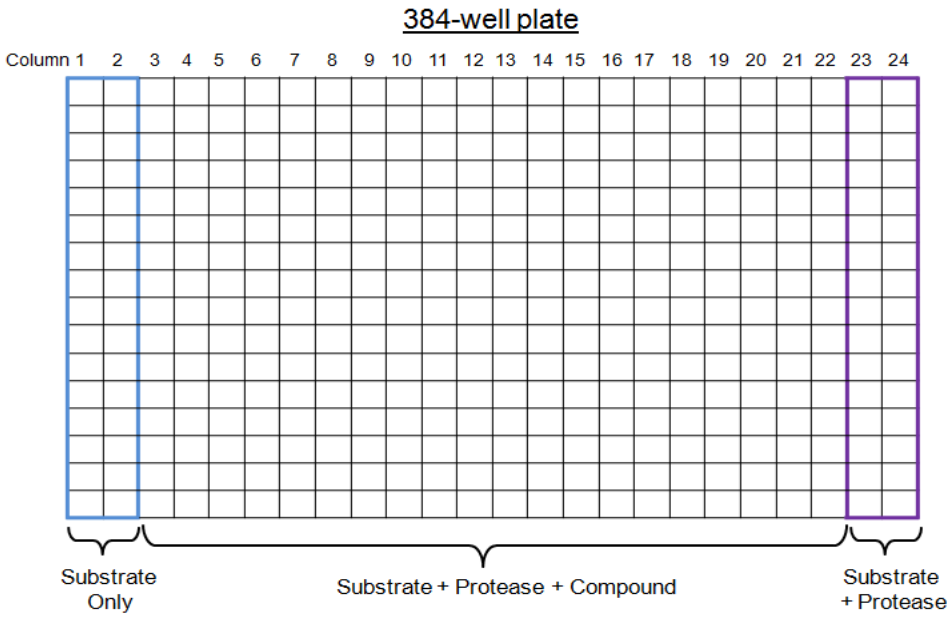

Fig. 45 The alignment of samples in the screening plate. The 2 left columns (blue) was positive control with substrate only; the two 2 columns (purple) was negative control with substrate and protease, the central 20 columns were the real compound screening.

Out of 14,000 wells screened, significant inhibition of emission ratio of 530 nm to 475 nm larger than 1.5 ($r_{FL530/FL475} > 1.5$) were shown in 51 wells. The criteria of $r_{FL530/FL475} > 1.5$ was chosen as $Mean - 3\sigma_{-}$ and $Mean \sim 2.5$ and $\sigma_{-} \sim 0.35$. A small scale screening of the 204 compounds which corresponded to 23 mixtures was applied, 23 compounds were shown positive in a one-compound-one-well basis. These compounds when then tested by western blot assay. All of the 23 mixtures can partially inhibit pre-SUMO1's maturation by SENP1 (Fig. 46).

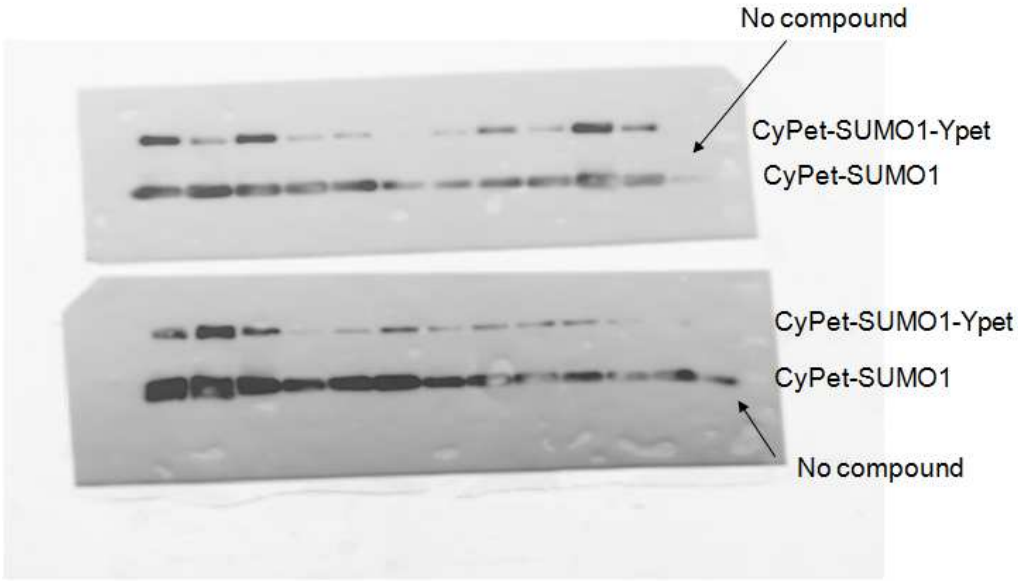

Fig. 46 Validation of SENP inhibitors picked from HTS assay. The protein amount used in the western blot assay was the same as the amount used in HTS assay. Compounds with $r_{FL530/FL475}$ decrease less than Mean-3xSD$_{-}$ were picked up.

Discussion

The developed FRET-based protease assay for protease kinetics study was converted into an *in vitro* HTS assay for SENP1 inhibitor. Although FRET technology has been widely used in biological research and extensive efforts have been take to develop it into HTS assay, it is very challenging to develop FRET-based HTS assay due to low FRET efficiencies of most FRET pairs. The highly efficient FRET pair, CyPet and YPet, provided a powerful tool for the high-sensitivity HTS assay development. The cleavage of substrate CyPet-(pre-SUMO1)-YPet by SENP1C resulted in significant FRET signal decrease. Ratiometric measurements and the critical screening Z' factor have been determined from various ratios of substrate to enzyme at different incubation time. As the high energy transfer efficiency of CyPet-YPet pair, both FRET signal and Z' factor were above satisfactory level for HTS for the optimized condition: mixture of 100 nM substrate and 100 pM protease incubated for 25-30 minutes. Optimal screening condition can be achieved at low concentrations of substrate (6 pmol) and protease (6 fmol) at economical effective manner with high quality and reproducibility in the screening campaign.

The strategy using fluorescent proteins as fluorescent marker for bound and free partner measurements can be a general method for HTS technology [217-219]. There are several advantages with this method: this approach is environmentally friendly and easy to handle as it does not require radioisotope labeling or

chemical modification of proteins; the fluorescent tagged proteins are in aqueous phase, which is mostly close to their natural environment in cells and the fluorescence intensity can be determined by general fluorescence plate reader, which is widely available.

Several assays have been developed for SENP or other protease assays in HTS platform [112, 113, 166, 167, 170, 171, 180, 212-214]. The development of the highly sensitive CyPet-YPet FRET for SENP inhibitor screening offered several advantages over other approaches. The high efficient FRET pair offered great signal to noise ratio in HTS format, the substrate gave six-fold signal changes before and after hydrolyzed by SENP, while the CFP-YFP pair only provided two-fold signal change (Fig. 10, Chapter I); the recombinant proteins can be generated by multiple methods, such as from bacterial cells, insect cells or mammalian cells, it can be readily adapted to cell-based protease HTS assay, while most other approaches, such as quenched QTGG-AMC tetrapeptide, SUMO-AMC and Tb-fluorescein-based TR-FRET methods, can only be carried out *in vitro*; comparing with those synthetic substrate, such as Tb-SUMO1-fluorescein, which needs chemical modifications and purifications *in vitro*, the genetically fusion substrate, CyPet-(pre-SUMO1)-YPet, offered almost 100% efficiency of fluorescence labeling; the full length substrate, offered a substrate which is most close to its natural substrate, therefore most likely mimic SENP native enzymatic activity. Other synthetic peptide substrates are very different to their natural substrate. The combination of this developed FRET-based HTS for

SENP endopeptidase inhibitor and previously developed FRET-based HTS for SUMO conjugation and deconjugation (Y. Song, J. Liao *in process*) provideed complete study tool for looking for SENP inhibitors.

In the developed FRET-based HTS assay, the ratiometric measurement of acceptor emission to donor emission used as criterion for signal measurement. However, this ratiometric measurement may be interfered by several factors and therefore may have higher load for secondary confirmation assays. First, self-fluorescent compounds may emit fluorescence at donor emission wavelength and therefore cause decrease of acceptor emission/donor emission ratio. Second, those self-fluorescent compounds which emit fluorescence at acceptor emission wavelength, although they may real inhibitors, will cause an increase of acceptor emission/donor emission ratio and therefore are disregarded as false-negative. Third, the fluorescence readings are very sensitive and may be affected by several processes and/or instrumentation-related interferes. For example, the plastic bottom of current used HTS assay plate often generate different levels of fluorescence depending on materials and these emissions often change the noise levels of assay. The quantitative FRET analysis described in previous chapters may provide a better strategy to characterize the compound inhibition or the absolute decrease of acceptor's and the absolute increase of donor's emission should be considered with the combination of acceptor emission/donor emission ratio to minimize the false-negative hints.

Even though no potent inhibitors for SENP1 were found after screening the approximate 55,000 compounds, the developed genetic-encoded FRET-based HTS assay for SENP1 inhibitor screening demonstrated high signal-to-noise ratio and good reproducibility. The discovery of protease inhibitors is a very challenging task in current scientific and industrial communities in the past [112, 113, 171]. Moreover, the product inhibition characterized in Chapter III may also affect the small chemical compound inhibitor's activities as the IC_{50} was ~3.8 μM when substrate concentration was 1.5 μM.

Recent efforts of screening a war-head focused cysteine protease library only leads to discoveries of modest irreversible inhibitors of SENP1 [113, 175]. One of which I believe is the lack of robust screening technologies which can provide starting points for subsequent medicinal chemistry. The strategy of using the high efficient CyPet/YPet FRET pair for protease inhibitor screening can be used as general approach for other protease inhibitor discovery. This approach provided an accurate and inexpensive strategy for protease inhibitor screenings. The sensitive FRET-based approach provided a powerful tool and can be expended to large-scale protease inhibitor screenings.

CONCLUSIOINS

Proteases are one of the most important enzyme classes in various signaling pathways and involved in many human diseases. SENP, the SUMO specific protease, performs two critical functions via an encoded cysteinyl proteinase activity: pre-SUMO maturation and SUMO-target deconjugaiton. A novel FRET-based protease assay was designed and developed to study the activities and specificities of SENPs in SUMOylation pathway. FRET was achieved by modifying the N- and C- terminus of related proteins with a pair of engineered fluorescent proteins, CyPet and YPet, which were optimized to provide higher energy transfer efficiency and quantum yield. The hydrolysis of fluorescent protein tagged pre-SUMO or SUMO-target complex by SENPs can be detected by the changes of FRET signals.

Firstly, the endopeptidase activities and specificities of SENPs toward pre-SUMOs were studied by the developed FRET-based protease assay. The specificities of SENP1/2/5/6/7C toward pre-SUMO1/2/3 were tested. The protease kinetics of pre-SUMO1's maturation by SENP1C was studied by quantitative FRET analysis with pre-established standard curve. Compare to widely-used two channel ratiometric FRET analysis, the detect fluorescence signal was differentiated to three parts: real FRET-induced acceptor's emission and direct emissions of donor and acceptor, which can be derived from pre-determined cross-talk ratio α and β. The pre-established standard curve related

the protein concentration to fluorescent signal. The novel mathematical algorithms were developed to depict the relationship between hydrolyzed protein concentration and detected fluorescent signal in the dynamic process. The kinetics constants K_M, k_{cat} and the k_{cat}/K_M ratio were obtained. The quantitative FRET analysis for protease kinetics studies was further developed as detecting emissions of donor and acceptor simultaneously, which diminished the errors from the standard curve establishment and fluorometer. The kinetics constants of pre-SUMO1/2/3's maturation by SENP1/2C were derived to compare the SENP endopeptidase substrate preference and the results were consistent to previous crystal structure analysis. The isopeptidase activities of SUMO1/2-RanGAP1C deconjugation by SENP1/2/5/6/7C were also studied by the similar assay. The protease kinetics study of SUMO1-RanGAP1C deconjugation by SENP1C was also performed to compare the differences of SENP's iso- and endo- peptidase activities.

Furthermore, the developed protease assay and novel quantitative FRET analysis were applied to another two applications in enzymatic studies of bio-mechanism and product inhibition characterizations. The collaborated work with Dr. Dimitrios Morikis group about pre-SUMO4's maturation has led to a successful protein engineering case study. Different mutations were generated to reverse pre-SUMO4 to pre-SUMO2 on electrostatic perturbative design. The effects of different mutations were quantified in the developed FRET-based protease assay and analyzed by the developed methodology of enzyme kinetics

study. Quantitative FRET analysis in protein binding affinity (to determine K_i) and protease kinetics studies (to determine IC_{50}) were combined to characterize the product inhibition of pre-SUMO1's maturation by SENP1C. The study of product inhibition of quantitative FRET analysis indicated the potential application of characterizing selected chemical compound inhibitors from HTS assay.

Last but not least, the FRET-based protease assay was converted to high-throughput screen assay to look for small chemical compounds which could specifically inhibit SENP1's endopeptidase activity. The screening conditions as protein concentration and incubation time were optimized to achieve satisfactory Z' factor, high signal-to-noise ratio and repeatability. 55,000 compounds were screened by the developed FRET-based HTS assay but without finding any potential inhibitors as it is pretty challenge to find cysteine protease inhibitors. However, the developed FRET-based HTS assay provided a powerful tool for large-scale and high-throughput applications.

Overall, the work described in this dissertation provides novel powerful tools for the study of protease kinetics and related applications, biomechanism and product inhibition in the SUMO pathway, and can be hopefully expanded to the research of other substrate-protease proteins in other signaling pathways.

REFERENCES

1. Muller, S., Hoege, C., Pyrowolakis, G., and Jentsch, S., *SUMO, ubiquitin's mysterious cousin.* Nature, 2001. **2**: p. 202-210.
2. Gill, G., *SUMO and ubiquitin in the nucleus: different functions, similar mechanisms?* Genes & Development, 2004. **18**(17): p. 2046-2059.
3. Schlesinger, D.H., Goldstein, G., and Niall, *The complete amino acid sequence of ubiquitin, an adenylate cyclase stimulating polypeptide probably universal in living cells.* Biochemistry, 1975. **14**(10): p. 2214-2218.
4. Johnson, E.S., *Protein modification by SUMO.* Annual Review of Biochemistry, 2004. **73**(1): p. 355-382.
5. Hay, R.T., *SUMO: a history of midification.* Molecular Cell, 2005. **18**(1): p. 1-12.
6. Hochstrasser, M., *SP-RING for SUMO: new functions bloom for a ubiquitin-like protein.* Cell, 2001. **107**: p. 5-8.
7. Uri Hanania, N.F.-M., Mily Ron and and A. Avni*, *Isolation of a novel SUMO protein from tomato that suppresses EIX-induced cell death.* Plant J., 1999. **19**(5): p. 533-541.
8. Bayer, P., Arndt, A., Metzger, S., Mahajan, R., Melchior, F., Jaenicke, R., and Becker, J., *Structure determination of the small ubiquitin-related modifier SUMO-1.* J. Mol. Biol, 1998. **280**: p. 275-286.
9. Shen, Z., Pardington-purtymun, P. E., Comequx, J. C. Moyzis, P. K., Chen, D. J., *UBL1, a Human Ubiquitin-like Protein Associating with Human RAD51RAD52 Proteins.* Genomics, 1996. **36**(2): p. 271-279.
10. Mannen, H., Tseng, H. M., Cho, C. and Li, S. S.-L., *Cloning and expression of human homolog HSMT3 to yeast SMT3 suppressor of MIF2 mutation in a centrometere protein gene.* Biochem Biophys Res Commun, 1996.
11. Chen, A., Mannen, H., Li, S. S.-L., *Characterization of mouse ubiquitin-like SMT3A and SMT3B cDNAs and gene/pseudogenes.* Biochem Mol Biol Int, 1998. **46**(6): p. 1161-1174.
12. Bohren, K.M., *A M55V Polymorphism in a Novel SUMO Gene (SUMO-4) Differentially Activates Heat Shock Transcription Factors and Is Associated with Susceptibility to Type I Diabetes Mellitus.* Journal of Biological Chemistry, 2004. **279**(26): p. 27233-27238.
13. Matunis, M.J., Coutavas, E., and Blobel, G., *A novel ubiquitin-like modification modulates the partitioning of the Ran-GTPase-activating protein RanGAP1 between the cytosol and the nuclear pore complex.* J. Cell Biol., 1996. **135**(6): p. 1457-1470.
14. Saitoh, H., and Hinchey, J., *Functional Heterogeneity of Small Ubiquitin-related Protein Modifiers SUMO-1 versus SUMO-2/3.* J. Biol. Chem, 2000. **275**(9): p. 6252-6258.

15. Rosas-Acosta, G., *A Universal Strategy for Proteomic Studies of SUMO and Other Ubiquitin-like Modifiers.* Molecular & Cellular Proteomics, 2004. **4**(1): p. 56-72.
16. Vertegaal, A.C.O., et al., *Distinct and Overlapping Sets of SUMO-1 and SUMO-2 Target Proteins Revealed by Quantitative Proteomics.* Molecular & Cellular Proteomics, 2006. **5**(12): p. 2298-2310.
17. Tatham, M.H., *Polymeric Chains of SUMO-2 and SUMO-3 Are Conjugated to Protein Substrates by SAE1/SAE2 and Ubc9.* Journal of Biological Chemistry, 2001. **276**(38): p. 35368-35374.
18. Ulrich, H.D., *The SUMO system: an overview.* Methods Mol Biol, 2009. **497**: p. 3-16.
19. Hannoun, Z., et al., *Post-translational modification by SUMO.* Toxicology, 2010. **278**(3): p. 288-293.
20. Johnson, E.S., Schwienhorst, I., Dohmen, R. J. and Blobel, G., *The ubiquitin-like protein Smt3p is activated for conjugation to other proteins by an Aos1p/Uba2p heterodimer.* EMBO J., 1997. **16**(18): p. 5509-5519.
21. Azuma, Y., *Expression and regulation of the mammalian SUMO-1 E1 enzyme.* The FASEB Journal, 2001.
22. Hayashi, T., et al., *Ubc9 Is Essential for Viability of Higher Eukaryotic Cells.* Experimental Cell Research, 2002. **280**(2): p. 212-221.
23. Tong, H., Hateboer, G., Perrakis, A., Bernards, R., and Sixma, T. K., *Crystal Structure of Murine/Human Ubc9 Provides Insight into the Variability of the Ubiquitin-conjugating System.* J. Biol. Chem, 1997. **272**(34): p. 21381-21387.
24. Bernier-Villamor, V., Sampson, D. A., Matunis, M. J., and Lima, C. D., *Structural Basis for E2-Mediated SUMO Conjugation Revealed by a Complex between Ubiquitin-Conjugating Enzyme Ubc9 and RanGAP1.* Cell, 2002. **108**: p. 345-356.
25. Tatham, M.H., Chen, Y., and Hay, R. T., *Role of Two Residues Proximal to the Active Site of Ubc9 in Substrate Recognition by the Ubc9·SUMO-1 Thiolester Complex.* Biochemistry, 2003. **42**: p. 3168-3179.
26. Tatham, M.H., Kim, S., Yu, B., Jaffray, E., Song J., Zheng J,. Rodriguez, M. S., Hay, R. T., and Chen Y., *Role of an N-Terminal Site of Ubc9 in SUMO-1, -2, and -3 Binding and Conjugation.* Biochemistry, 2003. **42**: p. 9959-9969.
27. Gareau, J.R. and C.D. Lima, *The SUMO pathway: emerging mechanisms that shape specificity, conjugation and recognition.* Nature Reviews Molecular Cell Biology, 2010. **11**(12): p. 861-871.
28. Pichler, A., Gast, A., Seeler, J. S., Dejean, A., and Melchior, F., *The Nucleoporin RanBP2 Has SUMO1 E3 Ligase Activity.* Cell, 2002. **108**: p. 109-120.
29. Kagey, M.H., Melhuish, T. A., and Wotton, D., *The Polycomb Protein Pc2 Is a SUMO E3.* Cell, 2003. **113**: p. 127-137.
30. Zhao, X., et al., *Regulation of MEF2 by Histone Deacetylase 4- and SIRT1 Deacetylase-Mediated Lysine Modifications.* Molecular and Cellular Biology, 2005. **25**(19): p. 8456-8464.

31. Geiss-Friedlander, R. and F. Melchior, *Concepts in sumoylation: a decade on.* Nature Reviews Molecular Cell Biology, 2007. **8**(12): p. 947-956.
32. Love, K.R., et al., *Mechanisms, biology and inhibitors of deubiquitinating enzymes.* Nature Chemical Biology, 2007. **3**(11): p. 697-705.
33. Hay, R.T., *SUMO-specific proteases: a twist in the tail.* Trends in Cell Biology, 2007. **17**(8): p. 370-376.
34. Drag, M. and G.S. Salvesen, *DeSUMOylating enzymes-SENPs.* IUBMB Life, 2008. **60**(11): p. 734-742.
35. Li, S.J. and M. Hochstrasser, *A new protease required for cell-cycle progression in yeast.* Nature, 1999. **398**(6724): p. 246-51.
36. Li, S.J. and M. Hochstrasser, *The yeast ULP2 (SMT4) gene encodes a novel protease specific for the ubiquitin-like Smt3 protein.* Mol Cell Biol, 2000. **20**(7): p. 2367-77.
37. Li, S.J. and M. Hochstrasser, *The Ulp1 SUMO isopeptidase: distinct domains required for viability, nuclear envelope localization, and substrate specificity.* J Cell Biol, 2003. **160**(7): p. 1069-81.
38. Panse, V.G., et al., *Unconventional tethering of Ulp1 to the transport channel of the nuclear pore complex by karyopherins.* Nat Cell Biol, 2003. **5**(1): p. 21-7.
39. Mendoza, H.M., et al., *NEDP1, a highly conserved cysteine protease that deNEDDylates Cullins.* J Biol Chem, 2003. **278**(28): p. 25637-43.
40. Wu, K., et al., *DEN1 is a dual function protease capable of processing the C terminus of Nedd8 and deconjugating hyper-neddylated CUL1.* J Biol Chem, 2003. **278**(31): p. 28882-91.
41. Yeh, E.T., L. Gong, and T. Kamitani, *Ubiquitin-like proteins: new wines in new bottles.* Gene, 2000. **248**(1-2): p. 1-14.
42. Xu, Z., Chan, H. Y., Lam, W. L., Lam, K. H., Lam, L. S. M., Ng, T. B., Au, S. W. N., *SUMO Proteases: Redox Regulation and Biological Consequences.* Antioxid. Redox Signaling, 2009. **11**(6): p. 1453-1484.
43. Gong, L., et al., *Differential regulation of sentrinized proteins by a novel sentrin-specific protease.* J Biol Chem, 2000. **275**(5): p. 3355-9.
44. Bailey, D. and P. O'Hare, *Characterization of the localization and proteolytic activity of the SUMO-specific protease, SENP1.* J Biol Chem, 2004. **279**(1): p. 692-703.
45. Bailey, D. and P. O'Hare, *Herpes simplex virus 1 ICP0 co-localizes with a SUMO-specific protease.* J Gen Virol, 2002. **83**(Pt 12): p. 2951-64.
46. Kim, Y.H., et al., *Desumoylation of homeodomain-interacting protein kinase 2 (HIPK2) through the cytoplasmic-nuclear shuttling of the SUMO-specific protease SENP1.* FEBS Lett, 2005. **579**(27): p. 6272-8.
47. Hang, J. and M. Dasso, *Association of the human SUMO-1 protease SENP2 with the nuclear pore.* J Biol Chem, 2002. **277**(22): p. 19961-6.
48. Zhang, H., H. Saitoh, and M.J. Matunis, *Enzymes of the SUMO modification pathway localize to filaments of the nuclear pore complex.* Mol Cell Biol, 2002. **22**(18): p. 6498-508.

49. Ross, S., et al., *SUMO-1 modification represses Sp3 transcriptional activation and modulates its subnuclear localization.* Mol Cell, 2002. **10**(4): p. 831-42.
50. Itahana, Y., E.T. Yeh, and Y. Zhang, *Nucleocytoplasmic shuttling modulates activity and ubiquitination-dependent turnover of SUMO-specific protease 2.* Mol Cell Biol, 2006. **26**(12): p. 4675-89.
51. Nishida, T., et al., *Characterization of a novel mammalian SUMO-1/Smt3-specific isopeptidase, a homologue of rat axam, which is an axin-binding protein promoting beta-catenin degradation.* J Biol Chem, 2001. **276**(42): p. 39060-6.
52. Best, J.L., et al., *SUMO-1 protease-1 regulates gene transcription through PML.* Mol Cell, 2002. **10**(4): p. 843-55.
53. Nishida, T., H. Tanaka, and H. Yasuda, *A novel mammalian Smt3-specific isopeptidase 1 (SMT3IP1) localized in the nucleolus at interphase.* Eur J Biochem, 2000. **267**(21): p. 6423-7.
54. Gong, L. and E.T. Yeh, *Characterization of a family of nucleolar SUMO-specific proteases with preference for SUMO-2 or SUMO-3.* J Biol Chem, 2006. **281**(23): p. 15869-77.
55. Kim, K.I., et al., *A new SUMO-1-specific protease, SUSP1, that is highly expressed in reproductive organs.* J Biol Chem, 2000. **275**(19): p. 14102-6.
56. Mukhopadhyay, D., et al., *SUSP1 antagonizes formation of highly SUMO2/3-conjugated species.* The Journal of Cell Biology, 2006. **174**(7): p. 939-949.
57. Kim, J.H. and S.H. Baek, *Emerging roles of desumoylating enzymes.* Biochimica et Biophysica Acta (BBA) - Molecular Basis of Disease, 2009. **1792**(3): p. 155-162.
58. Mossessova, E. and C.D. Lima, *Ulp1-SUMO crystal structure and genetic analysis reveal conserved interactions and a regulatory element essential for cell growth in yeast.* Mol Cell, 2000. **5**(5): p. 865-76.
59. Dong, C., et al., *The structure of SENP1–SUMO-2 complex suggests a structural basis for discrimination between SUMO paralogues during processing.* Biochemical Journal, 2006. **397**(2): p. 279.
60. Reverter, D. and C.D. Lima, *A Basis for SUMO Protease Specificity Provided by Analysis of Human Senp2 and a Senp2-SUMO Complex.* Structure, 2004. **12**(8): p. 1519-1531.
61. Shen, L., et al., *SUMO protease SENP1 induces isomerization of the scissile peptide bond.* Nat. Struct. Mol. Biol., 2006. **13**(12): p. 1069-1077.
62. Xu, Z., and Au, S. W. N., *Mapping residues of SUMO precursors essential in differential maturation by SUMO-specific protease, SENP1.* Biochem J., 2005. **386**: p. 325-330.
63. Reverter, D. and C.D. Lima, *Structural basis for SENP2 protease interactions with SUMO precursors and conjugated substrates.* Nature Structural & Molecular Biology, 2006. **13**(12): p. 1060-1068.
64. Di Bacco, A., et al., *The SUMO-specific protease SENP5 is required for cell division.* Mol Cell Biol, 2006. **26**(12): p. 4489-98.

65. Lima, C.D. and D. Reverter, *Structure of the Human SENP7 Catalytic Domain and Poly-SUMO Deconjugation Activities for SENP6 and SENP7.* Journal of Biological Chemistry, 2008. **283**(46): p. 32045-32055.
66. Hay, R.T., *Protein modification by SUMO.* Trends Biochem Sci, 2001. **26**(5): p. 332-3.
67. Schwartz, D.C., R. Felberbaum, and M. Hochstrasser, *The Ulp2 SUMO protease is required for cell division following termination of the DNA damage checkpoint.* Mol Cell Biol, 2007. **27**(19): p. 6948-61.
68. Zhao, J., *Sumoylation regulates diverse biological processes.* Cell Mol Life Sci, 2007. **64**(23): p. 3017-33.
69. Dohmen, R.J., *SUMO protein modification.* Biochim Biophys Acta, 2004. **1695**(1-3): p. 113-31.
70. Cheng, J., et al., *SENP1 enhances androgen receptor-dependent transcription through desumoylation of histone deacetylase 1.* Mol Cell Biol, 2004. **24**(13): p. 6021-8.
71. Kaikkonen, S., et al., *SUMO-specific protease 1 (SENP1) reverses the hormone-augmented SUMOylation of androgen receptor and modulates gene responses in prostate cancer cells.* Mol Endocrinol, 2009. **23**(3): p. 292-307.
72. Cheng, J., N.D. Perkins, and E.T. Yeh, *Differential regulation of c-Jun-dependent transcription by SUMO-specific proteases.* J Biol Chem, 2005. **280**(15): p. 14492-8.
73. Kadoya, T., et al., *Desumoylation activity of Axam, a novel Axin-binding protein, is involved in downregulation of beta-catenin.* Mol Cell Biol, 2002. **22**(11): p. 3803-19.
74. Yamamoto, H., et al., *Sumoylation is involved in beta-catenin-dependent activation of Tcf-4.* EMBO J, 2003. **22**(9): p. 2047-59.
75. Shitashige, M., et al., *Regulation of Wnt signaling by the nuclear pore complex.* Gastroenterology, 2008. **134**(7): p. 1961-71, 1971 e1-4.
76. Gregoire, S. and X.J. Yang, *Association with class IIa histone deacetylases upregulates the sumoylation of MEF2 transcription factors.* Mol Cell Biol, 2005. **25**(6): p. 2273-87.
77. Choi, S.J., et al., *Negative modulation of RXRalpha transcriptional activity by small ubiquitin-related modifier (SUMO) modification and its reversal by SUMO-specific protease SUSP1.* J Biol Chem, 2006. **281**(41): p. 30669-77.
78. Yamaguchi, T., et al., *Mutation of SENP1/SuPr-2 reveals an essential role for desumoylation in mouse development.* Mol Cell Biol, 2005. **25**(12): p. 5171-82.
79. Chiu, S.Y., et al., *SUMO-specific protease 2 is essential for modulating p53-Mdm2 in development of trophoblast stem cell niches and lineages.* PLoS Biol, 2008. **6**(12): p. e310.
80. Cheng, J., et al., *Role of desumoylation in the development of prostate cancer.* Neoplasia, 2006. **8**(8): p. 667-76.
81. Yates, K.E., et al., *Repression of the SUMO-specific protease Senp1 induces p53-dependent premature senescence in normal human fibroblasts.* Aging Cell, 2008. **7**(5): p. 609-21.

82. Li, X., et al., *SENP1 mediates TNF-induced desumoylation and cytoplasmic translocation of HIPK1 to enhance ASK1-dependent apoptosis.* Cell Death Differ, 2008. **15**(4): p. 739-50.
83. Alarcon-Vargas, D.a.R., Z., *SUMO in cancer-Wrestlers wanted.* Can Biol Ther, 2002. **1**: p. 237-242.
84. Seeler, J.S. and A. Dejean, *Nuclear and unclear functions of SUMO.* Nat Rev Mol Cell Biol, 2003. **4**(9): p. 690-9.
85. Jacques, C., et al., *Two-step differential expression analysis reveals a new set of genes involved in thyroid oncocytic tumors.* J Clin Endocrinol Metab, 2005. **90**(4): p. 2314-20.
86. Bawa-Khalfe, T. and E.T.H. Yeh, *SUMO Losing Balance: SUMO Proteases Disrupt SUMO Homeostasis to Facilitate Cancer Development and Progression.* Genes & Cancer, 2010. **1**(7): p. 748-752.
87. Han, Y., et al., *SENP3-mediated de-conjugation of SUMO2/3 from promyelocytic leukemia is correlated with accelerated cell proliferation under mild oxidative stress.* J Biol Chem, 2010. **285**(17): p. 12906-15.
88. Kuo, M.L., et al., *Arf-induced turnover of the nucleolar nucleophosmin-associated SUMO-2/3 protease Senp3.* Cell Cycle, 2008. **7**(21): p. 3378-87.
89. Kim, W.Y. and N.E. Sharpless, *The regulation of INK4/ARF in cancer and aging.* Cell, 2006. **127**(2): p. 265-75.
90. Wang, L. and S. Banerjee, *Differential PIAS3 expression in human malignancy.* Oncol Rep, 2004. **11**(6): p. 1319-24.
91. Mo, Y.Y. and S.J. Moschos, *Targeting Ubc9 for cancer therapy.* Expert Opin Ther Targets, 2005. **9**(6): p. 1203-16.
92. Mo, Y.Y., et al., *A role for Ubc9 in tumorigenesis.* Oncogene, 2005. **24**(16): p. 2677-83.
93. Mooney, S.M., et al., *Sumoylation of p68 and p72 RNA helicases affects protein stability and transactivation potential.* Biochemistry, 2010. **49**(1): p. 1-10.
94. Ding, X., et al., *Overexpression of SENP5 in oral squamous cell carcinoma and its association with differentiation.* Oncol Rep, 2008. **20**(5): p. 1041-5.
95. Tagawa, H., et al., *Molecular cytogenetic analysis of the breakpoint region at 6q21-22 in T-cell lymphoma/leukemia cell lines.* Genes Chromosomes Cancer, 2002. **34**(2): p. 175-85.
96. Kim, J.H., et al., *Transcriptional regulation of a metastasis suppressor gene by Tip60 and beta-catenin complexes.* Nature, 2005. **434**(7035): p. 921-6.
97. Kim, K.I. and S.H. Baek, *SUMOylation code in cancer development and metastasis.* Mol Cells, 2006. **22**(3): p. 247-53.
98. Bauer, A., et al., *Pontin52 and reptin52 function as antagonistic regulators of beta-catenin signalling activity.* EMBO J, 2000. **19**(22): p. 6121-30.
99. Vethantham, V., N. Rao, and J.L. Manley, *Sumoylation modulates the assembly and activity of the pre-mRNA 3' processing complex.* Mol Cell Biol, 2007. **27**(24): p. 8848-58.

100. Haindl, M., et al., *The nucleolar SUMO-specific protease SENP3 reverses SUMO modification of nucleophosmin and is required for rRNA processing.* EMBO Rep, 2008. **9**(3): p. 273-9.
101. Concha, N.O. and S.S. Abdel-Meguid, *Controlling apoptosis by inhibition of caspases.* Curr Med Chem, 2002. **9**(6): p. 713-26.
102. Joyce, J.A., et al., *Cathepsin cysteine proteases are effectors of invasive growth and angiogenesis during multistage tumorigenesis.* Cancer Cell, 2004. **5**(5): p. 443-53.
103. Pickart, C.M. and I.A. Rose, *Mechanism of ubiquitin carboxyl-terminal hydrolase. Borohydride and hydroxylamine inactivate in the presence of ubiquitin.* J Biol Chem, 1986. **261**(22): p. 10210-7.
104. Hershko, A. and I.A. Rose, *Ubiquitin-aldehyde: a general inhibitor of ubiquitin-recycling processes.* Proc Natl Acad Sci U S A, 1987. **84**(7): p. 1829-33.
105. Lam, Y.A., et al., *Editing of ubiquitin conjugates by an isopeptidase in the 26S proteasome.* Nature, 1997. **385**(6618): p. 737-40.
106. Borodovsky, A., et al., *Small-Molecule Inhibitors and Probes for Ubiquitin- and Ubiquitin-Like-Specific Proteases.* ChemBioChem, 2005. **6**(2): p. 287-291.
107. Hemelaar, J., et al., *Specific and Covalent Targeting of Conjugating and Deconjugating Enzymes of Ubiquitin-Like Proteins.* Molecular and Cellular Biology, 2003. **24**(1): p. 84-95.
108. Borodovsky, A., Ovaa, H., Kolli, N., Gan-Erdene, T., Wilkinson, K. D., Ploegh, H. L. and Kessler, B. M., *Chemistry-Based Functional Proteomics Reveals Novel Members of the Deubiquitinating Enzyme Family.* Chem. Biol., 2002. **9**: p. 1149-1159.
109. Mullally, J.E., et al., *Cyclopentenone prostaglandins of the J series inhibit the ubiquitin isopeptidase activity of the proteasome pathway.* J Biol Chem, 2001. **276**(32): p. 30366-73.
110. Wilkinson, K.D., T. Gan-Erdene, and N. Kolli, *Derivitization of the C-terminus of ubiquitin and ubiquitin-like proteins using intein chemistry: methods and uses.* Methods Enzymol, 2005. **399**: p. 37-51.
111. Qiao, Z., et al., *Design, synthesis, and biological evaluation of benzodiazepine-based SUMO-specific protease 1 inhibitors.* Bioorg Med Chem Lett, 2011. **21**(21): p. 6389-92.
112. Ponder, Elizabeth L., et al., *Functional Characterization of a SUMO Deconjugating Protease of Plasmodium falciparum Using Newly Identified Small Molecule Inhibitors.* Chemistry & Biology, 2011. **18**(6): p. 711-721.
113. Albrow, Victoria E., et al., *Development of Small Molecule Inhibitors and Probes of Human SUMO Deconjugating Proteases.* Chemistry & Biology, 2011. **18**(6): p. 722-732.
114. Berger, A.B., et al., *Identification of early intermediates of caspase activation using selective inhibitors and activity-based probes.* Mol Cell, 2006. **23**(4): p. 509-21.

115. Fonovic, M., et al., *Human cathepsin F: expression in baculovirus system, characterization and inhibition by protein inhibitors.* Biol Chem, 2004. **385**(6): p. 505-9.
116. Sexton, K.B., et al., *Design of cell-permeable, fluorescent activity-based probes for the lysosomal cysteine protease asparaginyl endopeptidase (AEP)/legumain.* Bioorg Med Chem Lett, 2007. **17**(3): p. 649-53.
117. Kato, D., et al., *Activity-based probes that target diverse cysteine protease families.* Nat Chem Biol, 2005. **1**(1): p. 33-8.
118. Sun, Y., et al., *FRET Microscopy in 2010: The Legacy of Theodor Förster on the 100th Anniversary of his Birth.* ChemPhysChem, 2011. **12**(3): p. 462-474.
119. Stryer, L., *Fluorescence energy transfer as a spectroscopic ruler.* Annu Rev Biochem, 1978. **47**: p. 819-46.
120. dos Remedios, C.G. and P.D. Moens, *Fluorescence resonance energy transfer spectroscopy is a reliable "ruler" for measuring structural changes in proteins. Dispelling the problem of the unknown orientation factor.* J Struct Biol, 1995. **115**(2): p. 175-85.
121. Stryer, L. and R.P. Haugland, *Energy transfer: a spectroscopic ruler.* Proc Natl Acad Sci U S A, 1967. **58**(2): p. 719-26.
122. Bucher, H., et al., *Controlled Transfer of Excitation Energy through Thin Layers.* Molecular Crystals, 1967. **2**(3): p. 199-&.
123. Haugland, R.P., J. Yguerabide, and L. Stryer, *Dependence of the kinetics of singlet-singlet energy transfer on spectral overlap.* Proc Natl Acad Sci U S A, 1969. **63**(1): p. 23-30.
124. Shaner, N.C., et al., *Improving the photostability of bright monomeric orange and red fluorescent proteins.* Nat Methods, 2008. **5**(6): p. 545-51.
125. Sapsford, K.E., L. Berti, and I.L. Medintz, *Materials for Fluorescence Resonance Energy Transfer Analysis: Beyond Traditional Donor–Acceptor Combinations.* Angewandte Chemie International Edition, 2006. **45**(28): p. 4562-4589.
126. Day, R.N. and M.W. Davidson, *The fluorescent protein palette: tools for cellular imaging.* Chem Soc Rev, 2009. **38**(10): p. 2887-921.
127. Day, R.N. and F. Schaufele, *Fluorescent protein tools for studying protein dynamics in living cells: a review.* J Biomed Opt, 2008. **13**(3): p. 031202.
128. Wallrabe, H. and A. Periasamy, *Imaging protein molecules using FRET and FLIM microscopy.* Curr Opin Biotechnol, 2005. **16**(1): p. 19-27.
129. Li, H., et al., *Actin cytoskeleton-dependent Rab GTPase-regulated angiotensin type I receptor lysosomal degradation studied by fluorescence lifetime imaging microscopy.* J Biomed Opt, 2010. **15**(5): p. 056003.
130. Li, H., et al., *Rab4 and Rab11 coordinately regulate the recycling of angiotensin II type I receptor as demonstrated by fluorescence resonance energy transfer microscopy.* J Biomed Opt, 2008. **13**(3): p. 031206.

131. Algar, W.R. and U.J. Krull, *Quantum dots as donors in fluorescence resonance energy transfer for the bioanalysis of nucleic acids, proteins, and other biological molecules.* Anal Bioanal Chem, 2008. **391**(5): p. 1609-18.
132. Resch-Genger, U., et al., *Quantum dots versus organic dyes as fluorescent labels.* Nat Methods, 2008. **5**(9): p. 763-75.
133. Medintz, I.L. and H. Mattoussi, *Quantum dot-based resonance energy transfer and its growing application in biology.* Phys Chem Chem Phys, 2009. **11**(1): p. 17-45.
134. Clapp, A.R., I.L. Medintz, and H. Mattoussi, *Förster Resonance Energy Transfer Investigations Using Quantum-Dot Fluorophores.* ChemPhysChem, 2006. **7**(1): p. 47-57.
135. Moshinsky, D.J., et al., *A widely applicable, high-throughput TR-FRET assay for the measurement of kinase autophosphorylation: VEGFR-2 as a prototype.* J Biomol Screen, 2003. **8**(4): p. 447-52.
136. Zhou, V., et al., *A time-resolved fluorescence resonance energy transfer-based HTS assay and a surface plasmon resonance-based binding assay for heat shock protein 90 inhibitors.* Anal Biochem, 2004. **331**(2): p. 349-57.
137. Xu, Z., et al., *Development of high-throughput TR-FRET and AlphaScreen assays for identification of potent inhibitors of PDK1.* J Biomol Screen, 2009. **14**(10): p. 1257-62.
138. Pyykko, I., et al., *Postural control in Meniere's disease and acoustic neurinoma when studied on a linearly oscillating platform.* Acta Otolaryngol Suppl, 1995. **520 Pt 1**: p. 19-21.
139. Lundin, K., et al., *Development of a time-resolved fluorescence resonance energy transfer assay (cell TR-FRET) for protein detection on intact cells.* Anal Biochem, 2001. **299**(1): p. 92-7.
140. Ponsioen, B., et al., *Detecting cAMP-induced Epac activation by fluorescence resonance energy transfer: Epac as a novel cAMP indicator.* EMBO Rep, 2004. **5**(12): p. 1176-80.
141. Allen, M.D., et al., *Reading dynamic kinase activity in living cells for high-throughput screening.* ACS Chem Biol, 2006. **1**(6): p. 371-6.
142. Gao, X. and J. Zhang, *Spatiotemporal analysis of differential Akt regulation in plasma membrane microdomains.* Mol Biol Cell, 2008. **19**(10): p. 4366-73.
143. Vinkenborg, J.L., et al., *Genetically encoded FRET sensors to monitor intracellular Zn2+ homeostasis.* Nat Methods, 2009. **6**(10): p. 737-40.
144. Tron, L., et al., *Flow cytometric measurement of fluorescence resonance energy transfer on cell surfaces. Quantitative evaluation of the transfer efficiency on a cell-by-cell basis.* Biophys J, 1984. **45**(5): p. 939-46.
145. Gordon, G.W., et al., *Quantitative fluorescence resonance energy transfer measurements using fluorescence microscopy.* Biophys J, 1998. **74**(5): p. 2702-13.

146. Tsuji, A., et al., *Direct observation of specific messenger RNA in a single living cell under a fluorescence microscope.* Biophys J, 2000. **78**(6): p. 3260-74.
147. Suzuki, Y., *Detection of the swings of the lever arm of a myosin motor by fluorescence resonance energy transfer of green and blue fluorescent proteins.* Methods, 2000. **22**(4): p. 355-63.
148. Kam, Z., T. Volberg, and B. Geiger, *Mapping of adherens junction components using microscopic resonance energy transfer imaging.* J Cell Sci, 1995. **108 (Pt 3)**: p. 1051-62.
149. Mahajan, N.P., et al., *Bcl-2 and Bax interactions in mitochondria probed with green fluorescent protein and fluorescence resonance energy transfer.* Nat Biotechnol, 1998. **16**(6): p. 547-52.
150. Ruiz-Velasco, V. and S.R. Ikeda, *Functional expression and FRET analysis of green fluorescent proteins fused to G-protein subunits in rat sympathetic neurons.* J Physiol, 2001. **537**(Pt 3): p. 679-92.
151. Elangovan, M., et al., *Characterization of one- and two-photon excitation fluorescence resonance energy transfer microscopy.* Methods, 2003. **29**(1): p. 58-73.
152. Mehta, K., et al., *A computational approach to inferring cellular protein-binding affinities from quantitative fluorescence resonance energy transfer imaging.* Proteomics, 2009. **9**(23): p. 5371-83.
153. Lam, A.D., et al., *Mapping dynamic protein interactions to insulin secretory granule behavior with TIRF-FRET.* Biophys J, 2010. **99**(4): p. 1311-20.
154. Albertazzi, L., et al., *Quantitative FRET analysis with the EGFP-mCherry fluorescent protein pair.* Photochem Photobiol, 2009. **85**(1): p. 287-97.
155. Padilla-Parra, S., et al., *Quantitative FRET analysis by fast acquisition time domain FLIM at high spatial resolution in living cells.* Biophys J, 2008. **95**(6): p. 2976-88.
156. Kenworthy, A.K., *Imaging protein-protein interactions using fluorescence resonance energy transfer microscopy.* Methods, 2001. **24**(3): p. 289-96.
157. Valentin, G., et al., *Photoconversion of YFP into a CFP-like species during acceptor photobleaching FRET experiments.* Nat Methods, 2005. **2**(11): p. 801.
158. Van Munster, E.B., et al., *Fluorescence resonance energy transfer (FRET) measurement by gradual acceptor photobleaching.* J Microsc, 2005. **218**(Pt 3): p. 253-62.
159. Peter, M., et al., *Multiphoton-FLIM quantification of the EGFP-mRFP1 FRET pair for localization of membrane receptor-kinase interactions.* Biophys J, 2005. **88**(2): p. 1224-37.
160. Cheng, A.K., et al., *Aptamer-based detection of epithelial tumor marker mucin 1 with quantum dot-based fluorescence readout.* Anal Chem, 2009. **81**(15): p. 6130-9.
161. Prasuhn, D.E., et al., *Quantum dot peptide biosensors for monitoring caspase 3 proteolysis and calcium ions.* ACS Nano, 2010. **4**(9): p. 5487-97.

162. Merchant, K.A., et al., *Characterizing the unfolded states of proteins using single-molecule FRET spectroscopy and molecular simulations.* Proc Natl Acad Sci U S A, 2007. **104**(5): p. 1528-33.
163. Bendix, P.M., M.S. Pedersen, and D. Stamou, *Quantification of nano-scale intermembrane contact areas by using fluorescence resonance energy transfer.* Proc Natl Acad Sci U S A, 2009. **106**(30): p. 12341-6.
164. Mikolajczyk, J., et al., *Small Ubiquitin-related Modifier (SUMO)-specific Proteases: PROFILING THE SPECIFICITIES AND ACTIVITIES OF HUMAN SENPs.* Journal of Biological Chemistry, 2007. **282**(36): p. 26217-26224.
165. Drag, M., et al., *Positional-scanning fluorigenic substrate libraries reveal unexpected specificity determinants of DUBs (deubiquitinating enzymes).* Biochemical Journal, 2008. **415**(3): p. 367.
166. Horton, R., et al., *A substrate for deubiquitinating enzymes based on time-resolved fluorescence resonance energy transfer between terbium and yellow fluorescent protein.* Analytical Biochemistry, 2007. **360**(1): p. 138-143.
167. Martin, S., et al., *A fluorescence-resonance-energy-transfer-based protease activity assay and its use to monitor paralog-specific small ubiquitin-like modifier processing.* Analytical Biochemistry, 2007. **363**(1): p. 83-90.
168. Drag, M., et al., *Activity profiling of human deSUMOylating enzymes (SENPs) with synthetic substrates suggests an unexpected specificity of two newly characterized members of the family.* Biochemical Journal, 2008. **409**(2): p. 461.
169. Kolli, N., et al., *Distribution and paralogue specificity of mammalian deSUMOylating enzymes.* Biochem J, 2010. **430**(2): p. 335-44.
170. Engels, I.H., et al., *A time-resolved fluorescence resonance energy transfer-based assay for DEN1 peptidase activity.* Anal Biochem, 2009. **390**(1): p. 85-7.
171. Carlson, C.B., R.A. Horton, and K.W. Vogel, *A toolbox approach to high-throughput TR-FRET-based SUMOylation and DeSUMOylation assays.* Assay Drug Dev Technol, 2009. **7**(4): p. 348-55.
172. Berney, C. and G. Danuser, *FRET or no FRET: a quantitative comparison.* Biophys J, 2003. **84**(6): p. 3992-4010.
173. Nguyen, A.W. and P.S. Daugherty, *Evolutionary optimization of fluorescent proteins for intracellular FRET.* Nature Biotechnology, 2005. **23**(3): p. 355-360.
174. Deu, E., M. Verdoes, and M. Bogyo, *New approaches for dissecting protease functions to improve probe development and drug discovery.* Nat Struct Mol Biol, 2012. **19**(1): p. 9-16.
175. Drag, M. and G.S. Salvesen, *Emerging principles in protease-based drug discovery.* Nat Rev Drug Discov, 2010. **9**(9): p. 690-701.
176. Wu, P. and L. Brand, *Resonance energy transfer: methods and applications.* Anal Biochem, 1994. **218**(1): p. 1-13.

177. Miyawaki, A., *Development of probes for cellular functions using fluorescent proteins and fluorescence resonance energy transfer.* Annu Rev Biochem, 2011. **80**: p. 357-73.
178. Jares-Erijman, E.A. and T.M. Jovin, *FRET imaging.* Nat Biotechnol, 2003. **21**(11): p. 1387-95.
179. Grecco, H.E. and P.J. Verveer, *FRET in cell biology: still shining in the age of super-resolution?* ChemPhysChem, 2011. **12**(3): p. 484-90.
180. Rouleau, N., et al., *Highly sensitive assays for SUMOylation and small ubiquitin-like modifier-dependent protein–protein interactions.* Analytical Biochemistry, 2008. **375**(2): p. 364-366.
181. Ullman, E.F., et al., *Luminescent oxygen channeling assay (LOCI): sensitive, broadly applicable homogeneous immunoassay method.* Clin Chem, 1996. **42**(9): p. 1518-26.
182. Ullman, E.F., et al., *Luminescent oxygen channeling immunoassay: measurement of particle binding kinetics by chemiluminescence.* Proc Natl Acad Sci U S A, 1994. **91**(12): p. 5426-30.
183. Dafforn, A., H. Kirakossian, and K. Lao, *Miniaturization of the luminescent oxygen channeling immunoassay (LOCI(TM)) for use in multiplex array formats and other biochips.* Clin Chem, 2000. **46**(9): p. 1495-7.
184. Liu, Y.P., et al., *Homogeneous, rapid luminescent oxygen channeling immunoassay (LOCI(TM)) for homocysteine.* Clin Chem, 2000. **46**(9): p. 1506-7.
185. Morrison, L.E., *Time-resolved detection of energy transfer: theory and application to immunoassays.* Anal Biochem, 1988. **174**(1): p. 101-20.
186. Xu, Z., et al., *Crystal structure of the SENP1 mutant C603S-SUMO complex reveals the hydrolytic mechanism of SUMO-specific protease.* Biochem J, 2006. **398**(3): p. 345-52.
187. Turk, B., *Targeting proteases: successes, failures and future prospects.* Nature Reviews Drug Discovery, 2006. **5**(9): p. 785-799.
188. Guo, D., et al., *A functional variant of SUMO4, a new I kappa B alpha modifier, is associated with type 1 diabetes.* Nat Genet, 2004. **36**(8): p. 837-41.
189. Wang, C.-Y. and J.-X. She, *SUMO4 and its role in type 1 diabetes pathogenesis.* Diabetes/Metabolism Research and Reviews, 2008. **24**(2): p. 93-102.
190. Bacher, S. and M.L. Schmitz, *The NF-kappaB pathway as a potential target for autoimmune disease therapy.* Curr Pharm Des, 2004. **10**(23): p. 2827-37.
191. Shaulian, E. and M. Karin, *AP-1 as a regulator of cell life and death.* Nat Cell Biol, 2002. **4**(5): p. E131-6.
192. Libermann, T.A. and L.F. Zerbini, *Targeting transcription factors for cancer gene therapy.* Curr Gene Ther, 2006. **6**(1): p. 17-33.
193. Ashida, R., et al., *AP-1 and colorectal cancer.* Inflammopharmacology, 2005. **13**(1-3): p. 113-25.

194. Guo, D., et al., *Proteomic analysis of SUMO4 substrates in HEK293 cells under serum starvation-induced stress.* Biochem Biophys Res Commun, 2005. **337**(4): p. 1308-18.
195. Bossis, G., et al., *Down-regulation of c-Fos/c-Jun AP-1 dimer activity by sumoylation.* Mol Cell Biol, 2005. **25**(16): p. 6964-79.
196. Salinas, S., et al., *SUMOylation regulates nucleo-cytoplasmic shuttling of Elk-1.* J Cell Biol, 2004. **165**(6): p. 767-73.
197. Owerbach, D., et al., *A proline-90 residue unique to SUMO-4 prevents maturation and sumoylation.* Biochemical and Biophysical Research Communications, 2005. **337**(2): p. 517-520.
198. Zhang, L., B. Mallik, and D. Morikis, *Immunophysical exploration of C3d-CR2(CCP1-2) interaction using molecular dynamics and electrostatics.* J Mol Biol, 2007. **369**(2): p. 567-83.
199. Morikis, D. and J.D. Lambris, *The electrostatic nature of C3d-complement receptor 2 association.* J Immunol, 2004. **172**(12): p. 7537-47.
200. Zhang, L. and D. Morikis, *Immunophysical properties and prediction of activities for vaccinia virus complement control protein and smallpox inhibitor of complement enzymes using molecular dynamics and electrostatics.* Biophys J, 2006. **90**(9): p. 3106-19.
201. Chae, K., et al., *Two SCA (stigma/style cysteine-rich adhesin) isoforms show structural differences that correlate with their levels of in vitro pollen tube adhesion activity.* J Biol Chem, 2007. **282**(46): p. 33845-58.
202. Cheng, Y. and W.H. Prusoff, *Relationship between the inhibition constant (K1) and the concentration of inhibitor which causes 50 per cent inhibition (I50) of an enzymatic reaction.* Biochem Pharmacol, 1973. **22**(23): p. 3099-108.
203. Krivov, G.G., M.V. Shapovalov, and R.L. Dunbrack, Jr., *Improved prediction of protein side-chain conformations with SCWRL4.* Proteins, 2009. **77**(4): p. 778-95.
204. Song, Y., V. Madahar, and J. Liao, *Development of FRET assay into quantitative and high-throughput screening technology platforms for protein-protein interactions.* Ann Biomed Eng, 2011. **39**(4): p. 1224-34.
205. Gorham, R.D., Jr., C.A. Kieslich, and D. Morikis, *Electrostatic clustering and free energy calculations provide a foundation for protein design and optimization.* Ann Biomed Eng, 2011. **39**(4): p. 1252-63.
206. Heun, P., *SUMOrganization of the nucleus.* Curr Opin Cell Biol, 2007. **19**(3): p. 350-5.
207. Yeh, E.T., *SUMOylation and De-SUMOylation: wrestling with life's processes.* J Biol Chem, 2009. **284**(13): p. 8223-7.
208. Bawa-Khalfe, T., et al., *Induction of the SUMO-specific protease 1 transcription by the androgen receptor in prostate cancer cells.* J Biol Chem, 2007. **282**(52): p. 37341-9.
209. Hemelaar, J., et al., *Specific and covalent targeting of conjugating and deconjugating enzymes of ubiquitin-like proteins.* Mol Cell Biol, 2004. **24**(1): p. 84-95.

210. Liu, Y., et al., *Discovery of inhibitors that elucidate the role of UCH-L1 activity in the H1299 lung cancer cell line.* Chem Biol, 2003. **10**(9): p. 837-46.
211. Tirat, A., et al., *Synthesis and characterization of fluorescent ubiquitin derivatives as highly sensitive substrates for the deubiquitinating enzymes UCH-L3 and USP-2.* Anal Biochem, 2005. **343**(2): p. 244-55.
212. Goldenberg, S.J., et al., *Strategies for the identification of novel inhibitors of deubiquitinating enzymes.* Biochem Soc Trans, 2008. **36**(Pt 5): p. 828-32.
213. Nicholson, B., et al., *Characterization of ubiquitin and ubiquitin-like-protein isopeptidase activities.* Protein Sci, 2008. **17**(6): p. 1035-43.
214. Leach, C.A., et al., *Detection and characterization of SUMO protease activity using a sensitive enzyme-based reporter assay.* Methods Mol Biol, 2009. **497**: p. 269-81.
215. Tian, X., et al., *Characterization of selective ubiquitin and ubiquitin-like protease inhibitors using a fluorescence-based multiplex assay format.* Assay Drug Dev Technol, 2011. **9**(2): p. 165-73.
216. Zhang, J.H., T.D. Chung, and K.R. Oldenburg, *A Simple Statistical Parameter for Use in Evaluation and Validation of High Throughput Screening Assays.* J Biomol Screen, 1999. **4**(2): p. 67-73.
217. Piston, D.W. and G.J. Kremers, *Fluorescent protein FRET: the good, the bad and the ugly.* Trends Biochem Sci, 2007. **32**(9): p. 407-14.
218. Giepmans, B.N., et al., *The fluorescent toolbox for assessing protein location and function.* Science, 2006. **312**(5771): p. 217-24.
219. Zhang, J., et al., *Creating new fluorescent probes for cell biology.* Nat Rev Mol Cell Biol, 2002. **3**(12): p. 906-18.